3.5 GHz Indoor Propagation Modeling and Channel Characterization

Sean A. Ha

Thesis submitted to the faculty of the Virginia Polytechnic Institute and State University in partial fulfillment of the requirements for the degree of

Master of Science
In
Electrical Engineering

Jeffrey H. Reed, Chair
Christopher R. Anderson
Robert W. McGwier

April 30, 2015
Blacksburg, Virginia

Keywords: 3.5 GHz, path loss, indoor propagation, channel model, MIMO, spectrum sharing

3.5 GHz Indoor Propagation Modeling and Channel Characterization

Sean A. Ha

(ABSTRACT)

In the push for spectrum sharing and open spectrum access, the 3.5 GHz frequency band is under consideration for small cells and general Wireless Local Area Networks (WLAN) in the United States. The same band is beginning to see deployment in China, Japan, and South Korea, for the 4G Long Term Evolution (LTE) cellular standard to increase coverage and capacity in urban areas through small cell deployment. However, since the adoption of this band is new, there is a distinct shortage of propagation data and accurate channel modeling at 3.5 GHz in indoor environments. These models are necessary for cellular coverage planning and evaluating the performance and feasibility of wireless systems.

This report presents the results of a fixed wireless channel measurement campaign at 3.5 GHz. Measurements were taken in environments typical of indoor wireless deployment: traditional urban indoor office, hallway, classroom, computer laboratory, and atrium areas, as well as within a hospital. Primarily Non Line of Sight (NLOS) experiments were carried out in areas with a controllable amount of partitions separating the transmitter and receiver in order to document material-based attenuation values. Indoor-to-outdoor measurements were carried out, focusing on attenuation due to common exterior building materials such as concrete, brick, wood, and reinforced glass.

Documented metrics include large scale path loss, log-normal shadowing, and channel power delay profiles combined with delay spread characteristics for multipath analysis. The statistical multi-antenna diversity gain was evaluated to gauge the benefit of using multi-antenna systems in an indoor environment, which has much greater spatial diversity than an outdoor environment. Measurements were compared to indoor path loss models used for WLAN planning in the low GHz range to investigate the applicability of extending these models to 3.5 GHz.

This work was supported by the Office of the Secretary of Defense (OSD).

To my late mother, Dung T. Young

Acknowledgements

First and foremost, I would like to thank my family, specifically, my father, Phat Ha, and my sister, Julie Mayer, for their unending patience and support through the ups and downs that have comprised the last two years. To you, I say: if nothing else, this manuscript serves as assurance that I won't end up some schmo working in a box factory.

On the academic front, I would, of course, like to thank my advisor, Jeffrey Reed, for overseeing my journey through the Master's program. Thanks also go out to my committee members, Bob McGwier and Chris Anderson, for reviewing and providing feedback for this manuscript. Dr. Anderson, in particular, presented me with a unique and edifying experience in helping with Navy radar measurements; he was also a great help in defining the conceptual foundation for much of the propagation layouts, as well as lending advice for publications created from this body of work.

Special thanks to Taeyoung Yang and Vuk Marojevic for invaluable supervision and guidance over the past year. Randall Nealy has proved equally invaluable as a reliable source of information for RF hardware instrumentation, advice, and debugging.

Thanks to all my labmates at Wireless @ VT for reliable academic discourse, punctuated with brief pockets of reprieve to deflect the long hours of graduate school ennui. In particular, the channel measurement system would have never been resurrected without Karim Said and Miao Yao's FPGA expertise. Thaddeus Czauski has also been a tremendous aid in helping haul equipment and coordinating logistical aspects of my experiments and thesis.

Finally, thanks to everyone in my personal circle of friends. Specifically, a shout-out to Joseph Walsh for those long nights we'd linger over brandy at 'Eat'.

All photos in this document are by the author.

Table of Contents

List of Figures

List of Tables

Chapter 1

Introduction

1.1 Motivation

Over the past two decades, people worldwide have been enjoying seamless inter-connectivity due to the rapid growth and deployment of wireless communication systems. The ubiquity and global adoption of wireless technology has allowed near-limitless innovation in the field of digital communications. One major wireless research trend in the area of cellular communications is leveraging small cell technology – cells with a range of up to 100 meters, as opposed to macrocells which cover multiple kilometers – to fill coverage gaps, promote automated coordination of disparate technologies in self-organizing/self-optimizing heterogeneous networks, and aid in the development of the globally-interconnected smart object infrastructure known as the Internet of Things (IoT).

However, the drawback is that the continued evolution of wireless technology requires a steady supply of available electromagnetic spectrum, which is an extremely limited resource. In response to the impending spectrum crisis, the U.S. President's Council of Advisors on Science and Technology recently released a report that recommended sharing of up to 1 GHz of federal government radio spectrum with non-government entities. The European Union made a similar announcement, calling for a more open, harmonious spectral environment. In December of 2012, the Federal Communications Commission (FCC) issued a Notice of Proposed Rule Making (NPRM) to solicit feedback on the possibility of sharing the 3550 to 3700 MHz band as a first step in this spectrum sharing scheme [1]. This band is envisioned to be shared according to a three-tier authorization mechanism using Dynamic Spectrum Access (DSA) technology, as shown in Figure 1.1.

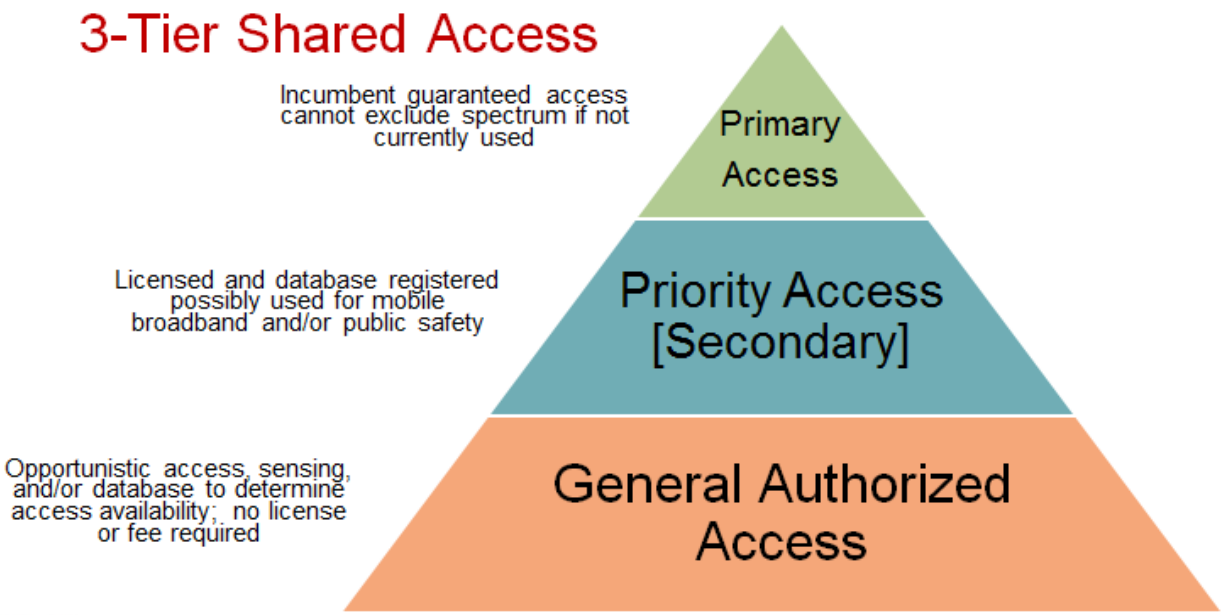

Figure 1.1: FCC proposed three-tier approach to spectrum sharing

The three proposed tiers of operation are incumbent access (Navy radar, federal and non-federal Fixed Satellite Service), priority access (hospitals and public-safety entities), and general authorized access (GAA) or the public. The new spectrum sharing policy offers new spectrum-sharing applications, such as rural broadband wireless services, wireless patient monitoring, agricultural monitoring, smart grid, and enhanced augmented reality. For example, the proposed-GAA Citizens Broadband Radio Service (CBRS) would enable unlicensed opportunistic devices to dynamically access the IoT in an effort to promote innovative wireless connectivity. In this manner, the 3.5 GHz band has been dubbed an "innovation band" where current and emerging wireless technologies strive for co-existence and lay the foundation for spectrum sharing in other frequency bands.

Even in the presence of primary and priority access users, there is vast potential for opportunistic spectrum sharing, as the 3.5 GHz band boasts sparse occupancy and abundant contiguous bandwidth. Small cells and heterogeneous networks may be deployed and lay initial claim to the band, while existing wireless technologies can co-exist and optimize their performance through opportunistic access of any unused bandwidth.

As a commercial example, the Time Division Duplexing (TD) version of the Long Term Evolution (LTE) cellular standard is already being primed for the 3.5 GHz band, otherwise known as Band 42/43 [2]. Forecasters predict that the band will provide greater capacity in

urban hot zones as the short-range propagation properties of the low GHz band will allow for pronounced frequency reuse [3].

In April of 2014, the FCC issued a Further Notice of Proposed Rulemaking (FNPRM), which addressed comments regarding the previous NPRM. The FNPRM proposed exclusion zones for incumbent users, a reserved GAA spectrum "floor" to further promote sharing and innovation in the band, and Contained Access Facilities (CAF) or indoor environments for Contained Access Users (CAU) for private, unencumbered utilization of up to 20 MHz of the GAA band [4].

Prior to deploying new wireless devices and systems, it is necessary to predict the performance of the new devices via channel models. Channel models are critical in spectrum planning as they allow us to assess the co-existence and compatibility of the band's primary and secondary users. Unfortunately, there is a distinct shortage of 3.5 GHz propagation characterization data and/or models in literature, due primarily to the relatively lackluster interest in the band over the past decade.

1.2 Objective

This thesis addresses the comprehensive documentation, validation, and statistical analysis of radio wave propagation parameters in the 3.5 GHz band of distances less than 100 meters in an indoor environment to facilitate indoor small cell deployment, spectrum sharing, and co-existence with primary users. Using measurements from our indoor propagation campaign, we compute statistical parameters such as large scale path loss and delay spread which help define and characterize the wireless channel. Path loss measurements are compared to predictions from empirical path loss models commonly used for low GHz Wireless Local Area Network (WLAN) system planning to gauge the performance of existing models in the 3.5 GHz frequency range and to determine if the same models may be applied for indoor picocell and femtocell deployments. Since spatial diversity in an indoor environment is much greater than in an outdoor environment, we employ multiple-antenna transmit and receive diversity using a vector channel model with four antenna elements to determine the performance gain of indoor multi-antenna wireless system deployments over outdoor deployments.

1.3 Organization of Thesis

This thesis is organized as follows.

Chapter 2 provides background on basic radio wave propagation theory, statistical channel parameters essential in channel characterization, basic channel modeling techniques, and a literature survey on existing channel models and propagation data at 3.5 GHz.

Chapter 3 provides an outline of the measurement system used for the propagation campaign, the measurement campaign test plan, and pictures and floor layouts for the various propagation scenarios under consideration.

Chapter 4 comprehensively documents and analyzes the measured channel characterization parameters described in Chapter 2. The impact of multiple antenna diversity gain is statistically derived and analyzed.

Chapter 5 statistically compares the recorded propagation measurements to existing indoor path loss models for the 3.5 GHz band.

Chapter 6 provides a summary and proposes future work on the topic of 3.5 GHz channel characterization.

Chapter 2

Background and Related Work

2.1 Radio Wave Propagation

In a wireless system, the transmitter and receiver communicate by trading electromagnetic waves between their respective antennas. When an electromagnetic wave collides with an object, the direction of propagation will be diverted through means such as reflection or scattering.

Reflection occurs when the object's dimensions are much larger than the wavelength of the signal and has applications in channel modeling, as shown with the two-ray model in Figure 2.1.

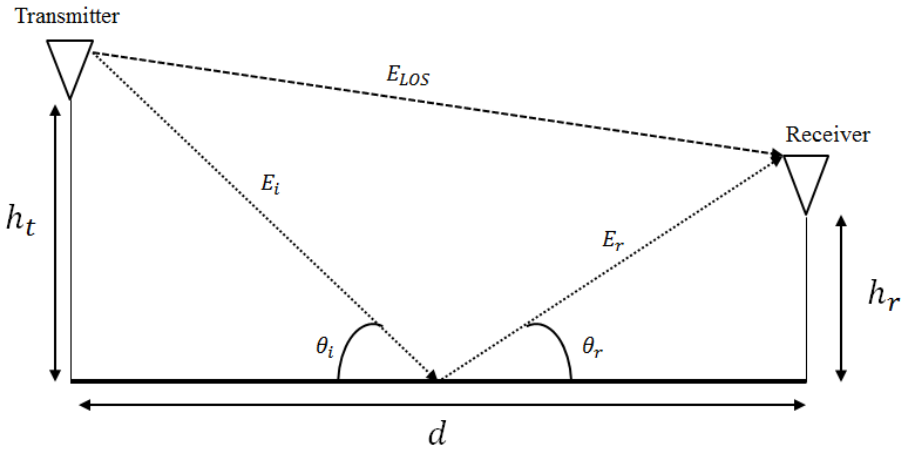

Figure 2.1: Two-ray model for reflection

The most common diversion of an electromagnetic wave, however, occurs when the object's dimensions are much smaller than the wavelength of the signal, which is known as scattering, as shown in Figure 2.2. As its name implies, scattering takes the energy of an incident radio wave and disperses it unpredictably in all directions.

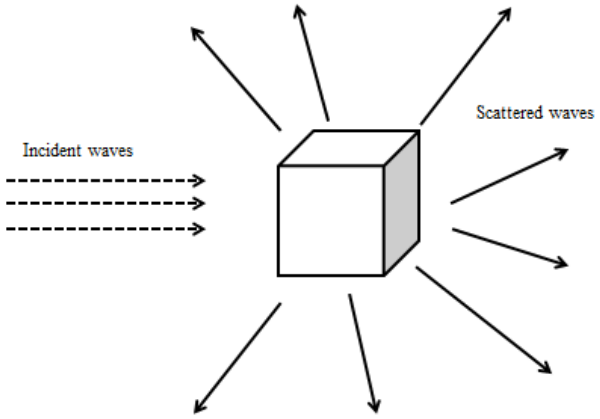

Figure 2.2: Scattering by a small object

Scattering, combined with propagation losses over distance, leads to a phenomenon known as *fading*. *Large-scale fading* accounts for the average loss in signal strength or amplitude over a period of time, and results from a combination of propagation over long distances - known as *path loss* - and scattering off of large objects, known as *shadowing*. *Small-scale fading* refers to rapid fluctuations in signal strength due to scattering over small objects close to the transmitter and receiver. Path loss is represented as monotonically decreasing, and obeys a log-linear regression. Figure 2.3 illustrates the difference in received power as a function of distance due to both small-scale and large-scale fading.

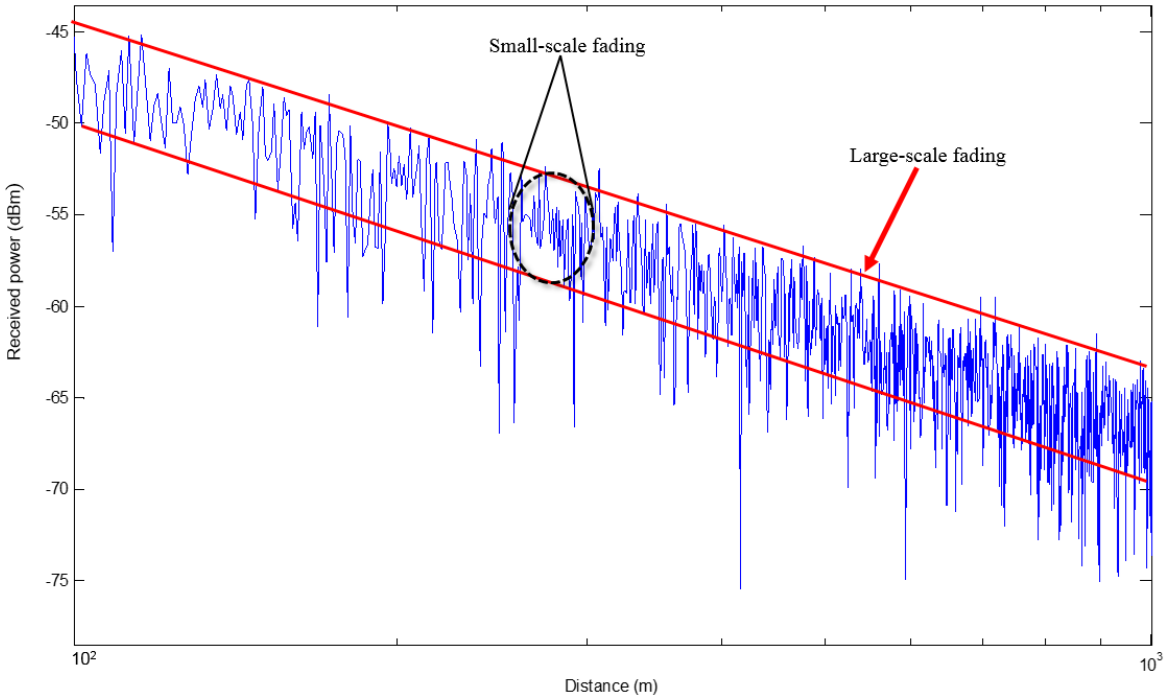

Figure 2.3: Large scale vs. small scale fading

As seen by the receiver, the scattering of radio waves off of many objects in the environment results in a phenomenon known as *multipath*. Multipath can be modeled as multiple copies of the transmitted signal arriving at the receiver with varying delays (phases) and amplitudes, as shown in Figure 2.4. The direct ray arrives at the receiver with zero delay and each subsequent received signal arrives with a non-zero excess delay. The phase misalignment of the signals may results in destructive interference, which can further reduce the received power of the signal, if not properly accounted for.

Also shown in Figure 2.4 is the power delay profile (PDP) of the wireless system due to the multipath caused by the surrounding environment. The PDP is a graph of received signal strength versus excess delay and is a visual indication of the multipath richness of a particular wireless channel.

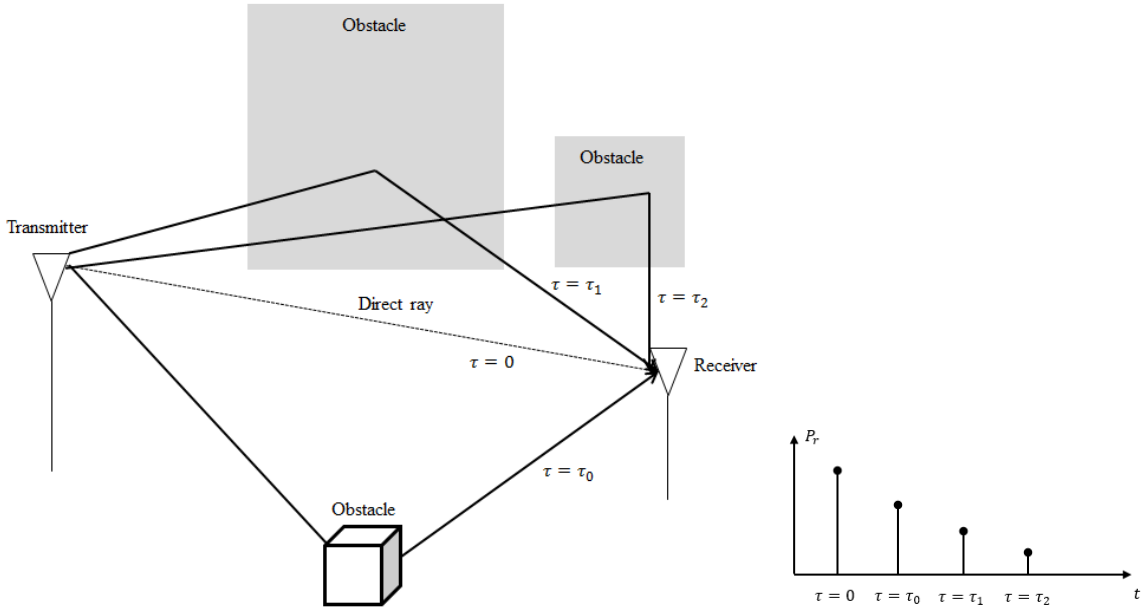

Figure 2.4: Multipath due to scattering and corresponding power delay profile

2.2 Channel Characterization Parameters

2.2.1 The Wireless Channel

The wireless channel is defined as the medium through which an electromagnetic wave travels from transmitter to receiver. One common way to represent the wireless channel, mathematically is by using the following, convolutional form

$$y(t) = h(t;\tau) * x(t) + n(t). \quad (1)$$

where $h(t;\tau)$ represents the wireless channel as a function of time t and delay τ, which may be thought of as a transfer function, $y(t)$ and $x(t)$ represent the received and transmitted signals, respectively, and $n(t)$ is Additive White Gaussian noise (AWGN). $h(t;\tau)$ is a function that depends implicitly on the propagation environment and can differ rapidly on an instant-by-instant basis, making it extremely difficult to fully characterize. As such, simplifying assumptions are made to characterize $h(t;\tau)$ in a manner that is computationally tractable.

One method of simplifying $h(t;\tau)$ is by referencing the measured power delay profile of a channel and expressing the channel as a function of τ, only, as shown in the following equation:

$$h(\tau) = \sum_{k=0}^{N-1} |P(\tau_k)|\, e^{j\angle P(\tau_k)} \delta(\tau - \tau_k)). \tag{2}$$

In (2), $P(\tau_k)$ is the value of the power delay profile at time delay τ_k, and N is the total number of multipath components. This form assumes that the channel is time-invariant (stationary) and is therefore a function of delay only. The channel property which results in delayed multipath components is known as the *time-dispersion* of the channel, as it is a measure of how the channel spreads a given input across a specific time window.

2.2.2 Delay Spread

The time dispersion of a channel can be expressed in terms of *delay spread*. We first define *mean excess delay* as

$$\bar{\tau} = \frac{\sum_{i=0}^{N-1} P(\tau_i)\, \tau_i}{\sum_{i=0}^{N-1} P(\tau_i)}. \tag{3}$$

The *RMS delay spread* of a channel can then be expressed as

$$\sigma_\tau = \sqrt{\overline{\tau^2} - (\bar{\tau})^2}. \tag{4}$$

with

$$\overline{\tau^2} = \frac{\sum_{i=0}^{N-1} P(\tau_i)\, \tau_i^2}{\sum_{i=0}^{N-1} P(\tau_i)}. \tag{5}$$

RMS delay spread is critically useful in wireless applications, as it is used to determine the channel's *coherence bandwidth*, or the bandwidth over which a channel remains constant. If a channel's coherence bandwidth is narrower than the bandwidth of the baseband transmitted signal, undesirable inter-symbol interference (ISI) will occur [5][5]. This knowledge can be

helpful in waveform design – for example, Orthogonal Frequency Division Multiplexing (OFDM)-based wireless systems rely on accurate coherence bandwidth measurements to save overhead by shortening the cyclic prefix (CP) length during of each symbol [6].

Another important delay spread metric is *max excess delay*, which is defined as the maximum delay τ_{MAX} such that, beyond τ_{MAX}, the received power due to multipath does not drop X dB below its maximum value [5]. The threshold X may be defined according to a specified standard or application.

Figure 2.5 illustrates how mean excess delay, RMS delay spread, and max excess delay are defined relative to a sample channel power delay profile.

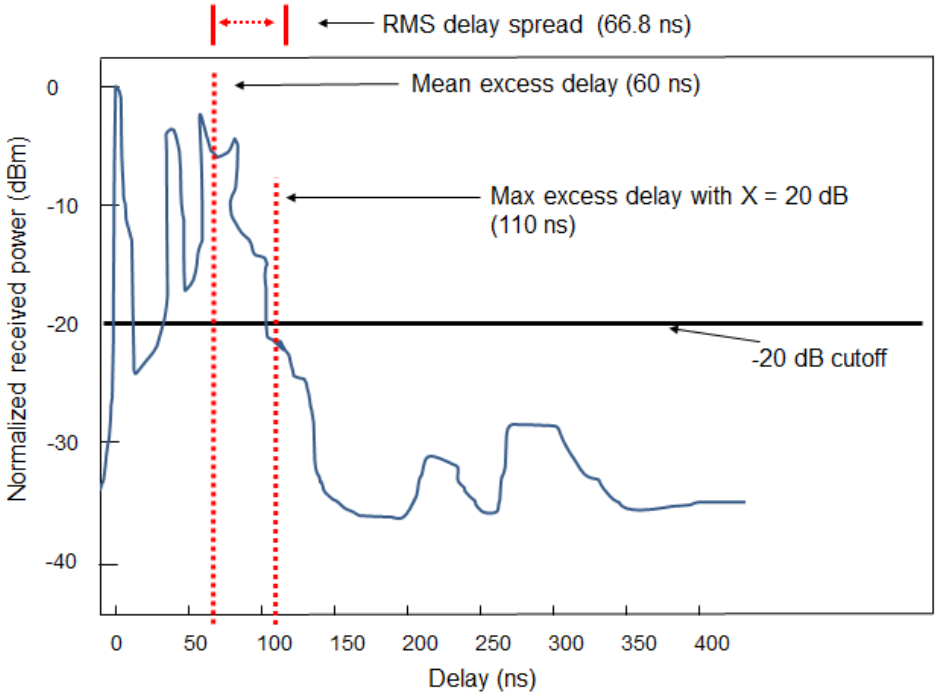

Figure 2.5: Channel delay characteristics with respect to a sample power delay profile

2.2.3 Envelope Correlation Coefficient

A multi-antenna system requires sufficient spatial correlation between each antenna element to obtain appreciable diversity gain. For a received signal at an antenna array, spatial correlation is most commonly quantified by the *envelope correlation coefficient* (ECC) of the signal. Assuming a time-invariant wireless channel, as defined in Equation (1), any two antenna elements x and y, the ECC between them between two delay instants τ_0 and τ_1 may be expressed as

$$\rho_{xy} = \frac{\int_{\tau_0}^{\tau_1}(r_x(\tau) - \bar{r_x})\big(r_y(\tau) - \bar{r_y}\big)dt}{\sqrt{\int_{\tau_0}^{\tau_1}(r_x(\tau) - \bar{r_x})^2 dt}\sqrt{\int_{\tau_0}^{\tau_1}\big(r_y(\tau) - \bar{r_y}\big)^2 d\tau}} \tag{6}$$

where $r_x(\tau)$ represents the received power envelope of signal $x(\tau)$. $\bar{r_x}$ represents the average received signal envelope power over the delay interval between τ_1 and τ_0, as expressed by

$$\bar{r_x} = \frac{1}{\tau_1 - \tau_0}\int_{\tau_0}^{\tau_1} r_x(t)\, d\tau \tag{7}$$

A lower correlation increases the difference in fading due to multipath at each element, and thus, allows for greater spatial diversity and greater diversity gains.

2.2.3 Large Scale Path Loss

As mentioned in Section 2.2.1, path loss is used to model the attenuation of a wireless channel as a function of the distance between the transmitter and receiver, as well as the characteristics of the surrounding propagation environment. The most common starting point for path loss calculation is the free-space path loss formula

$$P_R = P_T(L_P) \tag{8}$$

$$\bar{L}_P = \left(\frac{4\pi df}{c}\right)^2 \tag{9}$$

where P_R is the received power, P_T is the transmit power, d is the transmitter-receiver separation in meters, f is the frequency, and c is the speed of light in a vacuum. The quantity $\bar{L}_P$ is known as the *free-space path loss.*

Assuming frequency and distance to be constant, the relationship between non-free space path loss and the propagation environment can be expressed by

$$L_P \propto d^n \tag{10}$$

where n is the *path loss exponent* and encapsulates the attenuating effects of the propagation environment. Equation (9) shows that $n = 2$ for free space and increases as physical obstructions are introduced. Table 2.1 lists typical values of n for outdoor and indoor environments [5].

Table 2.1: Typical values of n for indoor propagation

Scenario	n
Free space	2
Urban cellular radio	2.7 – 3.5
Shadowed urban cellular radio	3 – 5
LOS in building	1.6 – 1.8
Obstructed in building	4 – 6

2.2.4 Log-Normal Shadowing

Shadowing accounts for the local variation in received power (or, equivalently, path loss) which is caused by the presence of large objects in the propagation environment. Shadowing may be expressed as a random process, determined by the random variable X_σ, which is log-normally distributed, as shown in Figure 2.6.

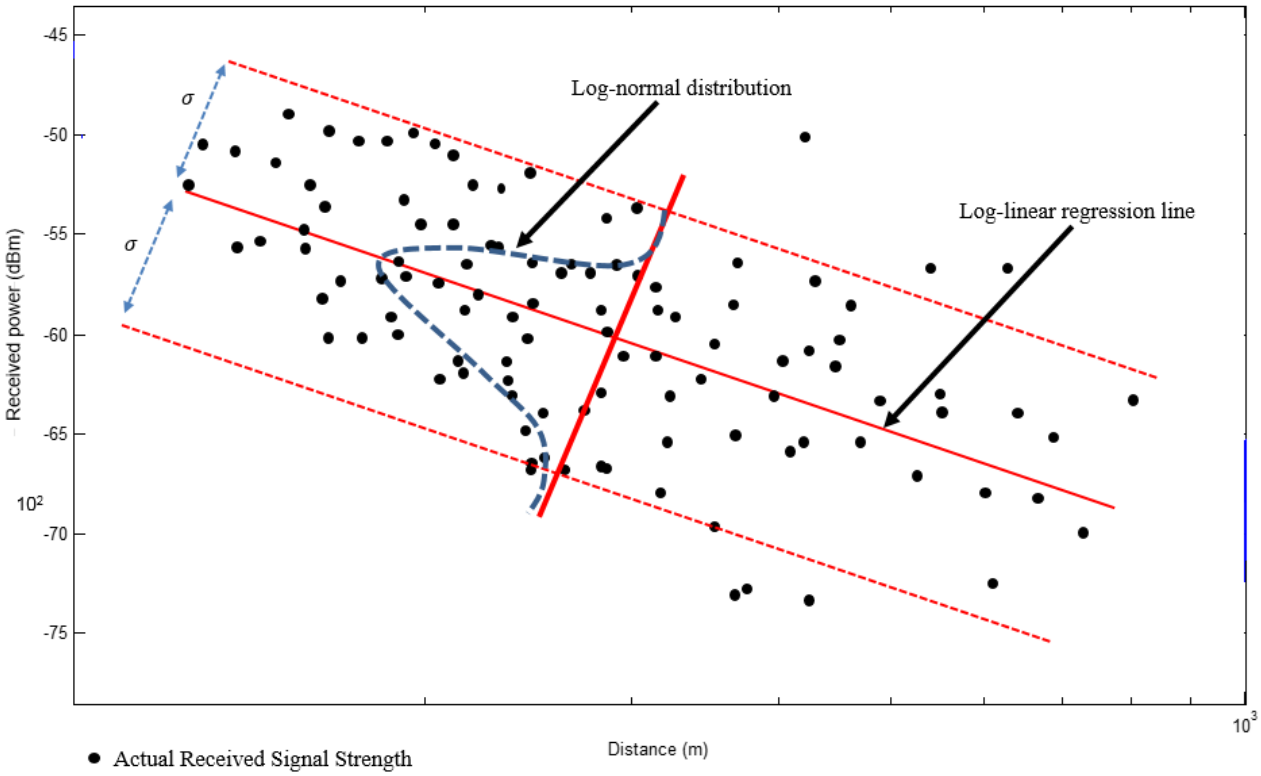

Figure 2.6: Sample received power measurements with log-normal shadowing

As shown in Figure 2.6, by fitting a log-linear regression line through the measured data, the log-normal shadowing may be statistically computed as the *root mean-squared error* (RMSE) of the received measurements. The path loss exponent may be similarly statistically derived as the slope of the fitted log-linear regression line.

Accounting for log-normal shadowing and converting from linear to dB, we define the more general and practical variant of the free-space path loss equation as

$$L_P = \hat{L}_P(d_0) + 10n \log_{10}\left(\frac{d}{d_0}\right) + X_\sigma \qquad (11)$$

where d_0 is the reference distance and $\hat{L}_P(d_0)$ is the measured path loss at d_0. Equation (11) is known as the *log-distance path loss model* and is the most basic of large scale path loss formulas which can be statistically derived from received power measurements.

2.3 Channel Modeling Techniques

Channel modeling consists of a broad set of techniques and tools, all of which attempt to model a certain behavior or aspect of a channel without having to fully characterize it. For wireless system deployment, large scale path loss is the most desired characteristic of a channel: that is, by how much does a channel attenuate signal power from transmitter to receiver?

The most basic path loss prediction technique is to apply the free space path loss formula given by Equation (9), as explained in the previous section; however, this model has limited utility as it assumes that the transmitter and receiver exist in a vacuum. Applying the log-distance path loss model given by Equation (11) will result in a more accurate prediction; however, the model only accounts for the presence of a discrete number of large objects and requires corrective measures to reach a usably accurate model.

There are three main categories of channel models: *empirical*, *deterministic*, and *statistical*. We define empirical models as models which expand upon the framework of the general path loss formula – they are based solely on prior observations and measurements and have no analytical basis. Despite their lack of theoretical foundation, empirical models are immensely popular as many generalize with enough accuracy for practical coverage planning and are incredibly simple to implement, analyze, and modify through correction factors, as the need arises.

The most widely-used empirical model is the Hata model [7], which can be defined as

$$L_H = 69.6 + 26.2\log_{10}(f) - 13.8\log_{10}(h_t) - a(h_r) + (44.9 - 6.55\log_{10}(h_t)\log_{10}(d) \quad (12)$$

where f is the frequency ranging from 150 – 1500 MHz, h_t and h_r are the heights of the transmit and receive antennas, respectively, and $a(h_r)$ is an applied correction factor based on the receive antenna height. Another popular empirical model is the Stanford University Interim (SUI) model [8], given by

$$L_{SUI} = A + 10n\log_{10}\left(\frac{d}{d_0}\right) + X_f + X_h + X_\sigma, \qquad d > d_0 \quad (13)$$

where A is the free space path loss at distance d_0, n is the model-specific path loss exponent derived terrain conditions, X_σ is the log-normal shadowing factor, X_f is the frequency correction factor for propagation above 2 GHz, and X_h is the correction factor for antenna height.

Deterministic models are environment-dependent, as they make use of radio wave propagation theory and ray tracing methods to predict the behavior of electromagnetic propagation at a fixed location. While highly accurate, they have poor extensibility and are highly computationally-intensive, though advances in computing power have greatly increased their practical usability over the past decade. Figure 2.7 outlines the process of generating a deterministic ray tracing model.

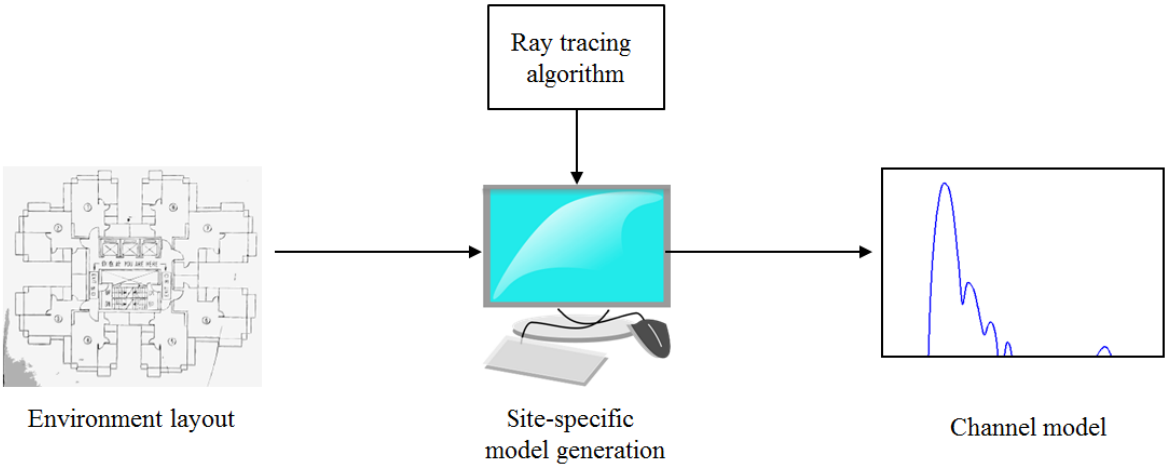

Figure 2.7: Generation of a deterministic ray tracing model

Statistical models use random variables to characterize the propagation environment by assigning probability distributions to channel parameters such as delay spread or small scale fading factors. Similar to empirical modeling, propagation experiments and statistical analysis are performed to validate the goodness-of-fit of each parameter distribution – adjustment factors are introduced as needed. Basic examples of statistical models include the Rayleigh and Rician fading models, which are based off of a set of commonly applied channel statistics and broadly applicable to many different environments.

A more constrained statistical model is the Saleh-Valenzeula (SV) model for indoor propagation, which is commonly used in modeling ultrawideband (UWB) communications [9]. Assuming that scatterers are not uniformly distributed in the propagation environment and are instead clustered into discrete groups, the SV model is able to extract features such as the arrival

rate and power decay of each individual cluster through statistical estimation of parameters derived from a channel's power delay profile.

In this work, we focus exclusively on empirical path loss channel models as determining the large scale path loss due to the environment is the first and most crucial step in wireless system planning. Exhaustively expanded empirical models have proven to be practical and accurate in predicting propagation behavior. Deterministic models produce results which are highly accurate; however, they are limited in flexibility as the model is entirely site-specific. Statistical models may be used to characterize channel parameters other than path loss; however, many assumptions about the propagation environment need to be made for the assigned statistical distributions to hold. Combined with the added mathematical complexity, a statistical model's utility to a practical use case, such as wireless coverage planning, is secondary to strictly large scale path loss models.

2.4 Literature Survey

2.4.1 3.5 GHz Propagation Measurement Campaigns

There have been abundant propagation studies at highly-used low-GHz frequency bands such as 2.4 or 5.8 GHz, but limited work in the 3.5 GHz band. In the literature, most propagation studies focus on Worldwide Interoperability for Microwave Access (WiMAX) which is the dominant commercial utility to have adopted the 3.5 GHz band. As a result, the majority of 3.5 GHz studies involve propagation centering on large outdoor macrocells, which range from one to several kilometers. Additionally, many propagation campaigns only focus on received power measurements (i.e. large scale path loss) and few capture the impact of other critical propagation metrics such as scattering or time dispersion.

The most extensive 3.5 GHz campaign in the literature carried out short-to-mid range fixed wireless access propagation campaign in rural, suburban, and urban environments in Cambridge, U.K., and compared path loss measurements to the free-space path loss model, the ECC model, the SUI model, and the COST-231 model [10]. As WiMAX adopted the band, multiple WiMAX-based path loss campaigns were carried out for urban and suburban macrocells for fixed and mobile broadband using WiMAX base stations [11] [12] [13] [14] [15] [16] [17]. One

study focused on propagation in rural areas such as fields, meadows, and forests with varying degrees of vegetation content [18].

Concerning small cells, an indoor-to-outdoor path loss campaign was carried out for small cells between 0.9 and 3.5 GHz [19], as well as an outdoor campaign [16] in a suburban apartment complex for distances of up to 25 meters. Concerning strictly indoor propagation, [20] measured path loss and delay spread for vector channels in hallway and office environments for distances of up to 10 meters.

Table 2.2 summarizes the results of the 3.5 GHz band measurement campaigns found in literature, along with the propagation-resulted results, such as the path loss exponent and the RMSE from the fitted log-linear regression line. Table 2.3 summarizes 3.5 GHz measurement campaigns which focus on comparing gathered measurements to existing channel models rather than extracting channel parameters.

Table 2.2: Measurement campaigns focused on gathering propagation data

Environment	Distance (m)	Antenna Height (m)		Path loss exponent and root mean squared error		Reference
		Tx	Rx	n	σ (dB)	
Suburban (offices)	50 - 500	43	1.5	3.0	1.35	[21]
Suburban (campus)		16	1.5	3.5	0.65	
Residential (indoor-to-outdoor)	1 - 110	1	1	3.8	-	[16]
Residential (indoor-to-outdoor)	1 - 100	1	1.5	3.9	7.1 - 12.4	[19]
Suburban	10 – 1000	15	2.5 – 4	3.7 – 4.9	7.7 – 9.6	[13]
Suburban	200 - 3500	20	3	3.6	9.5	[14]
Rural (forest)	1 - 110	0.9 – 1.6	0.9 – 1.6	1.87 - 3.01	2.76 – 5.98	[18]
Rural (open)				1.75 – 2.63	0.94 – 2.69	
Indoor	2 - 20	2.1	1.7	1.46 – 2.05	2.0 – 3.4	[20]

Table 2.3: Measurement campaigns focused on model comparisons

Environment	Distance (m)	Antenna Height (m)		Featured Models	RMSE σ (dB)	Ref.
		Tx	Rx			
Urban	250 - 2000	14 - 45	5 - 12	SUI / COST / ECC	10.6 / 8.2 / -	[10]
Suburban					8.8 / 7.5 / 6.9	
Rural					10.1 / 9.7 / 9.8	
Urban (on foot)	1 - 80	10	1.5	COST / SUI / Ray tracing	12.27 / 19.39 / 10.31	[16]
Urban (car)					14.27 / 20.11 / 11.30	
Suburban	100 -1000	2.5	1.5	Hata with - Longley Rice - Deygout - Epstein-Peterson	18.87 / 16.15 / 13.12	[11]
Suburban	50 - 2000	20 - 35	1.5	COST / SUI / ECC	13.29 / 11.99 / 11.16	[12]
Suburban	10 - 1000	15	2.5 - 4	Erceg / Hata / Walfisch-Ikegami	-	[13]
Suburban	200 - 1200	18	1.6	Walfisch-Ikegami / SUI / Hata	6.72 / 5.00 / 5.24	[15]
Urban	1 - 4500	42	1.5	ITU-R P.1411 / ITU-R P.1546 / SUI	24.71 / 20.00 / 14.33	[22]
Urban	100 - 1000	30	1.5	Walfisch-Ikegami / COST / Erceg	-	[17]
Indoor	2 - 20	2.1	1.7	M.2135, WINNER	-	[20]

Of note in Table 2.3 are the final three entries [17] [20] and [22], as both [20] and [22] derive delay spread statistics for the channel and [17] derives small-scale statistical parameters such as Rayleigh, Nakagami, and Ricean fading factors.

2.4.2 3.5 GHz Channel Models

As mentioned, several traditional empirical channel models have been extrapolated to 3.5 GHz [23] [24][25] [26] [27], however, all such models are for macrocells and have appreciable room for improvement when compared to gathered data, as seen in Table 2.3 [10] [28] [29]. For microcells, there is the ITU-R P.1546 [30], model and attempts have been made at extrapolating the Walfisch-Ikegami model [24] to distances of less than 100 meters.

Regarding indoor modeling, the COST-231 Multi-Wall (MW) empirical model has proven popular with commercial entities seeking to carry out basic indoor cell planning [24]. The Multi-Wall and Floor (MWF) model extended the COST-231 MW model to account for types and number of floors [31]. Along the same lines, the Motley-Keenan (MK) variation of the COST

model was developed and further factored the relative thickness of walls into the formula [32]. [33] suggests that both the COST MW and MK models are adequate in predicting indoor-to-outdoor propagation. The partition-based path loss model [34] uses precise, experimentally-derived attenuation factors for each partition. Finally, the ITU-R M.2135 model is a simple model which averages the losses due to walls and NLOS partitions into an empirical constant and has been used to model indoor hotspots [35].

There has also been an effort to generate new empirical models, such as the WINNER II project, which produced a comprehensive empirical model from 2 – 6 GHz with extensive correction factors to account for a variety of propagation scenarios, both indoor and outdoor [36]. However, as with most indoor models and propagation studies, the WINNER model was generated using data at 2.45 and 5.25 GHz and the 3.5 GHz applicability is an extrapolation in frequency.

Tables 2.4 and 2.5 summarize the results of the path loss models found in literature.

Table 2.4: Summary of outdoor propagation models for low GHz bands

Model	Frequency Range	Cell Type	Locations	Features	Reference
ECC-33	3.4 – 3.8 GHz	Macro	Urban Suburban	-	[23]
SUI	2 – 11 GHz	Macro Small	Urban Suburban Rural	Terrain Vegetation	[8]
Erceg	1.9 – 3.5 GHz	Micro	Urban Suburban Rural	Terrain Vegetation	[26]
Model 9999	150 – 3500 MHz	Macro	Urban Suburban Rural	-	[27]
COST-231	150 – 2000 MHz	Macro	Urban Suburban Rural	-	[24]
Walfisch-Ikegami	800 – 2000 MHz	Macro	Urban	Building height Street width Building separation	[24]
ITU-R P.1411	800 – 5000 MHz	Pico Micro	Urban Suburban Rural	Streets Over rooftops	[30]
ITU-R P.1546	300 – 3000 MHz	Small	Urban Suburban Rural	Climate regions	[37]

Table 2.5: Summary of indoor propagation models for low GHz bands

Model	Features	Reference
COST 231 Multi Wall	Loss from each wall classified as “light” or “heavy” and aggregated	[24]
ITU-R M.2135	NLOS loss consolidated into one attenuation term	[35]
WINNER II	Model categorized by LOS, NLOS, number and type of walls Loss from walls and floors aggregated via “light” or “heavy” categories	[36]
Adjusted Motley Keenan	Loss from each wall classified as “plaster”, “concrete”, or “soft” and aggregated, taking into account wall thickness	[32]
Multi Wall and Floor	Loss from each wall/floor classified by type (concrete, drywall, etc.) and aggregated	[31]
Partition-Based	Loss from each wall classified by empirical attenuation factors and aggregated	[34]

In summary, the scarcity of propagation measurements in the band has resulted in insufficient data with which to properly validate the performance of and/or modify existing channel models to arrive at a standard, suitable model for 3.5 GHz.

Chapter 3

Indoor Measurement Campaign

3.1 VIPER Software-Defined Measurement System

For our propagation measurement campaign, we employed a software-defined, wideband, vector channel sounder which uses a correlation receiver architecture to capture the power delay profile of the signal, allowing for received power and multipath analysis. The receiver uses four antennas elements, allowing for the study of multiple antenna diversity. The VIPER system was developed by Dr. Bill Newhall at Virginia Tech in 2003 for measurements at 2.05 GHz [38] and has been revived and adapted for use at the 3.5 GHz band.

3.1.1 Correlation Receiver Channel Sounding

To obtain the power delay profile of a wireless channel, we use a correlation receiver. The transmitter produces a pre-defined pseudorandom noise (PN) sequence which is modulated using Binary Phase Shift Keying (BPSK). At the receiver, the received signal is correlated with a local version of the PN sequence to determine the received power of the signal as a function of delay. The correlation receiver does not require time synchronization through either synchronized oscillators or direct cabling, as in the case of a vector network analyzer setup.

The operating parameters of the correlation receiver are listed in Table 3.1 [39].

Table 3.1: Parameters for correlation receiver

Parameter	Value
Chip Rate	80 MHz
Length of PN sequence	1023 chips
Temporal Resolution	12.5 ns
Maximum Multipath Delay	12.79 μs

3.1.2 VIPER Measurement System: Setup and Verification

The RF-front end of the VIPER system is flexible, as hardware components may be swapped out for the system to operate at desired frequencies. The RF parameters of the VIPER measurement system are listed in Table 3.2. A block diagram of the VIPER receiver is shown in Figure 3.1, with full pictures of the receiver shown in Figure 3.2.

Table 3.2: Parameters for VIPER measurement system

Parameter	Value	Notes
Center frequency	3.6 GHz	
Sampling Rate	1.0 GHz	
Transmit antenna	Wideband disc cone	
Receive antenna	4 monopoles	Mounted over ground plane λ/4 elements, λ/2 spacing
Tx antenna height	1.05 m	
Rx antenna height	1.35 m	
Transmit power	25 dBm	

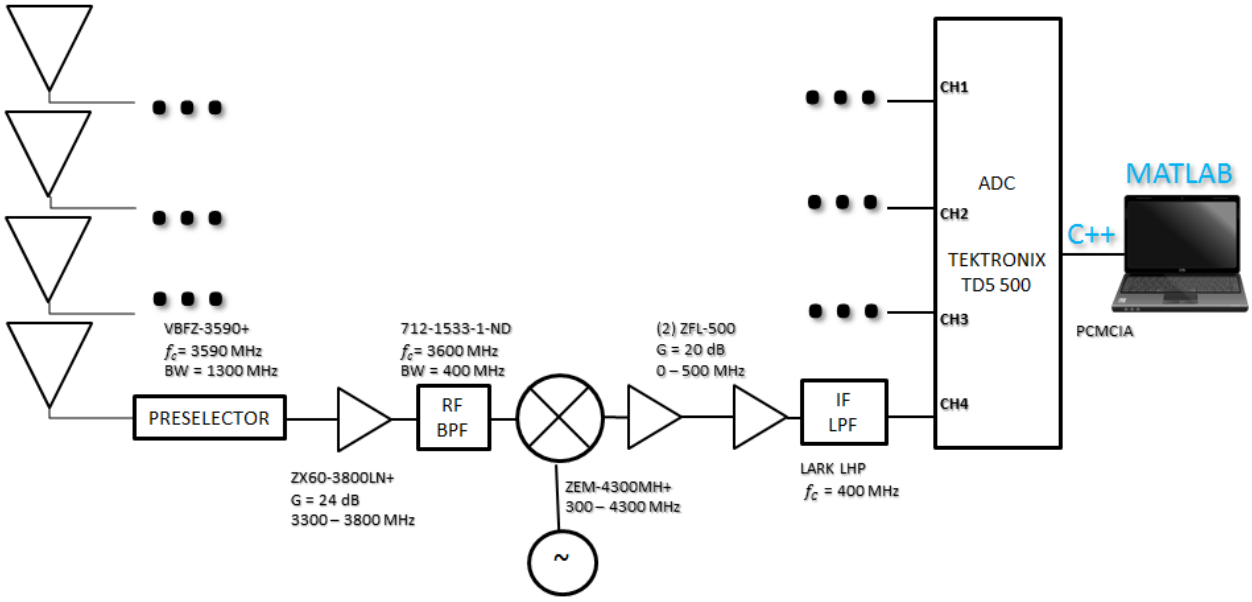

Figure 3.1: Block diagram of VIPER receiver

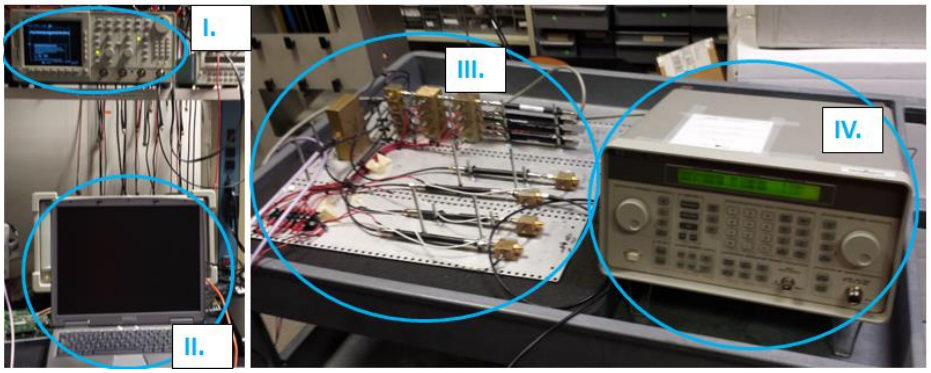

I. Tektronix TDS 580 Oscilloscope
II. Host PC running Windows 98
III. RF Front End
IV. Signal Generator for Downconversion

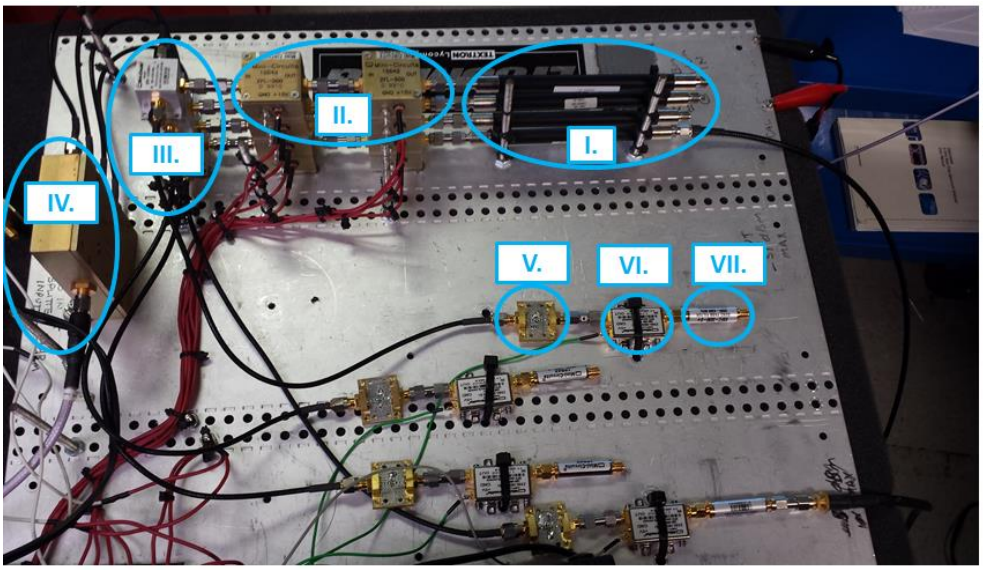

I. Low-pass filter: 400 MHz
II. 2x LNA: 500 MHz
III. 4x LO: 300 – 4300 MHz
IV. LO in: 4-way power splitter
V. 4x Band-pass filter: 3200 – 3800 MHz
VI. 4x LNA: 3300 – 3800 MHz
VII. 4x Pre-selector : 2940 – 4240 MHz

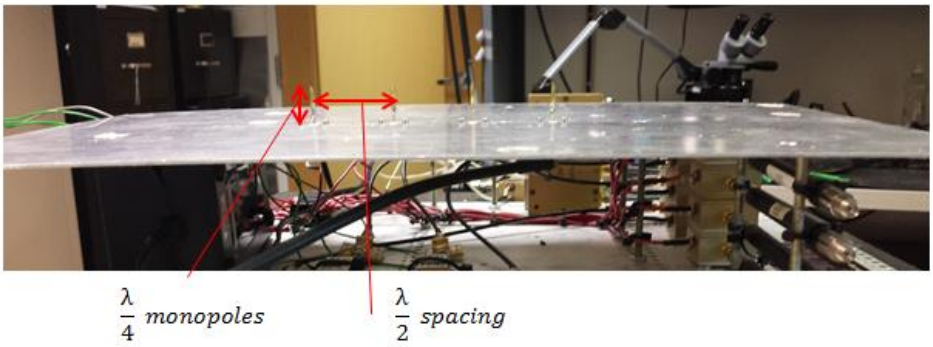

Figure 3.2: VIPER measurement system

Receiver equipment, RF front end, and receive antenna array

The VIPER measurement system uses a Local Oscillator (LO) to convert the received signal to an Intermediate Frequency (IF) of 150 MHz. After passing through a Low Pass Filter (LPF), the signal is converted into digital samples through an application written in C++ and finally into the MATLAB workspace where Digital Signal Processing (DSP) operations are performed to produce the final result. The MATLAB DSP operations are outlined in Figure 3.3.

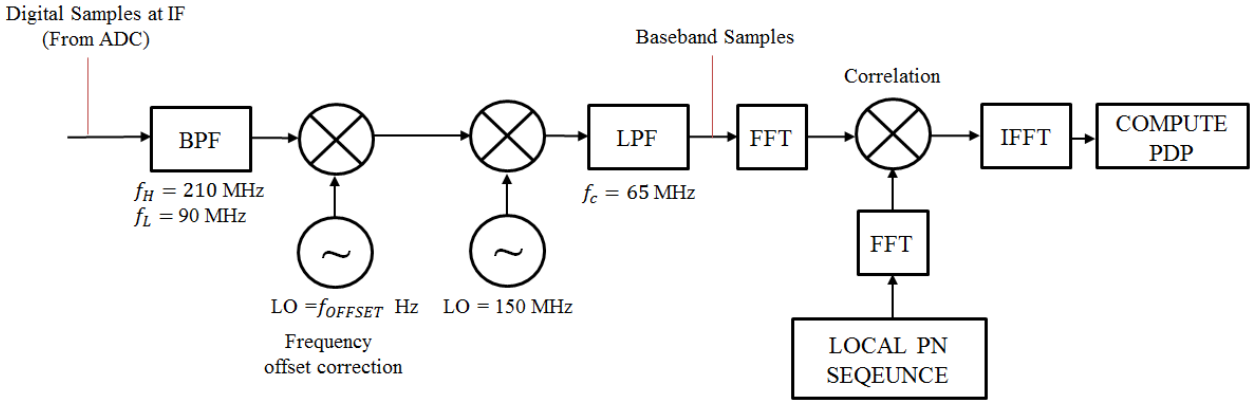

Figure 3.3: Block diagram of MATLAB DSP

Figure 3.4 shows the received power delay profile in the MATLAB workspace.

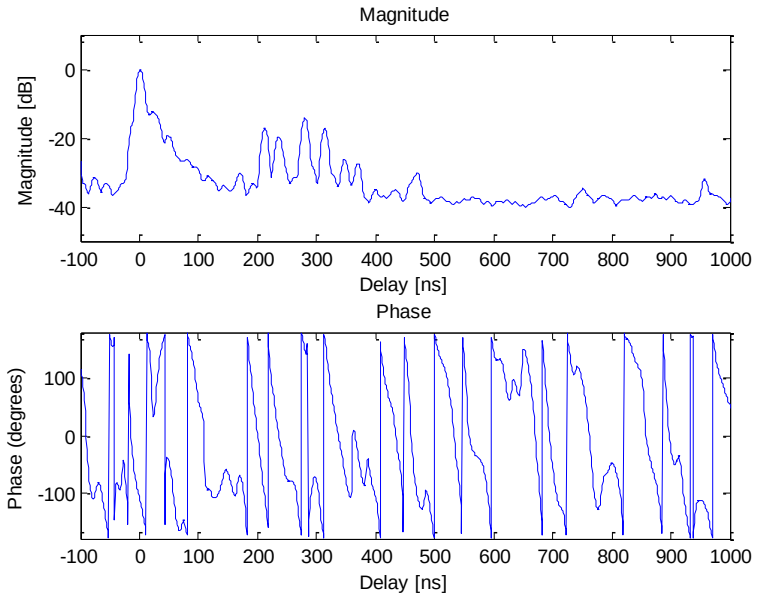

Figure 3.4: Received power delay profile in MATLAB

The Xilinx Spartan 3 FPGA board on a Universal Serial Radio Peripheral (USRP) N210 software-defined radio unit was used for the transmitter. The BPSK-modulated PN sequence was written to a digital pin output at a rate of 80 Mcps. A block diagram of the transmitter setup is shown in Figure 3.5.

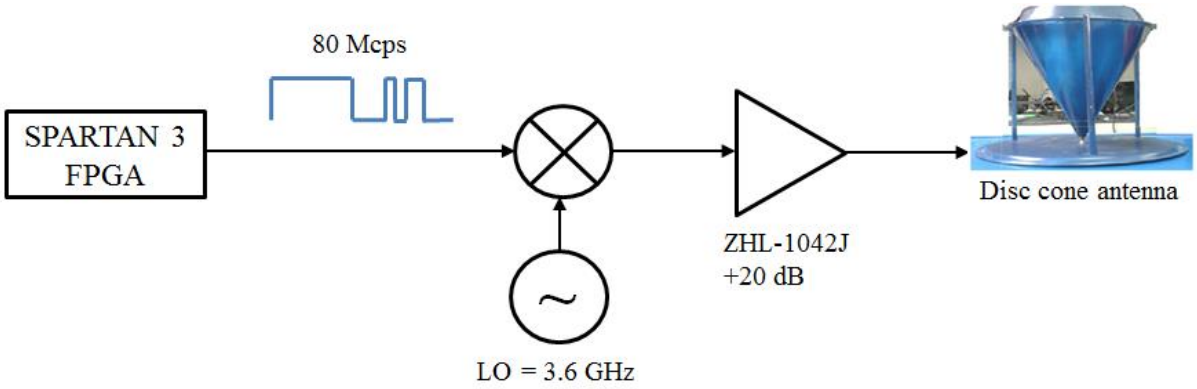

Figure 3.5: Transmitter block diagram

An example setup of the full VIPER transmitter/receiver configuration is shown in Figure 3.6.

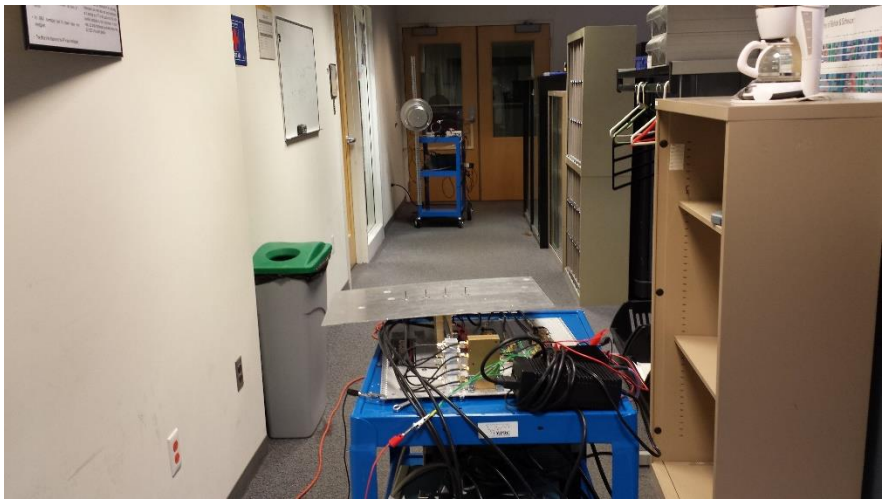

Figure 3.6: VIPER measurement system example setup: transmitter and receiver

3.2 Measurement Scenarios and Floor Plans

We consider three common indoor deployment environments: a traditional office building, an office building with a large atrium area, and a classroom/computer laboratory building. Additionally, we consider a traditional hospital patient monitoring room and surrounding hallway due to the candidacy of hospitals as a priority access environment for the 3.5 GHz band. Finally, we consider indoor-to-outdoor measurements to study how the signal penetrates common exterior building materials, to aid in co-existence studies and determine the feasibility of the FCC-proposed Contained Access Facilities.

For the measurement campaign, we focused on practical indoor use cases: specifically, we investigated primarily NLOS scenarios and transmitter/receiver separations of less than 100 meters. We adopted a 'Wi-Fi approach' to transmitter/receiver positioning by placing the transmitter in locations typical of WLAN access points and placed receivers in locations where a user would expect to maintain a reliable connection to the hypothetical access point, while obstructed by partitions. To supplement the practical access cases, a few baseline cases and extreme cases were also tested. A baseline case refers to a location without obstructions and an extreme case refers to a location where a user would have difficulty connecting to the access point.

For obstructed receiver locations, we ensured a reasonable, controllable amount of partitions separating the transmitter and receiver to easily quantify the contribution of each individual partition towards the overall signal attenuation.

Measurements were performed in and around office and academic buildings at Virginia Tech. Hospital measurements were performed at a nearby medical facility with simulated patient rooms used for student medical training and education.

3.2.1 Scenario 1: Office Environment

Scenario 1 measurements are representative of propagation performance in a traditional office building. Office rooms with cubicles and clutter such as computers, desks, and office chairs, as well as an adjoining hallway were considered. For the hallway environment, floor separation of 4.2 meters per floor was considered. Figures 3.7 and 3.8 show the floor layout and pictures of the office environment.

For the office room, NLOS locations were behind either a sheet of drywall in a conference room or outside in the hallway through a wire mesh glass door. For the hallway measurements, clear LOS locations (Rx 2.1 and 2.2) were recorded for baseline cases. Many obstructed cases near the transmitter were considered for practical cases, including cross-floor propagation. Extreme test cases were also considered (Rx 2.7 and Rx 2.9) to study the propagation behavior of a high number of non-uniform partitions.

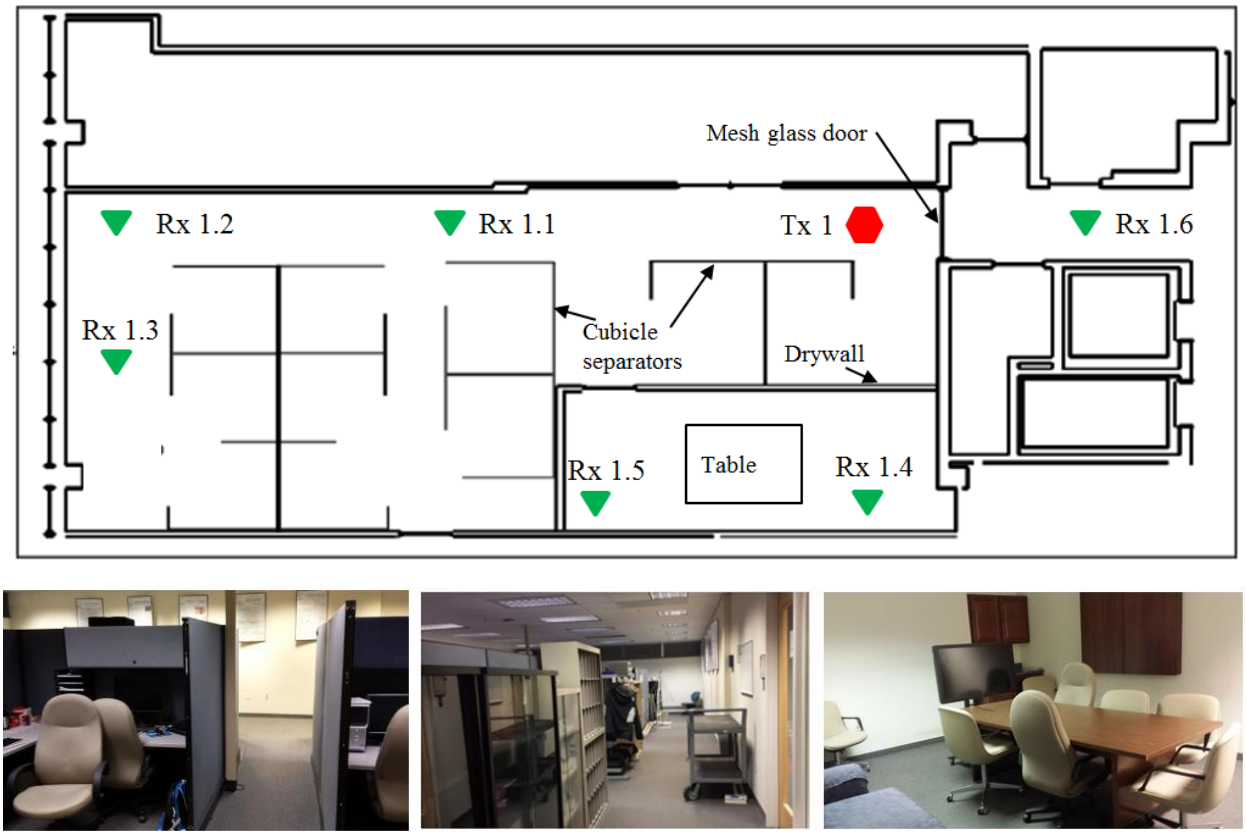

Figure 3.7: Layout and pictures for office scenario: cubicle office space

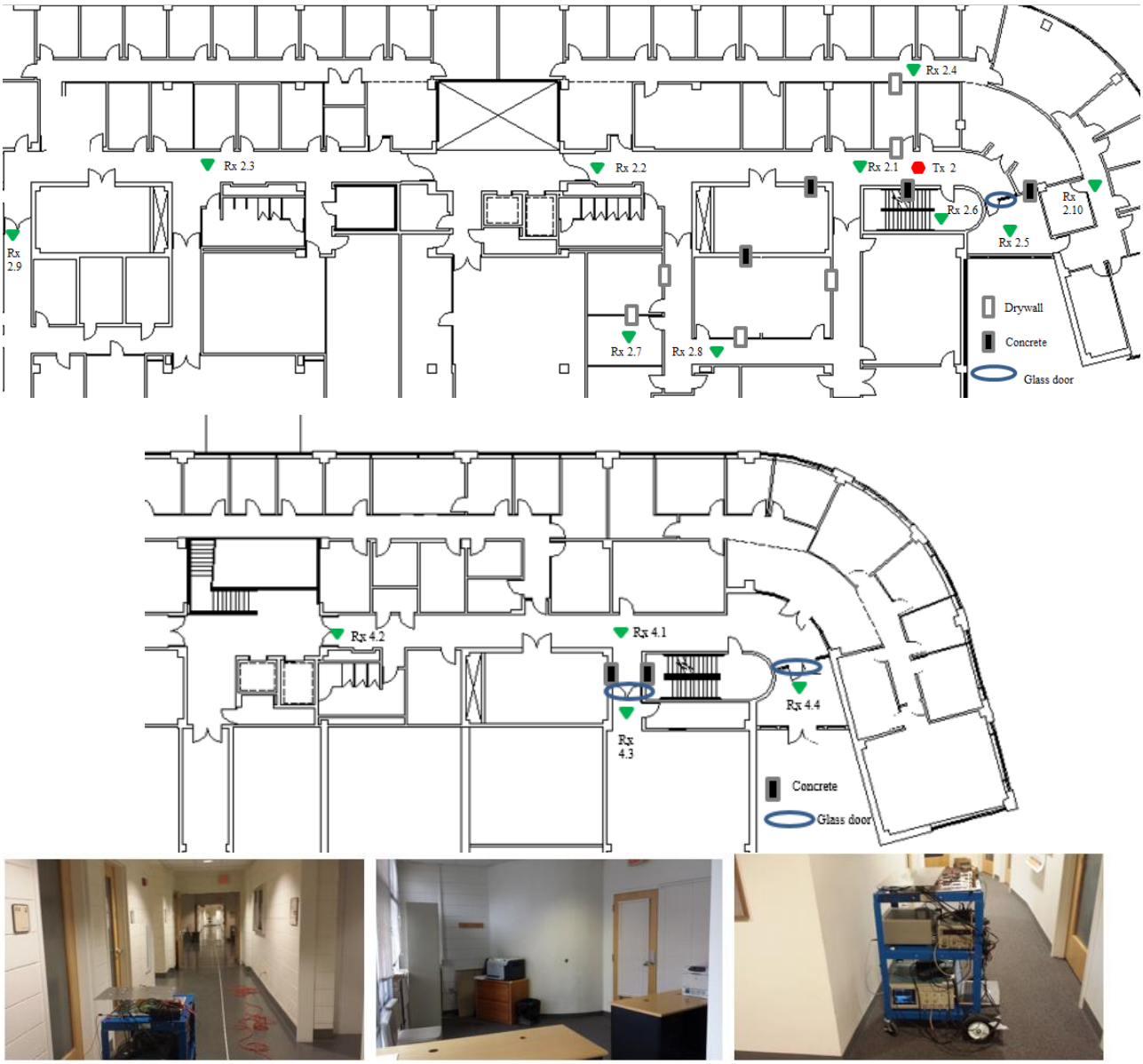

Figure 3.8: Layout and pictures for office scenario: hallway

Top: Same floor Bottom: One floor below

3.2.2 Scenario 2: Classroom and Computer Laboratory Environment

Scenario 2 measurements represent propagation performance in a computer laboratory or classroom building. Figure 3.9 displays the floor layout and pictures. Classrooms feature traditional student desks and chairs, and computer laboratories are outfitted with workbenches, computer workstations, and cabinets full of electronic kits and equipment. As shown in Figure 3.9, the building of interest features a long, snaking corridor – the unique hallway structure allows for a variable number of partitions separating the transmitter and receiver. For example, Rx 1.2 is typical of fairly standard and practical NLOS propagation, but locations such as Rx 2.2 and Rx 4.1 feature four to five walls of partitioning.

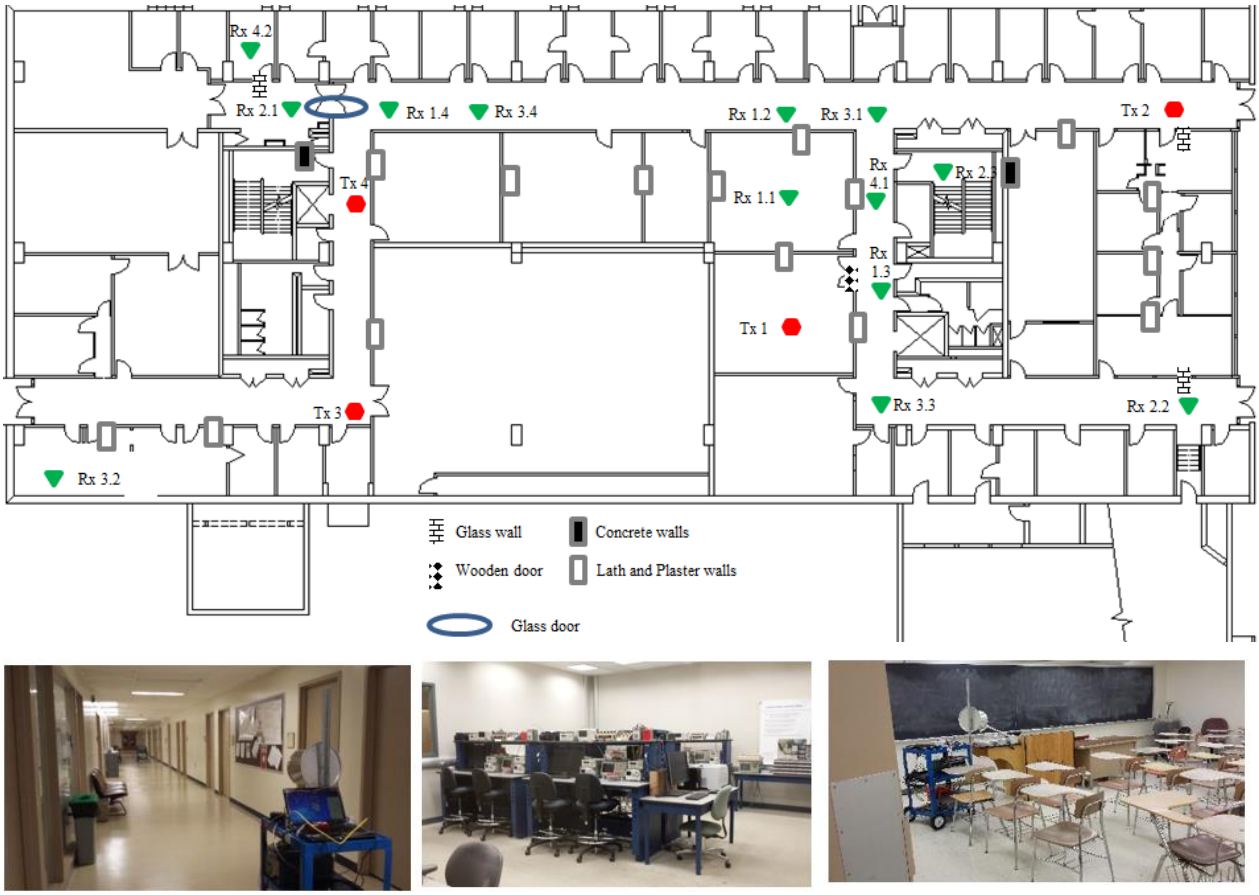

Figure 3.9: Layout and pictures for classroom/ computer laboratory scenario

3.2.3 Scenario 3: Atrium Environment

Scenario 3 measurements represent propagation performance in a building with an atrium or lobby area. Figure 3.10 shows the floor layout and pictures. The flanking classrooms and offices allow for cross-atrium, room-to-room measurements. The atrium is filled with chairs and desks and the classrooms are outfitted with office chairs, desks, and computers.

As shown in Figure 3.10, most of the measurement locations focus on the atrium, itself, (Tx 1 and Tx 2) in the transmitter/receiver path, to capture the effect of such a wide, open area within a building. The Tx 3 locations capture propagation through the atrium from office to office.

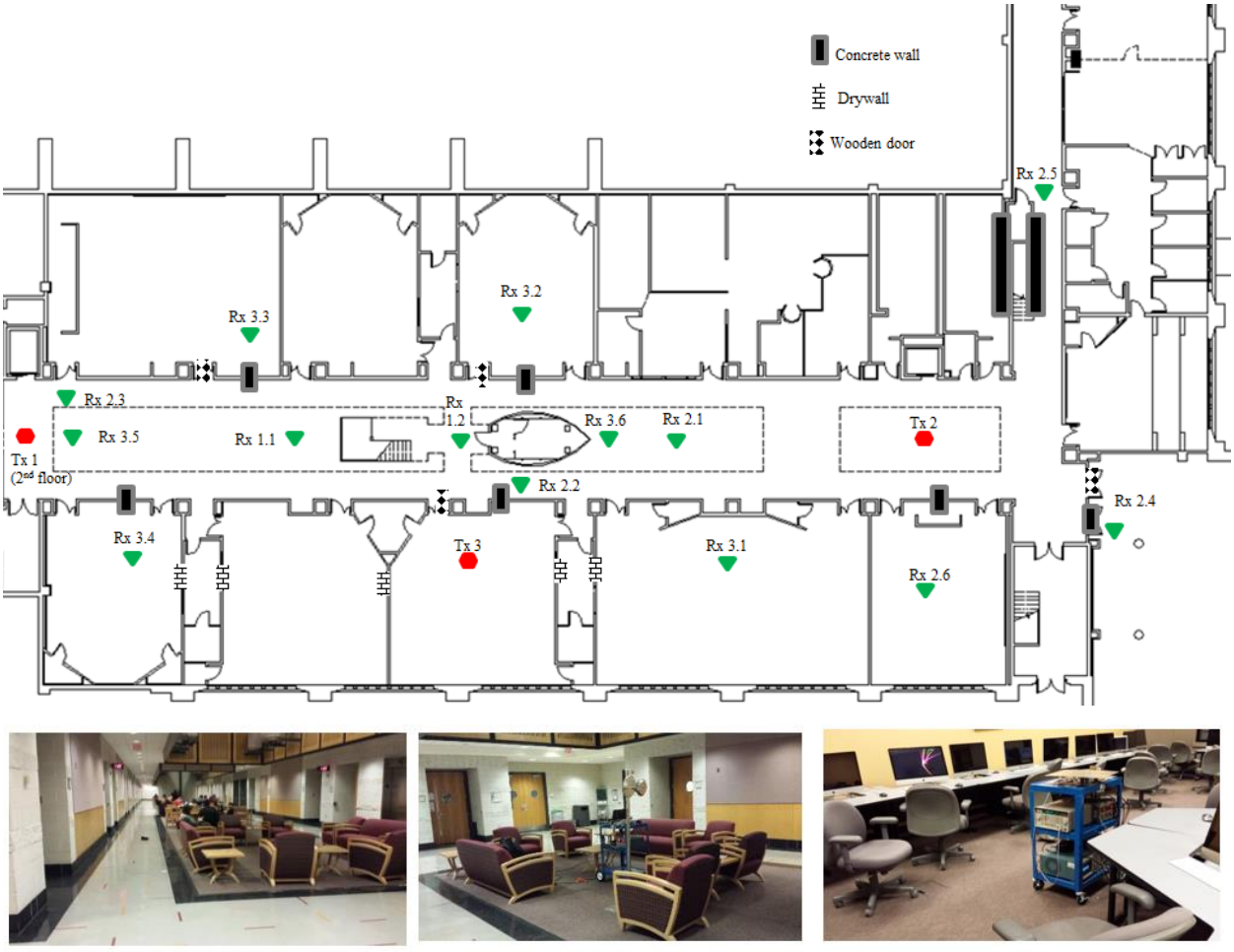

Figure 3.10: Layout and pictures for atrium scenario

3.2.4 Scenario 4: Hospital Environment

As part of the FCC's proposed three-tier spectrum sharing scheme, wireless systems in hospitals are being considered as a priority access use case. As such, it is critical to characterize propagation in a hospital environment as medical equipment may generate or be affected by electromagnetic interference (EMI), including electrocardiograms or telemetry systems [40]. The addition of expected spectral harmony with primary band users, existing WLAN technologies and EMI generated from medical equipment and processes leads to more complications. The added sensitivity of medical devices to EMI ensures that well-documented propagation behavior plays an essential role in wireless system deployment within hospitals [41].

We obtained propagation properties specific to a hospital environment due to its unique building construction and clutter distribution. Typically, hospital walls are constructed as dry partitions, where a steel frame is used to support a variety of materials. In most rooms, such as waiting rooms, offices, or patient sick rooms, the walls are made of drywall or player; however, operating rooms, Magnetic Resonance Therapy (MRT), or X-ray tomography feature metallic shielding. Specifically, MRT rooms feature full copper shielding, with an average of attenuation of 70 dB up to 90 dB [42]. The inhomogeneity of hospital walls and rooms leads to a large variance in propagation characteristics. Furthermore, certain areas such as laboratories, intensive care units, and patient diagnostic facilities feature an inordinately large amount of metallic medical equipment.

We observed the effect of propagation through two simulated hospital patient monitoring rooms, as well as surrounding hallways and offices. The hallways are narrow and the rooms in the area were tightly packed compared to an ordinary office building. The patient rooms are equipped with traditional medical fixtures such as sinks, storage cabinets, oxygen pumps, patient beds, and monitoring equipment. The environment also consisted of a control room with monitoring equipment and one-way reflective glass to observe both patient rooms. To account for the fact that hospital rooms and hallways may often be crowded with medical staff, several measurements were conducted with medical students running simulated diagnostic tests in the patient rooms to observe the effect of a large cluster of mobile bodies on propagation behavior. Figure 3.11 shows the floor layout and pictures.

Tx 1 and Tx 4 represent scenarios where the signal originates from the patient room, while Tx 2, Tx 3, and Tx 5 represent signals originating from adjacent office rooms or hallways. In the case of Tx 5, there were around 6-7 students performing diagnostic tests in Patient Room A.

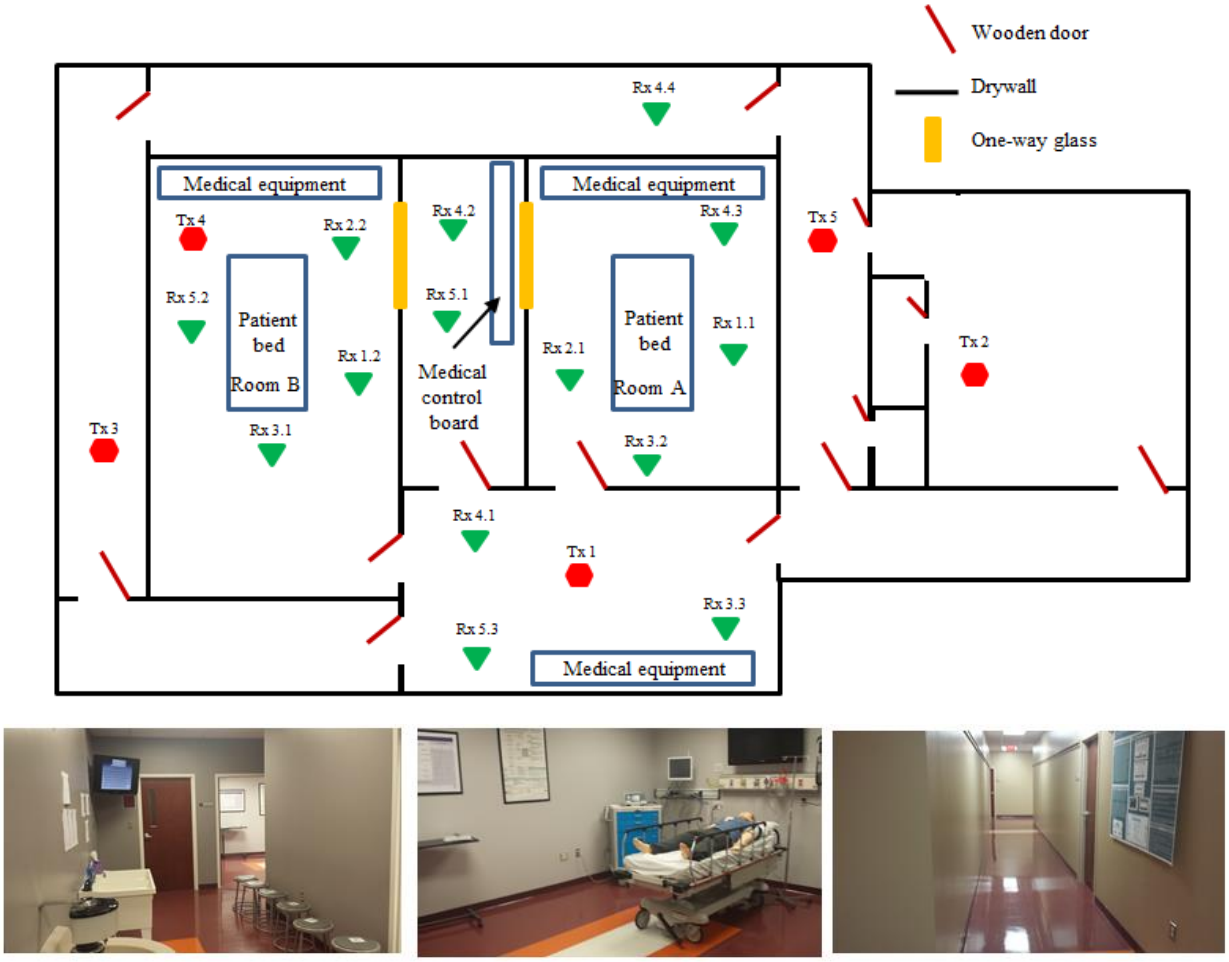

Figure 3.11: Layout and pictures for hospital scenario

3.2.5 Scenario 5: Indoor-to-Outdoor Measurements

We considered several indoor-to-outdoor locations to determine the extent to which a signal penetrates common external building materials. This study is highly important in determining the feasibility of Contained Access Facilities (CAFs) proposed by the FCC, as abundant external leakage would render the deployment of CAFs impractical.

In this scenario, we specifically we examined the effect through reinforced glass doors, wooden doors, glass paneling, limestone, concrete walls, and brick walls. Glass is standard exterior paneling material for corporate offices and other large office buildings. Concrete is standard structural material. Brick, while obsolete in terms of structure, has proven popular as an aesthetic façade. Figure 3.12 shows the setup for six measurement locations. Three measurements were captured at each location: near (5-8 meters), mid (10-18 meters), and far (20-35 meters). Receiver locations were directly in front the transmitter, resulting in completely unobstructed (i.e. LOS) propagation for the outdoor component.

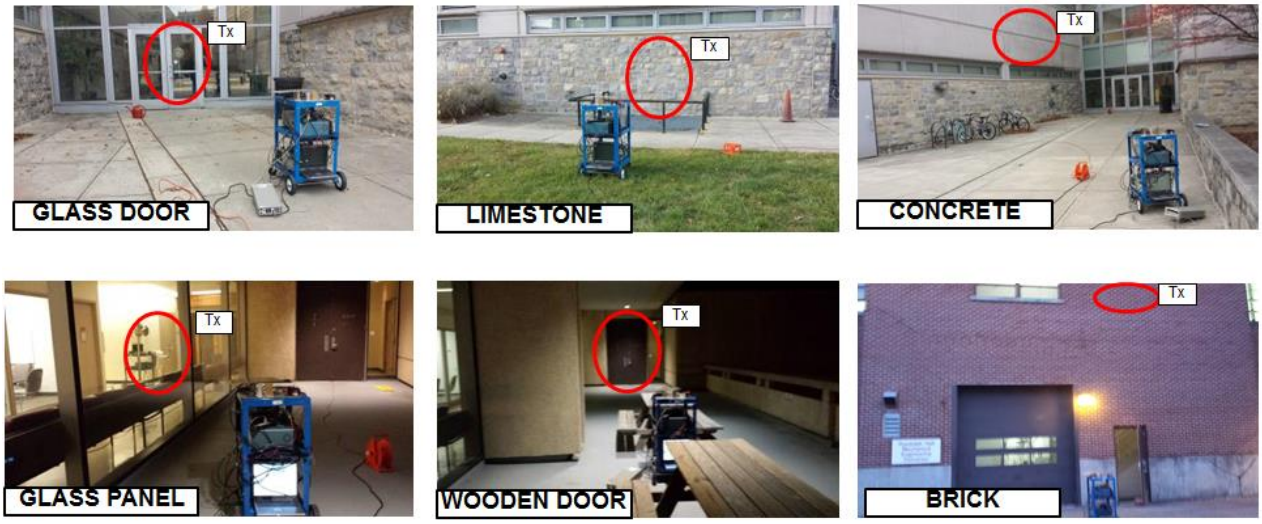

Figure 3.12: Pictures for indoor-to-outdoor measurement scenarios

3.3 Measurement Procedure

The transmitter and receiver were fixed to the locations shown in Section 3.2 for the duration of the measurements. The transmitter was set to continuously output the PN sequence and the signal at the receiver was captured every three seconds, resulting in one measurement snapshot. Every snapshot contains the received power and power delay profile for each of the four antenna elements. Received power measurements were computed as the total power across the entire signal bandwidth. At each location, 100 PDP snapshots were captured.

The distance between the transmitter and receiver was measured and recorded along with the number and type of partitions separating the transmitter and receiver. The results of this indoor measurement campaign are summarized in Chapter 4.

Chapter 4

Measurement Results and Analysis

4.1 Documentation and Analysis of Propagation Measurements

To determine the large scale path loss, the received power measurements were converted to path loss values by adding the transmit power to the VIPER system gain, and factoring in the gain of the transmit and receive antennas. Path loss measurements were aggregated for each scenario and the overall path loss exponent was statistically computed following the procedure outlined in section 2.2.3. Similarly, the shadowing standard deviation was statistically computed from the RMSE procedure outlined in section 2.2.4. The resulting log-linear regression line serves as the fitted log-distance path loss model for the set of measurement points in a particular scenario.

For each power delay profile, the RMS delay spread σ_τ and max excess delay τ_{MAX} (both referred to 20 dB) were derived, as outlined in section 2.2.2.

Tables 4.1 – 4.6 summarize the propagation results for the scenarios outlined in section 3.2. The tabulated values of path loss, RMS delay spread, and mean excess delay were obtained by averaging over all 100 recorded measurement snapshots for a given measurement location.

Figures 4.1, 4.3, 4.5, 4.7, and 4.9 display a scatter plot of the path loss measurements, complete with the corresponding log-linear regression line and statistically-derived path loss exponent and shadowing standard deviation. For comparison, the free space path loss is plotted against the resulting log-distance path loss model.

Figures 4.2, 4.4, 4.6, 4.8, and 4.10 display the measured RMS delay spread and max excess delay for each scenario. Photos of the measurements sites, as well as the average power delay profiles for each receiver location are documented in Appendix A and Appendix B.

4.1.1 Scenario 1: Office Environment Results

Table 4.1: Summary of propagation measurements for Scenario 1 (Office)

Receiver Location	Partitions	#	Distance (m)	Path loss (dB)	n	σ_τ (ns)	τ_{MAX} (ns)
1.1	-	-	5.76	57.16	2.17	17.66	95.55
1.2	-	-	13.0	63.23			
1.3	Cubicle separators	-	13.6	67.73			
1.4	Drywall	1	6.01	62.04			
1.5	Drywall	1	7.21	64.50			
1.6	Glass door (mesh)	1	4.21	58.56			
2.1	-	-	10.0	64.37	3.17	31.52	201.65
2.2	-	-	25.0	73.33			
2.3	-	-	50.0	81.98			
2.4	Concrete block	1	6.03	70.06			
	Drywall	1					
2.5	Concrete block	1	5.11	71.19			
2.6	Solid concrete	1	3.73	73.21			
2.7	Concrete block	2	17.49	94.31			
	Drywall	2					
2.8	Concrete block	1	15.78	82.63			
	Drywall	1					
2.9	Concrete block	2	64.01	99.15			
2.10	Concrete block	1	12.23	79.85			
	Drywall	2					
3.1	Ceiling/Floor	1	5.21	71.52	4.26	13.72	73.30
3.2	Ceiling/Floor	1	18.20	86.22			
3.3	Ceiling/Floor	1	7.54	89.38			
	Concrete block	1					
3.4	Ceiling/Floor	1	6.56	82.11			
	Glass door	1					

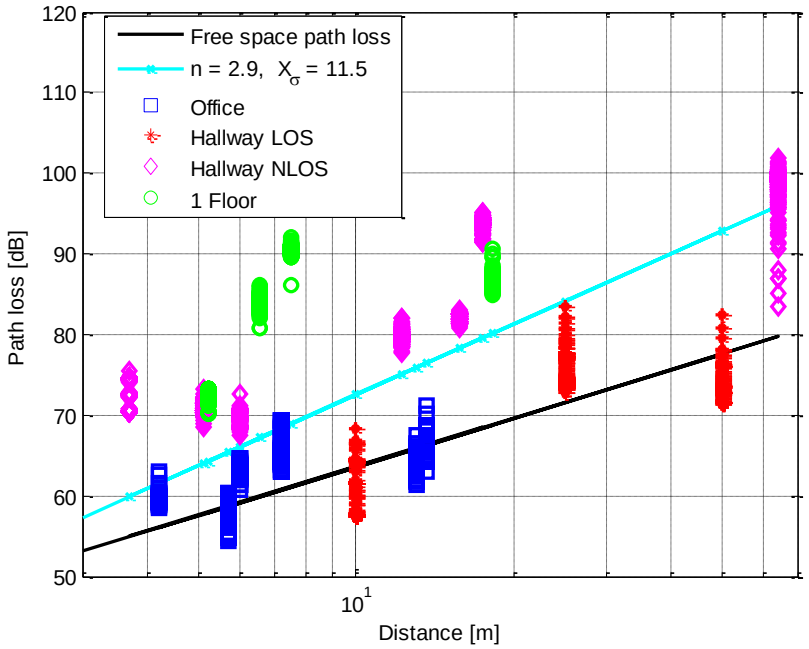

Figure 4.1: Scatter plot of measured path loss data for Scenario 1 (Office)

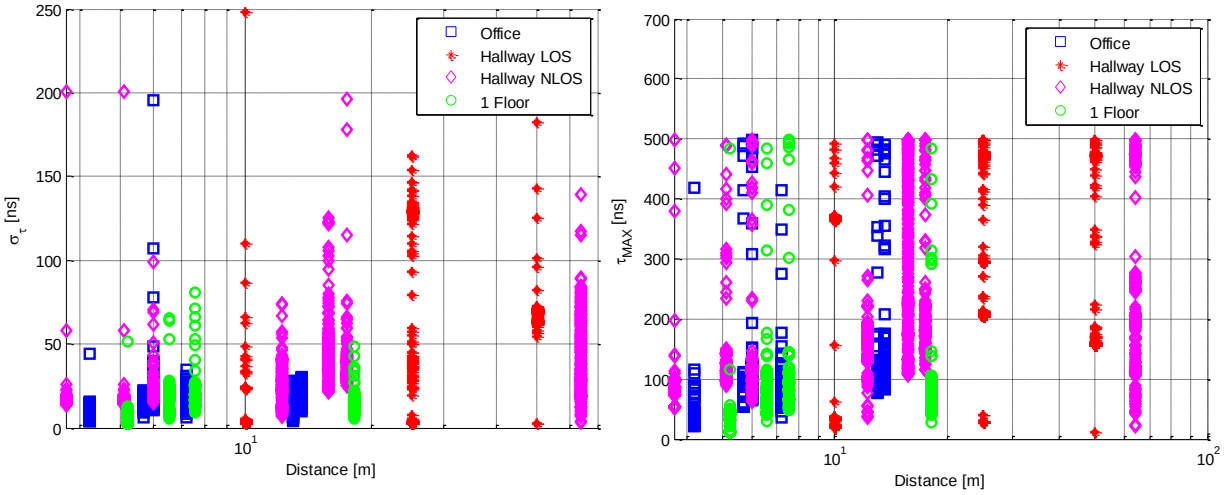

Figure 4.2: Scatter plot of measured delay spread data for Scenario 1 (Office)
Left: RMS delay spread Right: Max excess delay

For an office environment, the path loss is found to be slightly greater than free space, with the drywall separating office and meeting rooms contributing to most of the attenuation. In the LOS hallway environment, the path loss is slightly lower than free space, indicating the waveguide effect. The NLOS hallway path loss is about 10 dB greater due to propagation through various building materials such as multiple sheets of drywall or concrete. Attenuation in

the stairwell (Rx 2.6) is extremely high due to the presence of solid concrete, which is a thicker and more robust structural building material. The standard deviation is high due to the large differences between the four types of propagation environment.

Greater Tx/Rx separation as well as partitions with high attenuation lead to higher delay spreads, which is consistent as both situations introduce additional multipath. Hallway LOS delay distributions are identifiable by their bimodality; that is, there tends to be one very strong reflected component arriving at a fixed delay, rather than several weaker multipath components due to partitions.

Cross-floor propagation results in an additional attenuation loss of 17.5 dB, which is greater than the attenuation for any reasonable number of partitions for single-floor propagation. The delay spread increases accordingly, as well.

4.1.2 Scenario 2: Classroom and Computer Laboratory Environment Results

Table 4.2: Summary of propagation measurements for Scenario 2 (Classroom/Comp Lab)

Receiver Location	Partitions	#	Distance (m)	Path loss (dB)	n	σ_τ (ns)	τ_{MAX} (ns)
1.1	Plaster wall	1	9.71	65.78	2.40	19.77	102.54
1.2	Plaster wall	2	13.56	73.70			
1.3	Wooden door	1	5.12	60.71			
2.1	Glass door	1	53.43	77.15	3.18	38.10	205.38
2.2	Plaster wall	2	19.81	80.11			
	Glass wall	2					
2.3	Plaster wall	2	8.72	88.99			
	Concrete wall	1					
3.1	Plaster wall	2	33.09	97.20	3.00	37.31	209.35
	Concrete block	2					
3.2	Plaster wall	2	18.45	75.84			
3.3	Plaster wall	2	27.42	96.65			
	Concrete block	2					
3.4	Plaster wall	2	17.01	77.92			
	Concrete block	1					
4.1	Plaster wall	5	27.42	98.84	3.89	48.77	263.18
4.2	Concrete wall	1	12.01	85.80			
	Glass door	1					

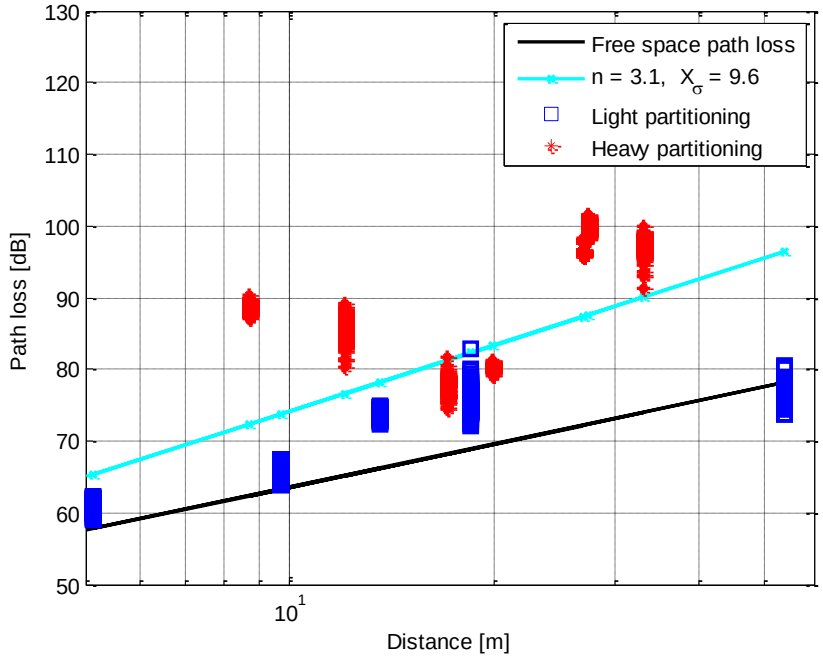

Figure 4.3: Scatter plot of measured path loss data for Scenario 2 (Classroom/Comp Lab)

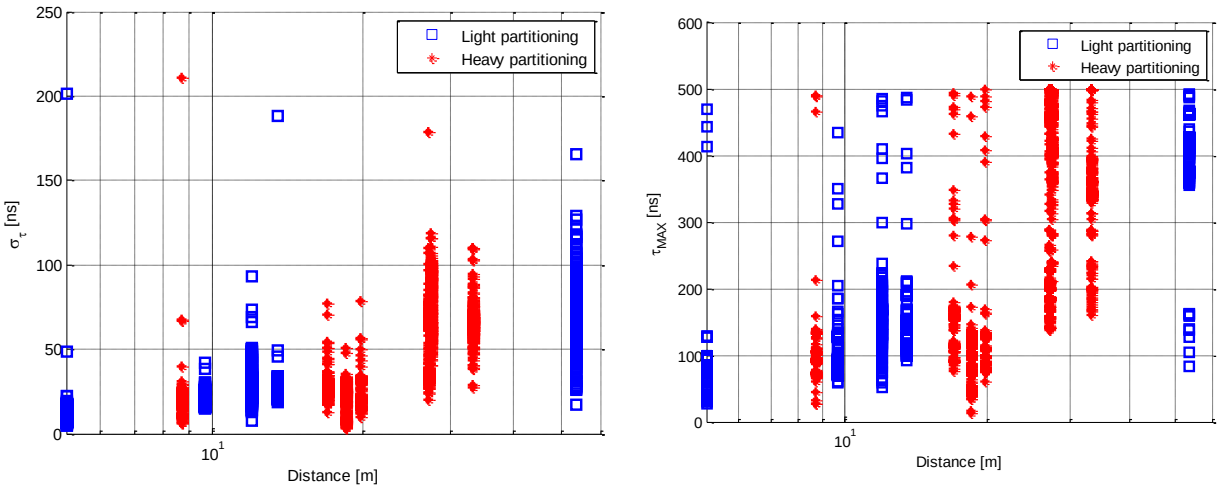

Figure 4.4: Scatter plot of measured delay spread data for Scenario 2 (Classroom/Comp Lab)
Left: RMS delay spread, Right: Max excess delay

As seen in Figures 4.3 and 4.4, there is a clear attenuation gap between light partitioning, which refers to 1-2 walls of transmitter/receiver separation, and heavy partitioning, referring to situations with more than 2 walls. The average attenuation increase is approximately 10 dB;

however, the variance is very large due to the different types of building materials. Plaster walls add attenuation of about 4.3 dB, for example, while concrete adds about 8.0 dB of attenuation.

The delay spread is similarly higher for a greater number of partitions, as expected due to the additional multipath introduced by more obstructions. The standard deviation is large due to the 10-15 dB attenuation gap between light and heavy partitioning situations.

4.1.3 Scenario 3: Atrium Environment Results

Table 4.3: Summary of propagation measurements for Scenario 3 (Atrium)

Receiver Location	Partitions	#	Distance (m)	Path loss (dB)	n	σ_τ (ns)	τ_{MAX} (ns)
1.1	-	-	16.66	63.10	2.12	33.15	170.93
1.2	Concrete staircase	1	26.25	76.16			
2.1	-	-	61.87	80.38	2.40	36.45	226.86
2.2	-	-	38.71	74.64			
2.3	-	-	15.24	69.42			
2.4	Concrete block	1	12.19	72.85			
2.5	Concrete staircase	-	18.70	81.08			
2.6	Concrete block	1	9.91	73.91			
3.1	Drywall	2	17.07	69.92	2.60	50.29	246.65
3.2	Drywall	1	14.63	74.61			
	Wooden door	1					
3.3	Drywall	1	27.50	85.44			
	Concrete block	2					
3.4	Drywall	3	24.30	77.03			
3.5	Concrete block	1	29.57	85.12			
3.6	Concrete block	1	9.14	71.64			

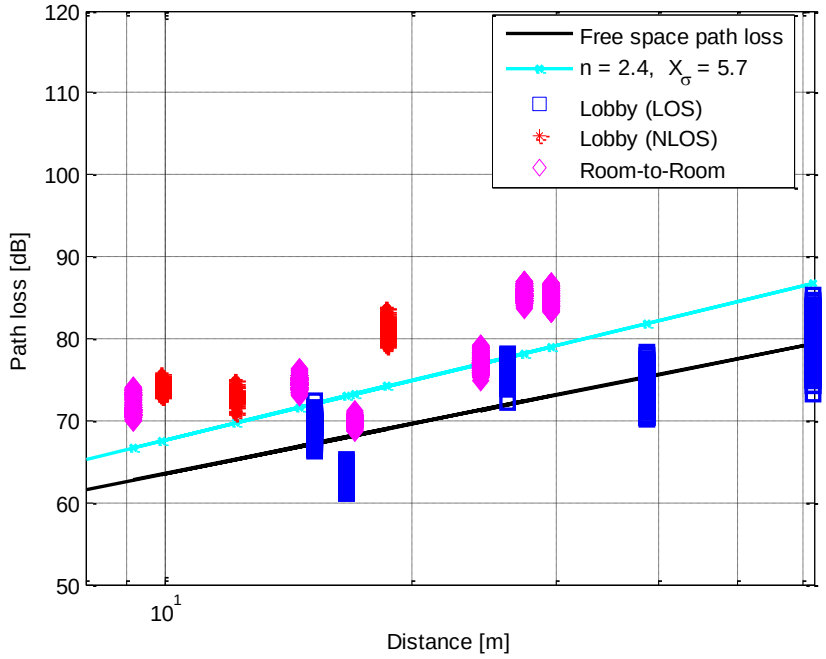

Figure 4.5: Scatter plot of measured path loss data for Scenario 3 (Atrium)

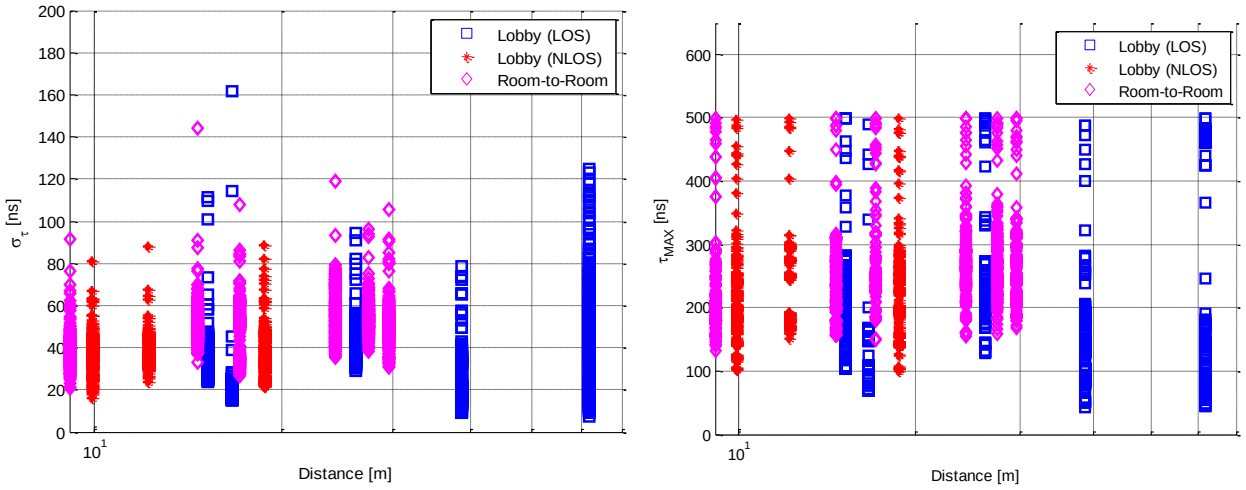

Figure 4.6: Scatter plot of measured delay spread data for Scenario 3 (Atrium)
Left: RMS delay spread, Right: Max excess delay

The path loss tends to be lower than the previous two scenarios due to wide, open lobby, containing far fewer obstructions. Room-to-room and lobby NLOS measurements are appropriately slightly higher in terms of loss; however the lack of a large amount of robust partitions leads to a relatively lower aggregate path loss exponent.

The delay spread is consistent with previous scenarios, including the noticeable bimodality in the lobby LOS cases as well as the general increase in delay for room-to-room propagation due to rooms having a greater concentration of clutter. Similar to the path loss results; however, the delay spread is much more uniform than the previous two scenarios, due to the consistency of the atrium environment.

4.1.4 Scenario 4: Hospital Environment Results

Table 4.4: Summary of propagation measurements for Scenario 4 (Hospital)

Receiver Location	Partitions	#	Distance (m)	Path loss (dB)	n	σ_τ (ns)	τ_{MAX} (ns)
1.1	Drywall	1	5.02	62.51	2.55	22.62	113.58
1.2	Drywall	1	9.45	68.02			
	Wooden door	1					
2.1	Drywall	3	7.62	73.24	3.53	30.55	153.17
2.2	Drywall	5	11.48	83.31			
3.1	Drywall	1	3.96	60.36	2.98	26.17	129.53
3.2	Drywall	3	11.01	77.01			
3.3	Drywall	1	13.22	77.11			
	Wooden door	1					
4.1	Drywall	2	4.57	62.59	2.87	26.32	125.25
4.2	One-way glass	1	5.18	64.13			
4.3	One-way glass	2	7.11	71.13			
4.4	Drywall	1	10.72	70.16			
5.1	Drywall	1	7.80	68.90	2.83	27.32	156.13
	One-way glass	1					
5.2	Drywall	1	12.05	74.66			
	One-way glass	2					
5.3	Drywall	2	8.10	69.34			

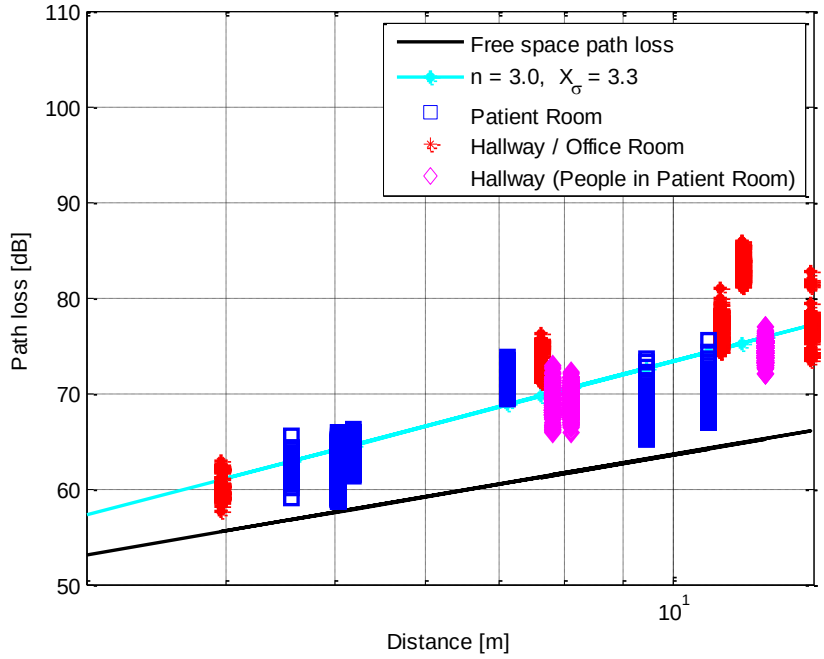

Figure 4.7: Scatter plot of measured path loss data for Scenario 4 (Hospital)

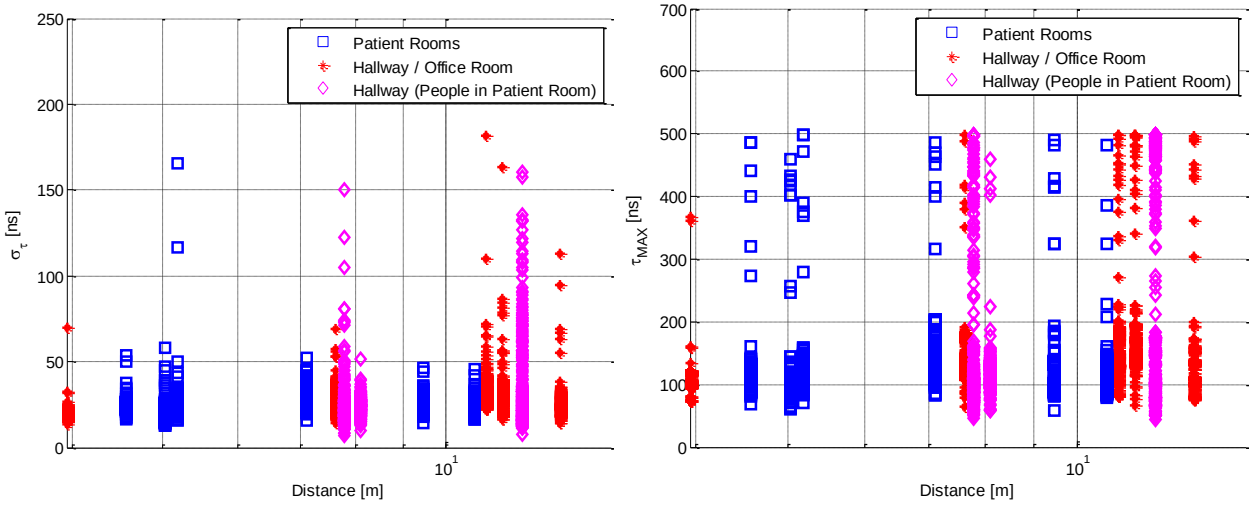

Figure 4.8: Scatter plot of measured delay spread data for Scenario 4 (Hospital)
Left: RMS delay spread, Right: Max excess delay

As seen in Figure 4.7, despite the relatively small number of light partitions, the path loss tends to be slightly higher than a traditional office building due to the enclosed, labyrinthine

nature of the environment. The presence of medical equipment and storage cabinets adds a significant amount of clutter to an environment that would typically consist of desks and chairs. The standard deviation is much lower due to the number and type of partitions (1-3 sheets of drywall) remaining generally consistent throughout the measurements. The one-way reflective glass has approximately the same attenuation as the surrounding drywall.

As seen in Figure 4.8, the delay spread and max excess delay tend to be higher in the presence of medical staff as the multipath increases. The max excess delay, in particular, exhibits noticeable bimodality, which can be attributed to the variability of people moving and shifting around in Patient Room A.

4.1.5 Scenario 5: Indoor-to-Outdoor Propagation Results

Table 4.5: Summary of propagation measurements for Scenario 5 (Indoor-to-Outdoor)

Receiver Location	Partitions	#	Distance (m)	Path loss (dB)	n	σ_τ (ns)	τ_{MAX} (ns)
1.1	Glass door	1	7.01	76.22	3.51	21.71	141.35
1.2			18.29	88.99			
1.3			35.36	92.59			
2.1	Concrete block Limestone wall	1	7.62	80.10	3.82	17.26	102.35
2.2			17.06	88.03			
2.3			23.46	95.47			
3.1	Glass panel	1	6.80	61.32	2.32	22.78	127.85
3.2			14.31	70.81			
3.3			18.23	75.61			
4.1	Wooden door	1	9.14	62.17	2.12	17.04	90.91
4.2			13.71	67.83			
4.3			22.86	73.90			
5.1	Drywall Concrete wall	1	8.17	74.82	3.31	16.68	116.58
5.2			18.77	86.34			
5.3			35.61	93.26			
6.1	Brick wall	1	7.25	71.41	3.03	14.58	86.48
6.2			13.08	75.21			
6.3			21.94	82.27			

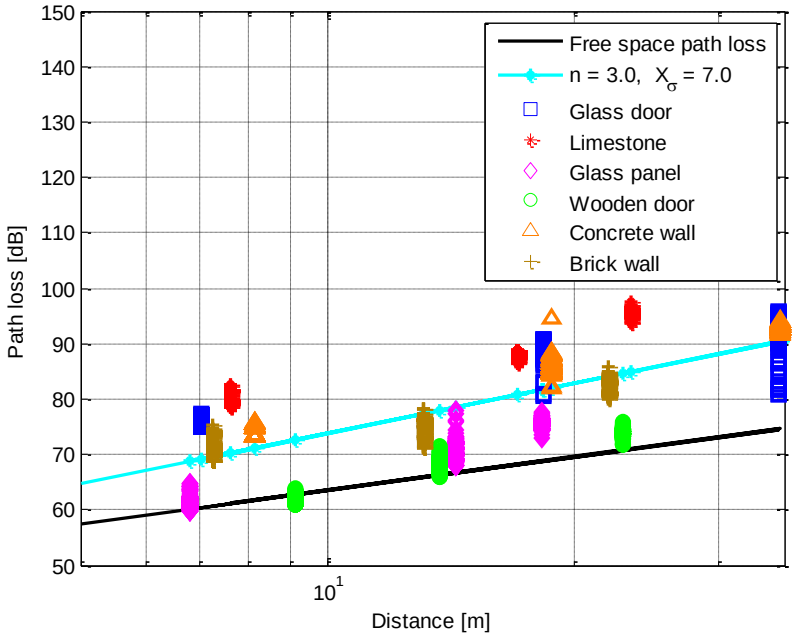

Figure 4.9: Scatter plot of measured path loss data for Scenario 5 (Indoor-to-Outdoor)

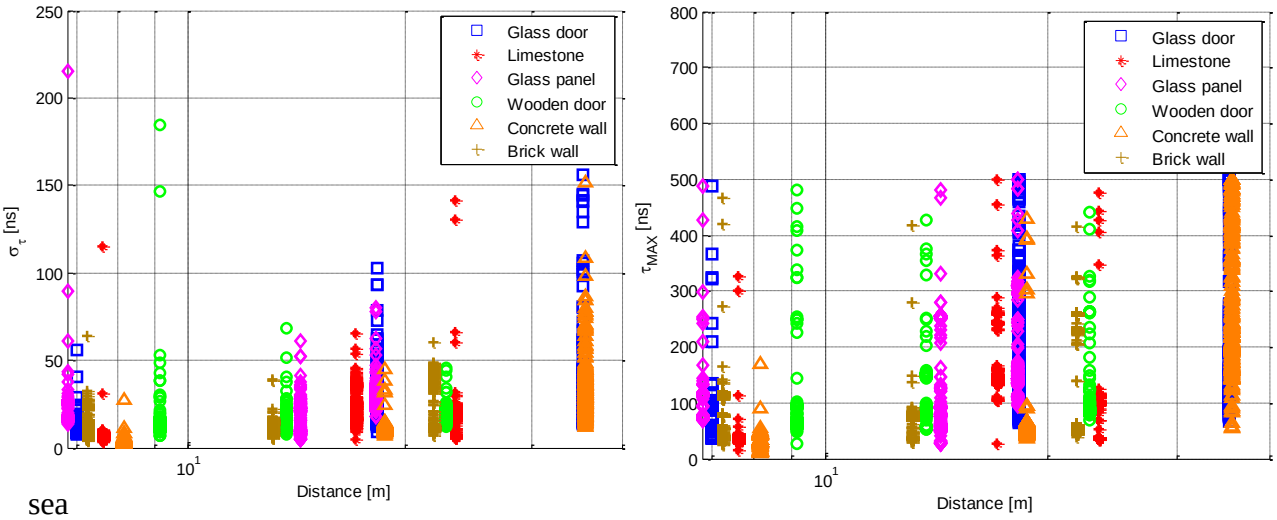

sea

Figure 4.10: Scatter plot of measured delay spread data for Scenario 5 (Indoor-to-Outdoor) Left: RMS delay spread, Right: Max excess delay

Indoor-to-outdoor measurements resulted in a slightly higher path loss than indoor environments, which is consistent with the fact that exterior building materials tend to be thicker and more robust, structurally, and have greater attenuation properties. Limestone, concrete and

brick feature the heaviest attenuation, as expected; however, reinforced glass used for glass doors does a similarly adequate job at containing indoor signals. Wood and glass panels do a poor job of containing signals, as their losses are nearly comparable to free space. These materials contributed to the noticeable attenuation gap of about 10 dB in the indoor-to-outdoor measurements.

Delay spread is generally lower due to the decrease in clustered objects which generate multipath. However, objects such as surrounding building architecture, other buildings, or nearby structures and/or vehicles contribute to a high max excess delay. Additionally, the homogenous nature of the outdoor environment compared to the indoor environment results in delay characteristics that are more uniform, even with the wide range of exterior building materials.

4.2 Attenuation Properties of Building Materials at 3.5 GHz

The authors of [34] proposed a minimum mean squared error method over all NLOS measurements to determine the attenuation properties of common indoor building materials. The empirically-determined attenuation values may be used in a partition-based path loss model where $L_{P,PB}$ is formulated as

$$L_{P,PB} = L_0 + 20log_{10}(d) + \sum_{i=1}^{N} n_i X_i \qquad (14)$$

where X_i is the attenuation value (dB) of the ith partition and n_i is the number of the ith partition dividing the transmitter and receiver.

Table 4.6 lists the measured attenuation of common indoor and indoor-to-outdoor building material installations as well as attenuation values. The materials listed are defined as full on-site installations, rather than individual material components: for example, *drywall* refers to a complete wall installation consisting of two individual sheets of drywall with composite materials in between.

For comparison purposes at Virginia Tech, attenuation values at 2.5 GHz band may be found in [43]. For further comparison purposes, Table 4.7 lists attenuation values for indoor building materials in office and hospital environments obtained at 2.4 GHz, in the literature. These documented values help to bolster the performance of multi-wall or partition-based path loss models, such as [24] [31] [32].

Table 4.6: Computed attenuation values for common indoor building materials at 3.5 GHz

Material	Thickness [cm]	Attenuation [dB]
Indoor		
Drywall	14.0	2.91
Glass door	-	2.86
Mesh glass door	-	2.45
Concrete block	13.0	8.02
Solid concrete	22.0	18.17
Plaster wall	20.0	4.30
Wooden door	3.50	1.35
Glass wall	-	0.99
Vinyl floor/concrete ceiling	120.0	15.65
Indoor-to-Outdoor		
Reinforced glass door	-	17.99
Limestone wall/Concrete block	20.0	21.07
Glass panel	-	4.02
Wooden door	3.50	1.35
Concrete wall/Drywall	20.0	16.32
Brick wall	25.0	10.61

Table 4.7: Reported attenuation values for building materials at 2.4 GHz

Material	Thickness [cm]	Attenuation [dB]	Reference
Concrete wall	25.0	21.6	[44]
Floor/ceiling	-	15.3	[45]
Wooden door	4.0	2.3	[44]
Glass wall	1.2	1.6	[44]
Glass window	-	3.0	[46]
Plasterboard	-	4.9	[47]
Chipwood	0.8	1.1	[44]
Thickwood	3.8	1.6	[44]
MRT wall (copper shielding)	0.016 (copper)	91.5	[48]
X-ray wall (lead facing)	0.05 – 0.25 (lead)	51.3	[48]
Operating room wall (CrNi steel facing)	0.08 (CrNi steel)	37.8	[48]
Concrete wall	10.0	7.0	[48]
Cinder block	-	4.0	[49]
Metal door	-	6.0	[49]

4.3 Impact of SIMO Diversity

In Single Input Multiple Output (SIMO) multi-antenna schemes, a receive spatial diversity gain may be achieved by intelligently combining the received signal power at each antenna element. Specifically, by applying a weighting technique known as Maximal Ratio Combining (MRC), we achieve optimal Signal-to-Noise Ratio (SNR) at the receiver [50]. Figure 4.11 illustrates the MRC process at the receiver.

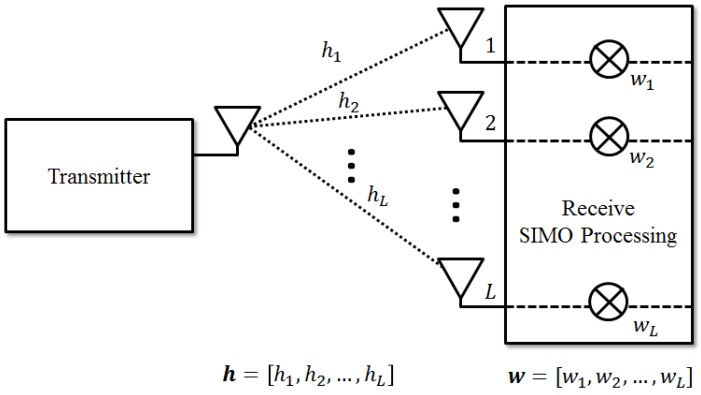

Figure 4.11: SIMO receive diversity processing

For a single antenna element in an array, the instantaneous received power at the ith element is computed as

$$P_i = |h_i|^2. \tag{15}$$

By applying MRC, the instantaneous received signal power is computed by weighting the received channel magnitude:

$$P_{MRC} = \boldsymbol{w^T h}. \tag{16}$$

To maximize SNR, the weights are chosen to be proportional to each channel's quality

$$\boldsymbol{w} = \boldsymbol{h}^{\dagger} \tag{17}$$

where † is the conjugate-transpose matrix operation.

The average received signal power over all antenna elements and all signal measurements is given by

$$\bar{P} = \frac{1}{LN_m}\sum_{i=1}^{L}\sum_{n=1}^{N_m}\left|h_i^{(n)}\right|^2 \qquad (18)$$

where N_m is the total number of measurements.

The Cumulative Distribution Function (CDF) of the normalized ratio of $P_1/\bar{P}$ and $P_{MRC}/\bar{P}$ is plotted for each of the five scenarios from section 4.1. P_{MRC} is normalized by -3 dB in the case of 1 x 2, and -6 dB in the case of 1 x 4 to compare the absolute gain of MRC over a single received antenna element. The measured envelope correlation coefficient between antenna elements for each scenario is listed in Table 4.8, along with the diversity gain at 1% and 10% outage probability levels.

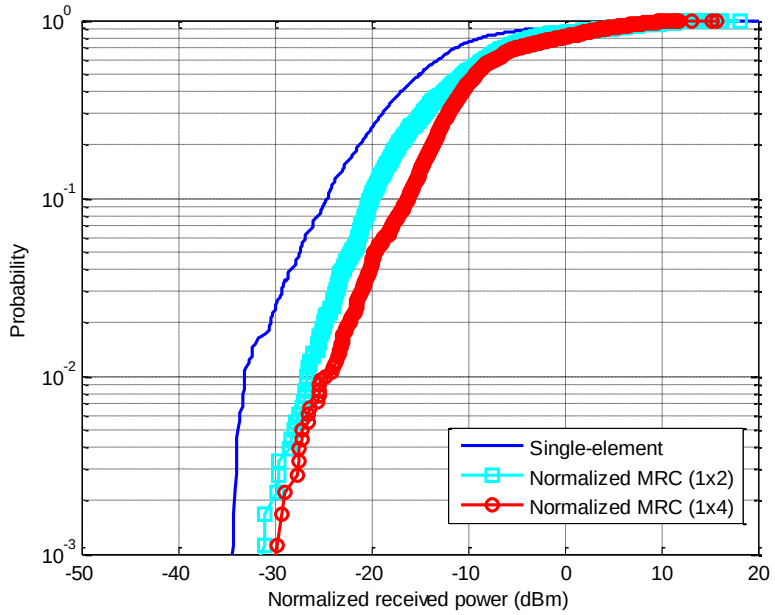

Figure 4.12: SIMO diversity: normalized received power CDF for Scenario 1 (Office)

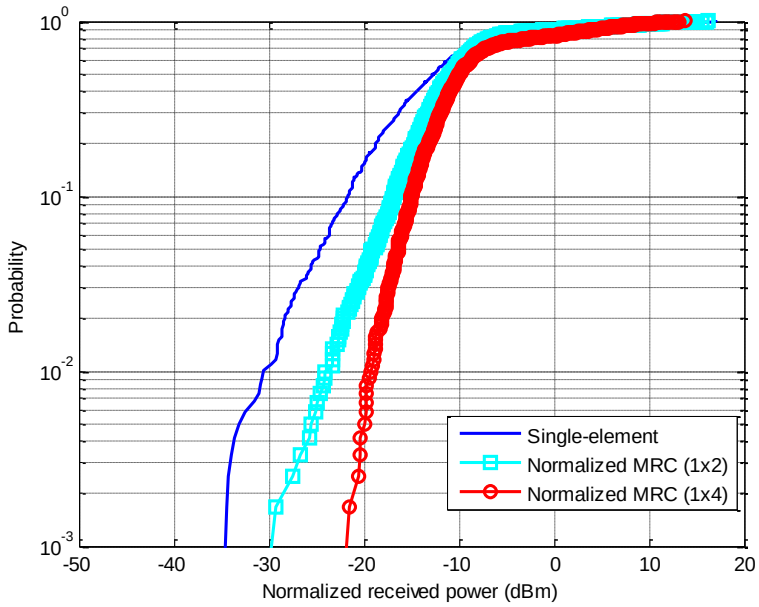

Figure 4.13: SIMO diversity: normalized received power CDF for Scenario 2 (Classroom/Comp Lab)

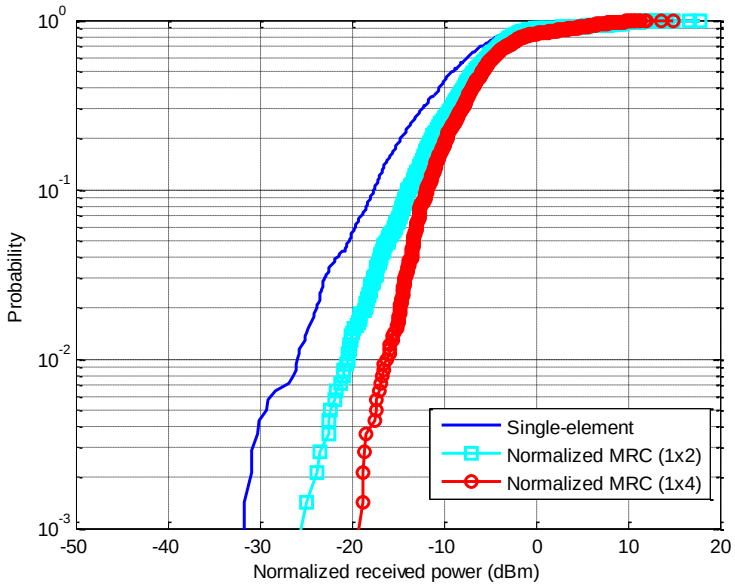

Figure 4.14: SIMO diversity: normalized received power CDF for Scenario 3 (Atrium)

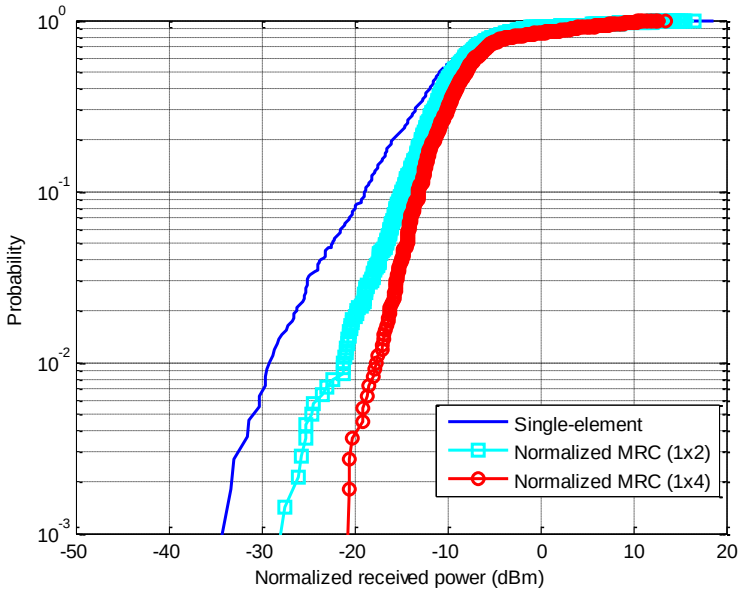

Figure 4.15: SIMO diversity: normalized received power CDF for Scenario 4 (Hospital)

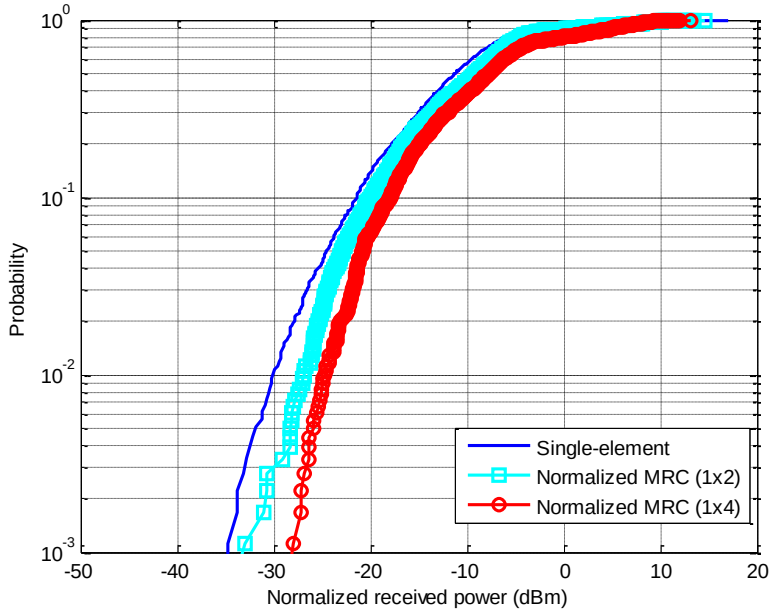

Figure 4.16: SIMO diversity: normalized received power CDF for Scenario 5 (Indoor-to-Outdoor)

Table 4.8: Envelope correlation coefficient and receive diversity gain for each scenario

Environment	Envelope Correlation Coefficient						1x2 MRC [dB]		1x4 MRC [dB]	
	ρ_{12}	ρ_{13}	ρ_{14}	ρ_{23}	ρ_{24}	ρ_{34}	10%	1%	10%	1%
Office	0.098	0.265	0.284	0.109	0.314	0.120	4.1	6.9	8.6	9.3
Classroom/Comp Lab	0.099	0.291	0.263	0.113	0.349	0.115	4.8	6.4	6.1	11.2
Atrium	0.084	0.196	0.298	0.156	0.311	0.106	3.6	5.4	7.1	9.4
Hospital	0.064	0.402	0.394	0.178	0.425	0.116	4.0	7.7	5.7	11.3
Indoor-to-Outdoor	0.642	0.623	0.719	0.557	0.703	0.690	1.5	3.2	3.3	5.3

As seen in Figures 4.11 – 4.15 and reported in Table 4.8, the typical indoor receive diversity gain averages **8-10 dB** from single element to 1 x 4 MRC due to the inhomogeneous propagation environment, clutter, and partitioning resulting in increased channel diversity.

Compared to typical LOS outdoor receive diversity gains at 2.05 GHz [38], as well as the recorded **4-5 dB** of gain from indoor-to-outdoor scenarios from this measurement campaign, *there is a significant improvement of up to **6 dB***. The loss in indoor-to-outdoor diversity gain is attributed to the increase in environmental uniformity and unobstructed outdoor component when comparing an indoor and outdoor environment.

Compared to 1 x 2 MRC, 1 x 4 MRC offers approximately **1-2 dB** of additional gain in indoor-to-outdoor scenarios with a strong outdoor LOS component. Thus, the extra complexity due to two additional antennas is generally not worth the additional gain for indoor-to-outdoor propagation; however, indoor receivers will see a performance increase of about **4-5 dB** from 1 x 2 MRC to 1 x 4 MRC.

4.4 Impact of MIMO Diversity

Similar to a multiple receive antenna configuration, a Multiple Input Multiple Output (MIMO) systems operate by intelligently combining both transmit and receive signals to further increase received signal power by exploiting spatial diversity. Figure 4.17 illustrates the general process for MIMO processing, assuming L receive antennas and K transmit antennas.

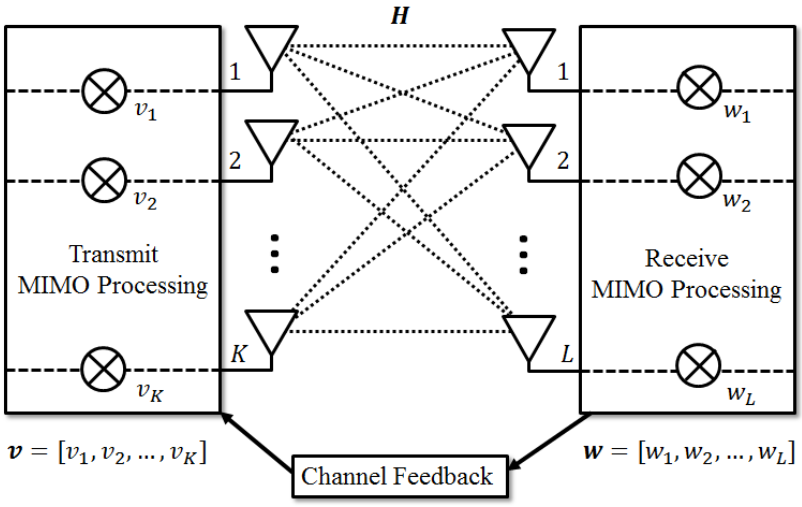

Figure 4.17: MIMO diversity processing

The channel at a given measurement is expressed as a $K \times L$ matrix $\boldsymbol{H}$. The received power, resulting from the complete weighting process, from transmitter to receiver is defined as

$$P = \left|\boldsymbol{v}\boldsymbol{H}^{\dagger}\boldsymbol{w}\right| \tag{19}$$

where $\boldsymbol{w}$ is a $L \times 1$ vector of receive combining weights, and $\boldsymbol{v}$ is a $1 \times K$ vector of transmit combining weights [51]. MIMO processing design involves determining $\boldsymbol{v}$ and $\boldsymbol{w}$ to achieve desired spatial steering effects, ranging from simple transmit diversity which increases received SNR to beamforming techniques which direct signal power in specific directions. The transmitter is provided channel information through a feedback channel.

We consider three popular methods for determining the weight vectors to increase SNR at the receiver: Alamouti Space-Time Coding for 2 x 1 transmit diversity, Transmit Antenna Selection with MRC (TAS/MRC) and Maximal Ratio Transmission with MRC (MRT/MRC).

Alamouti coding is a space-time code used for transmit diversity combining, mostly commonly with a 2 x 1 configuration. The channel matrix is derived as:

$$\boldsymbol{H} = \begin{bmatrix} h_1 & h_2 \\ h_2^* & -h_1^* \end{bmatrix} \tag{20}$$

and the transmitted symbols $[x_1, x_2]$ are weighted by this channel matrix across two time-slots.

TAS/MRC operates by simply selecting the transmit antennas that leads to the best quality channels [52]. Assuming that the system selects only *one* transmit antenna, the optimal antenna k^* is chosen as the maximum channel magnitude over all receive antennas:

$$k^* = \text{argmax}_{k'=1,2,\ldots,K} \sum_{l=1}^{L} \left| h_{k'}^{(l)} \right| \tag{21}$$

The transmit weight vector is chosen as

$$\boldsymbol{v_{TAS}} = [\delta_{1k^*}, \delta_{2k^*}, \ldots, \delta_{Kk^*}] \tag{22}$$

where $\delta_{(.)}$ is the Kronecker delta function. The receive weight vector is chosen as

$$\boldsymbol{w_{TAS}} = (\boldsymbol{H v_{TAS}})^{\dagger} \tag{23}$$

In the case of MRT/MRC, the orthonormal eigenvector $\boldsymbol{u_{MAX}}$ corresponding to the maximum eigenvalue λ_{MAX} of the matrix $\boldsymbol{H}^{\dagger}\boldsymbol{H}$ is computed [52]. The transmit weight vector is then selected as

$$\boldsymbol{v_{MRT}} = \boldsymbol{u_{MAX}} \tag{24}$$

and, as in the case of TAS/MRC, the receive weight vector is selected as

$$\boldsymbol{w_{MRT}} = (\boldsymbol{H v_{MRT}})^{\dagger} \tag{25}$$

For each scenario, simulated measurements were carried out by shifting the transmit antenna over by a half-wavelength, parallel to the receive antenna array, until four sets of measurements were captured. This procedure is summarized in Figure 4.18.

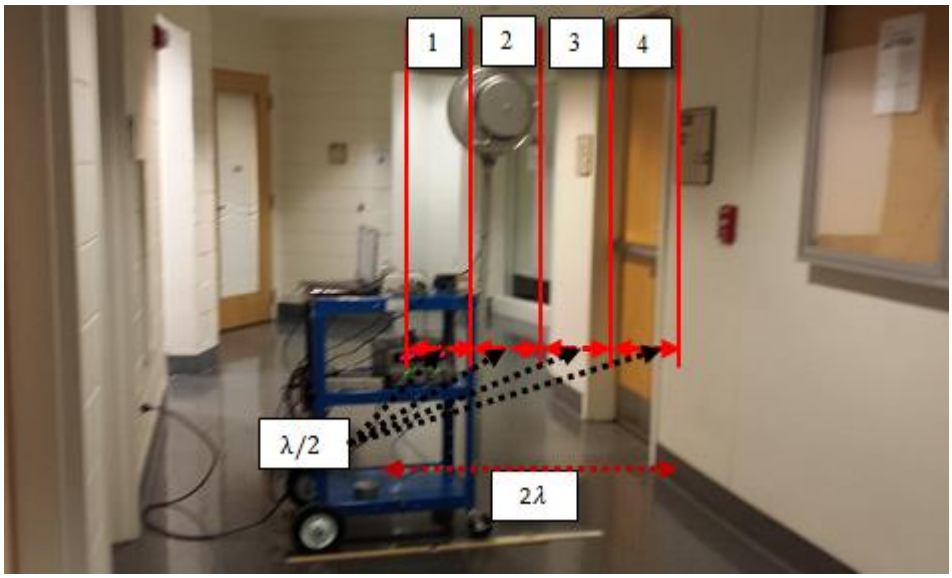

Figure 4.18: Simulated transmit antenna array for MIMO measurements (Note: distances not to scale)

It is assumed that the channel is time-invariant for the duration of the four sets of measurements. Due to the lack of synchronization between the measurements when adjusting the transmitter for the simulated transmit array, it was not possible to compute envelope correlation coefficients for the transmit antenna elements.

A set of MIMO measurements, which consisted of 100 PDP snapshots at a fixed receiver location, was captured for each of the five scenarios outlined in section 3.2. The five fixed receiver locations are listed in Table 4.9.

Table 4.9: Fixed receiver locations for MIMO measurements

Environment	Receiver Location	Corresponding floor plan figure (Chapter 3)	Corresponding table (Chapter 4)
Office	Rx 2.7	Figure 3.8	Table 4.1
Classroom/Comp Lab	Rx 4.1	Figure 3.9	Table 4.2
Atrium	Rx 2.3	Figure 3.10	Table 4.3
Hospital	Rx 4.3	Figure 3.11	Table 4.4
Indoor-to-Outdoor	Rx 1.2	Figure 3.12	Table 4.5

Figures 4.19 – 4.23 display the received power CDF for each scenario with normalized 2 x 1 Alamouti coding, normalized 2 x 2 TAS/MRC, normalized 4 x 4 TAS/MRC, and normalized 4 x 4 MRT/MRC. with the results summarized in Table 4.10.

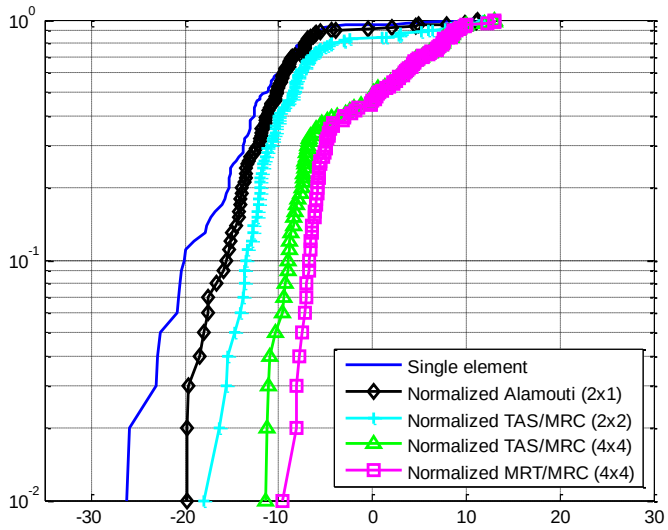

Figure 4.19: MIMO diversity: normalized received power CDF for Scenario 1 (Office)

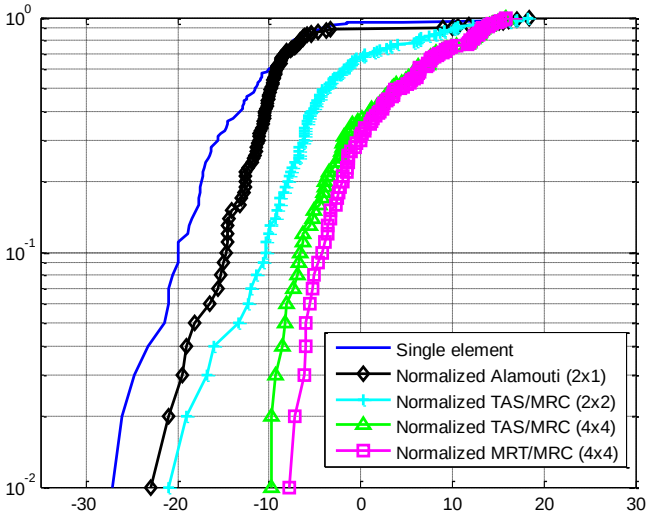

Figure 4.20: MIMO diversity: normalized received power CDF for Scenario 2 (Classroom/Comp Lab)

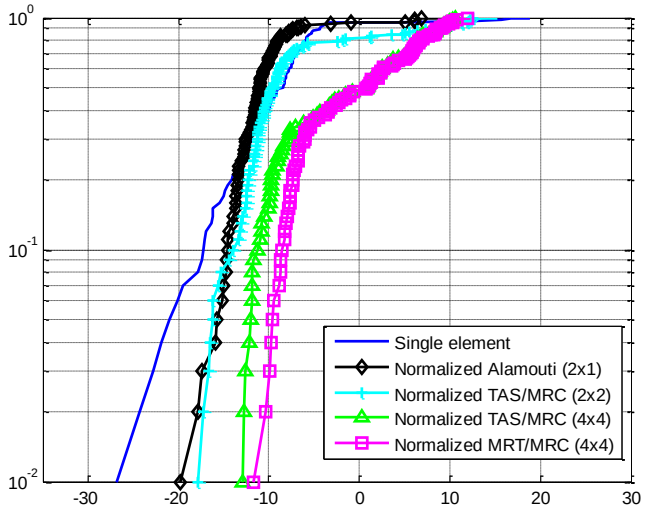

Figure 4.21: MIMO diversity: normalized received power CDF for Scenario 3 (Atrium)

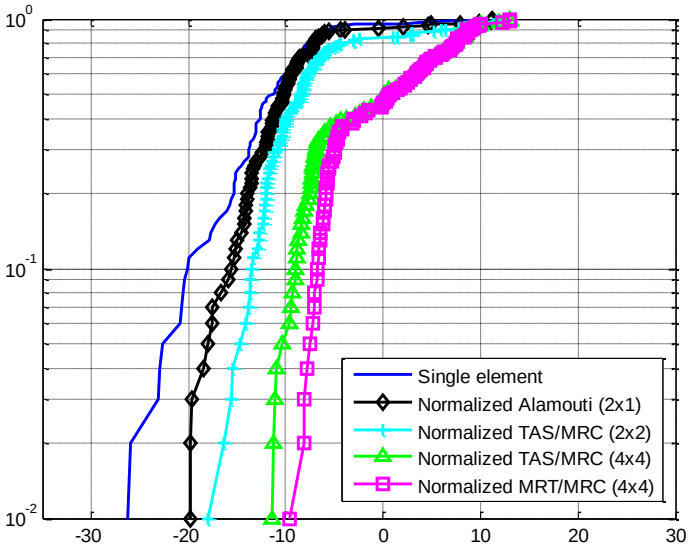

Figure 4.22: MIMO diversity: normalized received power CDF for Scenario 4 (Hospital)

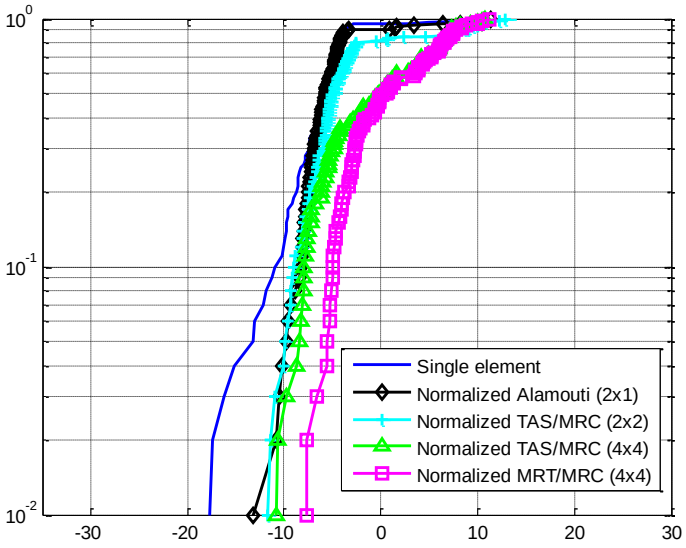

Figure 4.23: MIMO diversity: normalized received power CDF for Scenario 5 (Indoor-to-Outdoor)

Table 4.10: MIMO diversity gain for each scenario

Environment	2x1 Alamouti [dB]		2x2 TAS/MRC [dB]		4x4 TAS/MRC [dB]		4x4 MRT/MRC [dB]	
	10%	1%	10%	1%	10%	1%	10%	1%
Office	4.7	6.2	6.6	8.0	11.2	14.8	14.2	17.4
Classroom/Comp Lab	5.3	6.1	6.0	9.6	13.4	17.3	15.8	19.8
Atrium	2.6	6.3	3.0	8.1	5.4	13.0	9.3	14.2
Hospital	4.5	6.4	6.6	8.3	10.8	14.9	13.3	19.3
Indoor-to-Outdoor	2.1	4.5	2.3	6.6	2.6	6.8	5.2	10.0

Due to the simulated nature of the transmit antenna array, the results correspond to a lower bound on the MIMO diversity gain. In indoor environments, 2 x 1 transmit diversity offers approximately **4-5 dB** of gain and 2 x 2 TAS/MRC offers approximately **6-7 dB** of gain. 4 x 4 TAS/MRC offers approximately **12-13 dB** of gain and MRT/MRC offers **15-16 dB** of gain. Consequently, 2 x 1 MIMO systems and 4 x 4 TAS/MRC offer the most gain for relatively complexity. The diversity gain is greater for the classroom/comp lab environment due to the increase in partitions and clutter. Diversity is reduced in the atrium due to the wide, open nature of the environment. Diversity is slightly reduced in the hospital due to the reduced number of partitions.

For indoor-to-outdoor propagation, MIMO diversity provides a gain of approximately **5-6 dB lower** than strictly indoor propagation cases for 4 x 4 MIMO cases and approximately **3-4 dB lower** for 2 x 1 and 2 x 2 MIMO cases. Consequently, MIMO may play a critical role in indoor propagation for 3.5 GHz as high diversity indoors will greatly boost MIMO performance by approximately **15-16 dB** with MRT/MRC, while signals propagating outside the facility will have a lower gain of about **7-8 dB**, which, when combined with the attenuation properties of exterior building materials, may aid in keeping signals below the designated received power threshold to meet CAF regulations.

Chapter 5

Indoor Path Loss Models for 3.5 GHz

5.1 Indoor Path Loss Models Under Consideration

Accurate empirical path loss models specifically for 3.5 GHz in indoor environments do not exist, therefore we investigate the applicability of common WLAN path loss models in the low GHz range. Specifically, we investigate the accuracy of simplified path loss models which encapsulate indoor propagation loss into a single mathematical coefficient such as WINNER II and ITU-R M.2135, as well as more thorough models which explicitly formulate the contribution of each individual partition material into an aggregate term such as Cost-231 Multi-Wall or Multi-Wall and Floor. While these models are theoretically valid for any frequency range, little work has been done to test or verify their performance specifically at 3.5 GHz.

5.1.1 ITU-R M.2135 Indoor Hotspot Model

The M.2135 model is recommended by the ITU for modeling indoor hotspots and is a simplified path loss model where the loss due to indoor channel characteristics is lumped into a single attenuation term [35]. The LOS loss is defined as

$$L_{P,M2135} = 16.9 \log_{10}(d) + 32.8 + 20 \log_{10}(f) \quad (26)$$

and the NLOS loss is defined as

$$L_{P,M2135} = 43.3 \log_{10}(d) + 11.5 + 20 \log_{10}(f) \quad (27)$$

where f is the operating frequency in GHz.

5.1.2 WINNER II Model

The WINNER II model is significant due to its extensive collection of empirical correction factors, allowing it to adapt to a range of specific scenarios [36]. Though it is mainly applicable for outdoor propagation, it can be applied to indoor models, as well. The path loss formula is defined as

$$L_{P,WINNER} = Alog_{10}(d) + B + Clog_{10}\left(\frac{f}{5}\right) + X + FL \tag{28}$$

where f is the frequency in GHz, and the parameters A, B, C and X are given by Table A. n is the path loss exponent and FL is the floor loss, defined as

$$FL = 17 + 4(n_f - 1), n_f > 0 \tag{29}$$

where n_f is the number of floors. The parameters A, B, and C, and X are given in Table 5.1.

Table 5.1: Parameters for WINNER model

Scenario	LOS	*A*	*B*	*C*	*X*
Indoor office	Yes	18.7	46.8	20	0
Room-to-room	No	36.8	43.8	20	$5(n_w - 1)$ (light walls) $12(n_w - 1)$ (heavy walls)
Hallway-to-room	No	20	46.4	20	$5(n_w)$ (light walls) $12(n_w)$ (heavy walls)

5.1.3 COST-231 Multi-Wall Model

The COST 231 Multi-Wall model is based on the number of floors and walls between the transmitter and receiver [24]. The model is defined by

$$L_{P,COST} = L_0 + 20log_{10}(d) + k_f^{\left[\frac{(k_f+2)}{k_f+1}-0.46\right]}L_f + \sum_{i=1}^{k_w} K_w^{(i)} L_{wi} \quad (30)$$

with the parameters listed in Table 5.2. Table 5.3 lists the possible values for $L_w^{(i)}$.

Table 5.2: Parameters for COST-231 MW model

Parameter	Definition
L_0	Free space path loss at a distance of 1 m
k_f	Number of penetrated floors
L_f	Loss due to adjacent floors
k_w	Number of wall types
$K_w^{(i)}$	Number of walls of category i
$L_w^{(i)}$	Loss of walls of category i

Table 5.3: Attenuation values for COST-231 MW model partitions

Category	Attenuation (dB)
Light	3.4
Heavy	6.9

As seen in Table 5.3, there are only two fixed attenuation values for the model, depending on the attenuation strength of the partition material in question.

5.1.4 Multi-Wall and Floor Model

The Multi-Wall and Floor (MWF) [31] model was derived from the COST 231 Multi-Wall model and is commonly used in basic WLAN planning for urban indoor propagation. As its name suggests, the model separates the losses due to the walls and floors into categories of penetration loss magnitude by material. The path loss is defined as

$$L_{P,MWF} = L_0 + 10nlog_{10}(d) + \sum_{i=1}^{I}\sum_{k=1}^{K_w^{(i)}} L_{wk}^{(i)} + \sum_{j=1}^{J}\sum_{k=1}^{K_f^{(j)}} L_{fk}^{(j)} \quad (31)$$

with the parameters listed in Table 5.4. Table 5.5 lists common values of L_{wk} and L_{fk} for types of walls and ceilings.

Table 5.4: Parameters for MWF model

Parameter	Definition
L_0	Measured path loss at a reference distance of 1 meter
n	Path loss exponent
d	Transmitter-receiver separation [m]
$L_{wk}^{(i)}$	Attenuation due to wall type i, k-th traversed wall
$L_{fk}^{(j)}$	Attenuation due to floor type j, k-th traversed floor
I	Total number of wall types
J	Total number of floor types
$K_w^{(i)}$	Number of walls of category i
$K_f^{(j)}$	Number of floors of category j

Table 5.5: Attenuation values for MWF model partitions (obtained at 5.8 GHz)

Material	Thickness (cm)	Attenuation (dB)
Plywood	0.4	0.9
Gypsum wall	13.5	3.0
Rough chipboard	1.5	1.0
Glass plate	-	2.5
Double-glazed window	2.0	12
Concrete	10	16
Concrete	20	29
Office floor	-	19

Compared to the COST MW model, the MWF has much greater range and flexibility in terms of partition attenuation factors; however, the formula obeys the same general structure as the COST MW model.

5.2 Comparison of Path Loss Models

The predicted path loss values for the four channel models outlined in section 5.1 were computed and statistically compared against the basic free-space path loss model, and the fitted log-distance model computed from the indoor propagation campaign. Figure 5.1 displays a bar graph of the RMSE and mean error of the predicted path loss values compared to the measured path loss values – the prediction error values are also listed in Tables 5.6 and 5.7. For the log-distance model, the mean error is not displayed or listed since it is always zero.

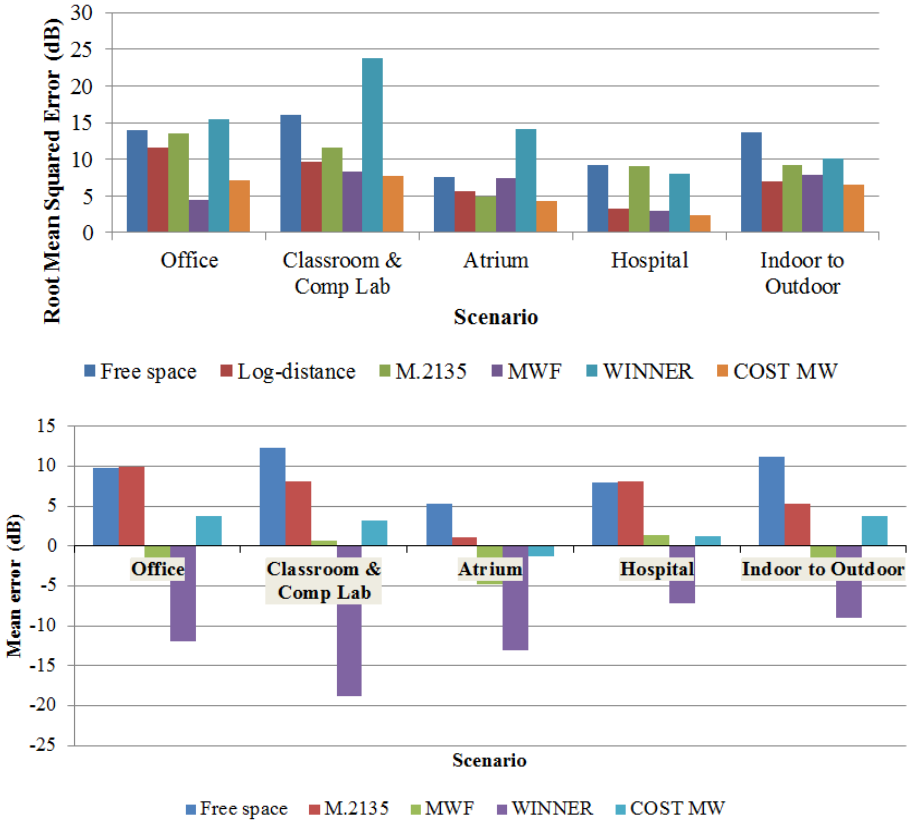

Figure 5.1: Prediction error of path loss models and measured path loss data. Top: RMSE Bottom: Mean Error

Table 5.6: RMSE for path loss models

Environment	Office	Classroom/comp lab	Atrium	Hospital	Indoor-to-Outdoor
Model	**Root mean squared error (σ_e [dB])**				
Free space	13.95	16.02	7.56	9.16	13.64
Log-distance	11.56	9.63	5.70	3.30	7.04
M.2135	13.54	11.56	4.96	9.13	9.24
MWF	**4.41**	8.29	7.49	2.91	7.88
WINNER	15.41	23.83	14.08	8.09	10.12
COST MW	7.20	**7.68**	**4.26**	**2.41**	**6.54**

Table 5.7: Mean error for path loss models

Environment	Office	Classroom/comp lab	Atrium	Hospital	Indoor-to-Outdoor
Model	**Mean error (μ_e [dB])**				
Free space	9.84	12.36	5.30	8.00	11.15
Log-distance	-	-	-	-	-
M.2135	9.96	8.16	**1.06**	8.11	5.36
MWF	**-1.63**	**0.66**	-4.78	1.44	-3.98
WINNER	-11.98	-18.87	-13.08	-7.23	-9.03
COST MW	3.79	3.15	-1.23	**1.21**	**3.74**

As seen in Tables 5.6 – 5.7 and Figure 5.1, path loss in typical office building environments favors models which explicitly factor the attenuation values of partitions in the model's formulation. The Cost MW and MWF models greatly outperform WINNER and M.2135 models and have comparatively high accuracy, typically outperforming the baseline log-distance model by 2 dB of RMSE and reaching up to 7 dB of RMSE in the case of the office scenario. Across all scenarios, the partition-based models average approximately 5 dB of RMSE from the measured path loss models.

Although the M.2135 model is generally outperformed by the log-distance model, M.2135 is comparatively simple and provides a solid rough prediction of the path loss. As seen in the atrium environment, the M.2135 performs well in heavy LOS scenarios and outperforms both the MWF model, as well as the log-distance model. Consequently, in a wide, open indoor environment, the M.2135 model serves as an adequate starting point before delving into more site-specific, partition-based channel modeling.

The WINNER model tends to over-predict path loss and has generally poor accuracy – it is regularly outperformed by both the log-distance model as well as the free space path loss model.

For the hospital environment, the COST MW model manages to come within 2.4 dB of RMSE of the measured data. Thus, in the case of patient monitoring rooms and medical offices, the additional clutter due to medical equipment has little impact on partition-based path loss prediction.

For indoor-to-outdoor propagation, due to the introduction of the outdoor component, the models do not perform nearly as well: even the most accurate model – the COST MW model – results in a performance increase of only approximately 0.5 dB of RMSE over the log-distance model. Correction factors may be introduced to account for the outdoor component ; however, a more appropriate approach would involve developing a short-range path loss model specifically to predict indoor-to-outdoor propagation.

To visualize the spread of the error distribution for each model, Figure 5.2 displays graphs of the CDF of the RMSE between the measured data and the data predicted by each path loss model. In the atrium and indoor-to-outdoor environments, the spread tends to be more uniform across most of the model predictions, as both scenarios are more uniform environments. The spread is more distributed in the highly-NLOS office and classroom/comp lab environments. There is interesting behavior in the hospital environment, however, as the models with a free-space distance-based component (FPSL, Cost MW, MWF) and all other models exhibit almost identical spreads.

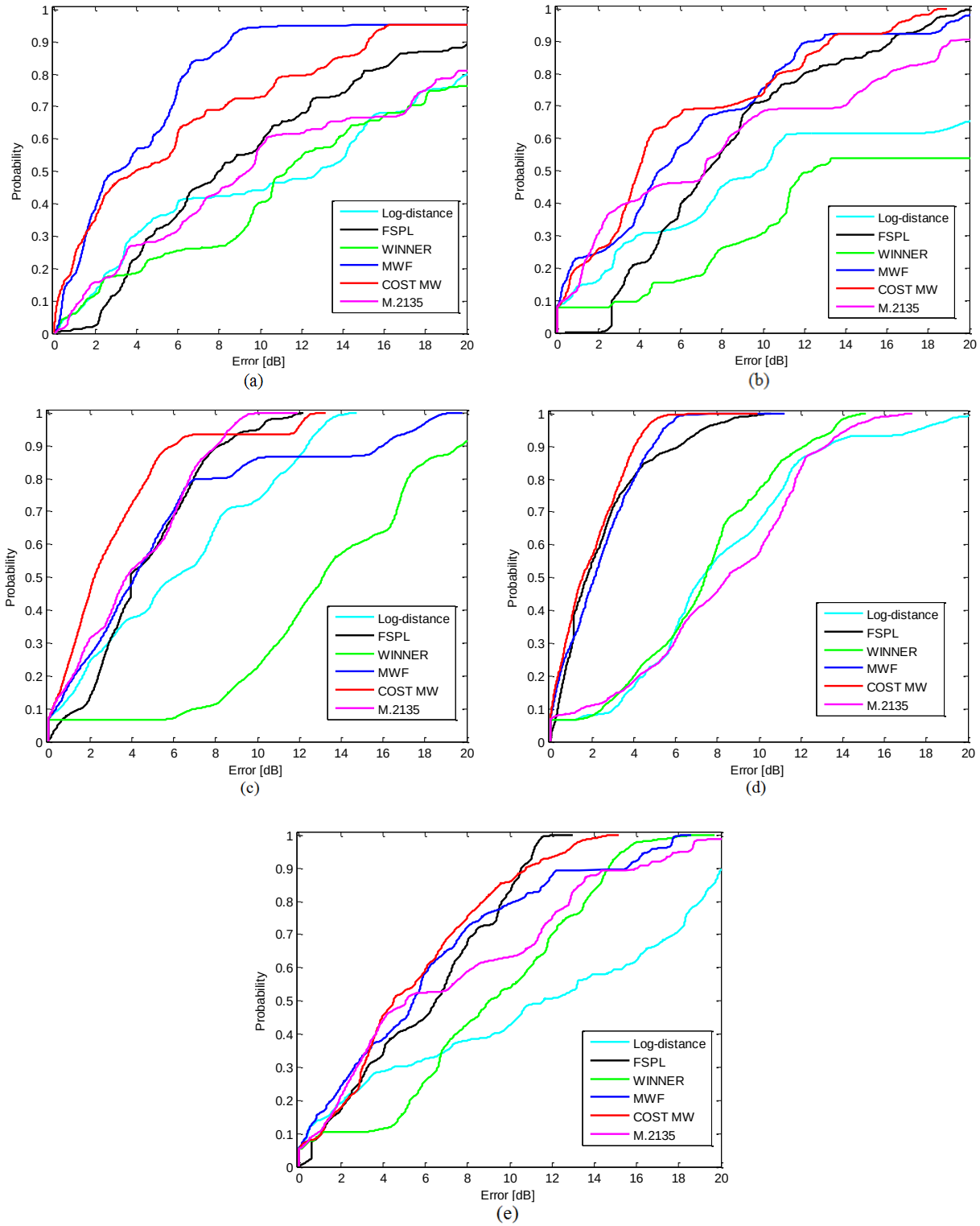

Figure 5.2: Error CDFs for path loss models. a) Office, b) Classroom/Comp Lab, c) Atrium, d) Hospital, e) Indoor-to-Outdoor

Chapter 6

Conclusions

6.1 Summary of Results

This thesis serves as documentation and analysis of propagation data for indoor scenarios at 3.5 GHz to facilitate the deployment of small cells and spectrum sharing technology. The motivation for this propagation research was prompted by the FCC's decision to open the 3.5 GHz band as an "innovation band" to promote opportunistic spectrum access, paving the way for less congested and optimized spectrum. Along with research opportunities with spectrum sharing systems, the commercial potential in the band is very high with 4G TD-LTE targeting the deployment of small cells in the band to increase coverage and capacity in urban areas.

An indoor propagation campaign was carried out and fundamental, critical propagation metrics such as large scale path loss and delay spread characteristics were recorded and analyzed. Typical indoor path loss exponents ranged between 2.4 and 3.1, which is consistent with similar propagation studies in the low GHz range. Indoor-to-outdoor measurements resulted in a greater path loss exponent between 2.1 and 3.8 which is expected due to the addition of robust exterior building materials.

Delay spread characteristics were consistent with indoor propagation studies at low GHz bands and with the transmitter/receiver separation, number of obstructions, and presence of mobile bodies in the environment. Exterior building materials such as reinforced glass, limestone, and concrete do an adequate job of containing signals (15+ dB of attenuation) and motivate the designation and regulation of Contained Access Facilities proposed by the FCC's FNPRM.

Using multiple receive antennas for indoor receive diversity resulted in 8-10 dB of gain, which is a significant improvement over indoor-to-outdoor scenarios, which yielded 4-5 dB of gain in the low GHz range. Taking advantage of both transmit and receive diversity using 4 x 4

MIMO resulted in 15-16 dB of gain for indoor environments, which is approximately 7-8 dB higher than gain for indoor-to-outdoor propagation. Employing even a simple 2 x 1 MIMO scheme in indoor environments may boost performance by 4-5 dB. Thus, using MIMO, we may greatly increase performance of indoor wireless deployments while keeping overall transmit power values low to further motivate the concept of Contained Access Facilities for indoor wireless deployments.

Existing path loss models were statistically compared against recorded measurements: models which explicitly attributed the excess indoor attenuation to partition materials yielded the most accurate predictions: they predicted within 5-6 dB of RMSE and as low as 2.4 dB of RMSE from measured path loss values and consistently outperformed the fitted log-distance model. However, simplified models such as M.2135 may perform well as a 'back of the envelope' prediction. The documentation of attenuation values of common internal and external building materials will further bolster the performance of the partition-based category of channel models as well as help characterize path loss and signal propagation behavior in indoor environments.

6.2 Future Work

There is a significant amount of propagation work to be done at 3.5 GHz. Residental environments, as well as industrial environments, such as factories, laboratories, or power plants must be considered. Outdoor-to-indoor and small cell outdoor urban measurement campaigns are also critically important, as they allow for co-existence studies with the primary user. These studies would be ideally supplemented with radar path loss measurements and radar channel characterization.

With regard to channel modelling, statistical channel parameters of the 3.5 GHz band are needed, such as small-scale fading parameters (e.g. Rayleigh or Nakagami fading factors) and statistical models must be tested or developed, specifically at 3.5 GHz.

To further facilitate the push for spectrum sharing, especially as the low GHz spectrum becomes heavily saturated. Small cells will play a big role in the planning for heterogeneous networks and IoT, so future propagation campaigns need to be carried out under the assumption that current and future wireless networks will be expected to harmoniously co-exist.

References

[1] "Enabling Innovative Small Cell Use in 3.5 GHz Band NPRM & Order" FCC 12-148, Federal Communications Commission, Dec. 2012

[2] 3GPP, "User Equipment (UE) radio transmission and reception" Technical Specification 36.101.

[3] "Special Research Report on LTE TDD Services in the 3.5 GHz bands", white paper, Heavy Reading, Nov. 2013

[4] "Proposes Creation of New Citizens Broadband Radio Service in 3.5 GHz" FCC 14-49, Apr. 2014

[5] T. S. Rappaport, *Wireless Communications: Principles and Practice (2nd Edition)*, Prentice Hall, 2002

[6] A. Goldsmith, *Wireless Communications*. Cambridge, U.K.: Cambridge Univ. Press, 2005

[7] M. Hata, "Empirical formula for propagation loss in land mobile radio services," *Vehicular Technology, IEEE Transactions on* , vol.29, no.3, pp.317,325, Aug. 1980

[8] K.V. S. Hari, K.P. Sheikh, and C. Bushue, "Interim channel models for G2 MMDS fixed wireless applications," *IEEE 802.16.3c-00/49r2*

[9] A.A.M. Saleh; R.A. Valenzuela, "A Statistical Model for Indoor Multipath Propagation," *Selected Areas in Communications, IEEE Journal on* , vol.5, no.2, pp.128,137, February 1987

[10] V. S. Abhayawardhana, I. J. Wassell, D. Crosby, M. P. Sellars, and M. G. Brown, "Comparison of empirical propagation path loss models for fixed wireless access systems," in *Vehicular Technology Conference, 2005. VTC 2005-Spring. 2005 IEEE 61st*, 2005, pp. 73-77 Vol. 1.

[11] C. Kin Lien and T. Kurner, "Effect of terrain irregularities and clutter distribution on wave propagation at 3.5 GHz in suburban area," in *Antennas and Propagation (EuCAP), 2010 Proceedings of the Fourth European Conference on*, 2010, pp. 1-5.

[12] Y. A. Alqudah and A. Tahat, "Path loss and propagation models at 3.5 GHz using deployed WiMAX network," in *Information Networking (ICOIN), 2011 International Conference on*, 2011, pp. 301-305.

[13] W. Joseph, L. Roelens, and L. Martens, "Path Loss Model for Wireless Applications at 3500 MHz," in *Antennas and Propagation Society International Symposium 2006, IEEE*, 2006, pp. 4751-4754.

[14] K. Sun, P. Wang, and Y. Li, "Path loss models for suburban scenario at 2.3GHz, 2.6GHz and 3.5GHz," in *Antennas, Propagation and EM Theory, 2008. ISAPE 2008. 8th International Symposium on*, 2008, pp. 438-441.

[15] J. Baumgarten, C. Kin Lien, A. Hecker, T. Kurner, M. Braun, and P. Zahn, "Performance of prediction models in suburban/rural residential areas at 860, 2300 and 3500 MHz," in *Antennas and Propagation (EUCAP), 2012 6th European Conference on*, 2012, pp. 1412-1416.

[16] M. Barbiroli, C. Carciofi, V. Degli Esposti, F. Fuschini, P. Grazioso, D. Guiducci, *et al.*, "Characterization of WiMAX propagation in microcellular and picocellular environments," in *Antennas and Propagation (EuCAP), 2010 Proceedings of the Fourth European Conference on*, 2010, pp. 1-5.

[17] G. L. Ramos, R. D. Vieira, Gonc, x, C. alves do Rego, P. T. Pereira, *et al.*, "Urban measurements and propagation models comparison of a 3.5 GHz signal for broadband wireless systems," in *Antennas and Propagation (EuCAP), 2010 Proceedings of the Fourth European Conference on*, 2010, pp. 1-5.

[18] J. A. Gay-Fernandez and I. Cuinas, "Peer to Peer Wireless Propagation Measurements and Path-Loss Modeling in Vegetated Environments," *Antennas and Propagation, IEEE Transactions on*, vol. 61, pp. 3302-3311, 2013.

[19] A. Valcarce and Z. Jie, "Empirical Indoor-to-Outdoor Propagation Model for Residential Areas at 0.9-3.5 GHz," *Antennas and Wireless Propagation Letters, IEEE*, vol. 9, pp. 682-685, 2010.

[20] Z. Jing and J. Zhang, "Propagation characteristics in indoor office scenario at 3.5 GHz," in *Communications and Networking in China (CHINACOM), 2013 8th International ICST Conference on*, 2013, pp. 332-336.

[21] D. De Luca, F. Fiano, F. Mazzenga, C. Monti, S. Ridolfi, and F. Vallone, "Outdoor Path Loss Models for IEEE 802.16 in Suburban and Campus-Like Environments," in *IEEE International Conference on Communications, 2007. ICC '07*, 2007, pp. 4902-4906.

[22] C. V. R. Ron and L. A. R. Da Silva Mello, "Propagation measurements at 3.5 GHz in a dense urban area," in *Antennas and Propagation (EuCAP), 2010 Proceedings of the Fourth European Conference on*, 2010, pp. 1-4.

[23] Electronic Communication Committee (ECC) within the European Conference of Postal and Telecommunications Administration (CEPT), “The analysis of the coexistence of FWA cells in the 3.4 - 3.8 GHz band,” tech. rep., ECC Report 33, May 2003.

[24] COST Action 231, “Digital mobile radio towards future generation systems, final report,” tech. rep., European Communities, EUR 18957,1999.

[25] V. Erceg, et al., “Channel models for fixed wireless applications,” tech. rep., IEEE 802.16 Broadband Wireless Access Working Group, January 2001.

[26] V. Erceg, et al. "An empirically based path loss model for wireless channels in suburban environments." *IEEE Journal on Selected Areas in Communications,* 17.7 (1999): 1205-1211.

[27] N. Shabbir, H. Kashif, "Radio Resource Management in WiMAX", MS Thesis, Bleking Institute of Technology, Karlskrona Sweden, 2009.

[28] J. Milanovic, S. Rimac-Drlje, and K. Bejuk, "Comparison of Propagation Models Accuracy for WiMAX on 3.5 GHz," in *ICECS 2007. 14th IEEE International Conference on Electronics, Circuits and Systems, 2007.* 2007, pp. 111-114.

[29] M. Shahjahan, A. Q. Abdulla Hes-Shafi, “Analysis of Propagation Models for WiMAX at 3.5 GHz,” MS thesis, Blekinge Institute of Technology, Karlskrona, Sweden, 2009.

[30] Propagation data and prediction method for the planning of short-range outdoor radiocommunication systems and radio local area networks in the frequency range 300 MHz to 100 GHz, ITU-R P.1411-7, Sept. 2013

[31] M. Lott and I. Forkel, "A multi-wall-and-floor model for indoor radio propagation," in *Vehicular Technology Conference, 2001. VTC 2001 Spring. IEEE VTS 53rd*, 2001, pp. 464-468 vol.1.

[32] A. G. M. Lima and L. F. Menezes, "Motley-Keenan model adjusted to the thickness of the wall," in *2005 SBMO/IEEE MTT-S International Conference on Microwave and Optoelectronics,* 2005, pp. 180-182.

[33] T. Sadiki; P. Paimblanc, "Modelling New Indoor Propagation Models for WLAN Based on Empirical Results," *11th International Conference on Computer Modelling and Simulation, 2009. UKSIM '09.*, vol., no., pp.585,588, 25-27 March 2009

[34] G. Durgin; T.S. Rappaport; H. Xu, "Measurements and models for radio path loss and penetration loss in and around homes and trees at 5.85 GHz," *IEEE Transactions on Communications*, vol.46, no.11, pp.1484, 1496, Nov 1998

[35] Guidelines for evaluation of radio interface technologies for IMT-Advanced, ITU-R Report M.2135, Nov. 2008.

[36] E. Tragos, S. A. Kyriazakos, and A. Mihovska, "D 6.12.3 Report on validation and implementation of key WINNER cooperation functionalities, ", Nov. 2007

[37] Method for point-to-area predictions for terrestrial services in the frequency range 30 MHz to 3000 MHz, ITU-R P.1546-5, Sept. 2013

[38] W. G. Newhall, "Radio channel measurements and modeling for smart antenna array systems using a software radio receiver," Ph.D. Dissertation, Virginia Polytechnic Institute and State University, http://scholar.lib.vt.edu/theses/index.html, May 2003

[39] R.J. Pirkl; G.D. Durgin, "Optimal Sliding Correlator Channel Sounder Design," *IEEE Transactions on Wireless Communications*, vol.7, no.9, pp.3488,3497, September 2008

[40] J. F. Coll, "RF Channel Characterization in Industrial, Hospital and Home Environments," Lic. Thesis, Royal Institute of Technology, Communication system Dept., 2012

[41] E. Hanada, Y. Antoku, S. Tani, M. Kimura, A. Hasegawa, S. Urano, K. Ohe, M. Yamaki, and Y. Nose, "Electromagnetic interference on medical equipment by low-power mobile telecommunication systems," *IEEE Transactions on Electromagnetic Compatibility*, vol. 42, no. 4, pp. 470 –476, Nov. 2000.

[42] T.M. Schafer; J. Maurer; J. von Hagen; W. Wiesbeck, "Experimental characterization of radio wave propagation in hospitals," *IEEE Transactions on Electromagnetic Compatibility*, vol.47, no.2, pp.304,311, May 2005

[43] C. R. Anderson, "Design and implementation of an ultrabroadband millimeter-wavelength vector sliding correlator channel sounder and in-building measurements at 2.5 & 60 GHz," MS Thesis, Virginia Polytechnic Inst. State University, Blacksburg, VA, May 2002

[44] Y.E. Mohammed; A.S Abdallah; Y.A. Liu, "Characterization of indoor penetration loss at ISM band," *Asia-Pacific Conference on Environmental Electromagnetics, 2003* , vol., no., pp.25,28, 4-7 Nov. 2003

[45] R. R. Skidmore, " A Comprehensive Method and System for the Design and Deployment of Wireless Data Networks," Ph.D. Dissertation, Virginia Polytechnic Institute and State University, http://scholar.lib.vt.edu/theses/index.html, April 2003

[46] B.T. Ahmed; I.A. Calvo; J.L.M. Campos; "Materials' Insertion Loss at Three Frequency Bands," *Progress In Electromagnetics Research Letters* 39 (2013): 199-205.

[47] A. Kara; H.L. Bertoni, "Blockage/shadowing and polarization measurements at 2.45 GHz for interference evaluation between Bluetooth and IEEE 802.11 WLAN," *IEEE Antennas and Propagation Society International Symposium, 2001,* pp.376,379 vol.3, 8-13 July 2001

[48] T.M Schafer; J. Maurer; J. von Hagen; W Wiesbeck, "Experimental characterization of radio wave propagation in hospitals," *IEEE Transactions on Electromagnetic Compatibility*, vol.47, no.2, pp.304,311, May 2005

[49] J.C. Stein, "Indoor radio WLAN performance part II: Range performance in a dense office environment." *Intersil Corporation*, 1998

[50] R. Janaswamy, *Radiowave Propagation and Smart Antennas for Wireless Communications*. Kluwer Academic Publishers, 2000

[51] Keun Chul Hwang; Kwang Bok Lee, "Efficient weight vector representation for closed-loop transmit diversity,". *IEEE International Conference on Communications, 2002*, vol.2, no., pp.732,736 vol.2, 2002

[52] Ching-Hok Tse; Kun-Wah Yip; Tung-Sang Ng, "Performance tradeoffs between maximum ratio transmission and switched-transmit diversity,"*11th IEEE International Symposium on Mobile Radio Communications*, 2000, vol.2, no., pp.1485,1489 vol.2, 2000

Appendix A

Transmitter/Receiver Setup and Site Photos

A.1 Scenario 1 (Office)

Figure A.1: Site photos for Scenario 1: Tx 1, Rx 1.1 – 1.6

Figure A.2: Site photos for Scenario 1: Tx 2, Tx 3, Rx 2.1 – 2.7

Figure A.3: Site photos for Scenario 1: Rx 2.8 – 2.10, Rx 3.1 – 3.4

A.2 Scenario 2 (Classroom/Computer Laboratory)

Figure A.4: Site photos for Scenario 2: Tx 1, Tx 2, Rx 1.1 – 1.3, Rx 2.1 – 2.3

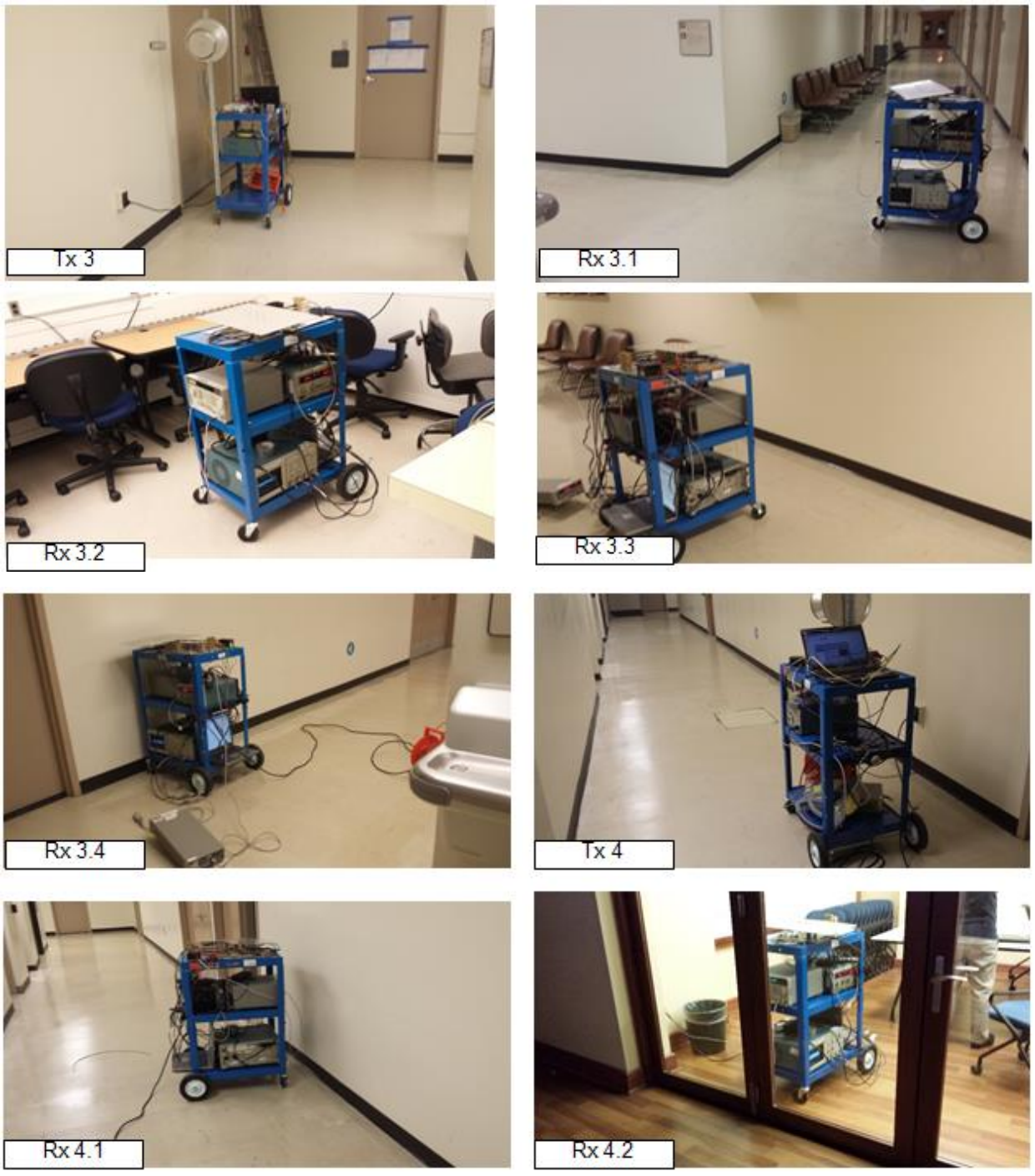

Figure A.5: Site photos for Scenario 2: Tx 3, Tx 4, Rx 3.1 – 3.4, Rx 4.1 – 4.2

A.3 Scenario 3 (Atrium)

Figure A.6: Site photos for Scenario 3: Tx 1, Tx 2, Rx 1.1 – 1.2, Rx 2.1 – 2.4

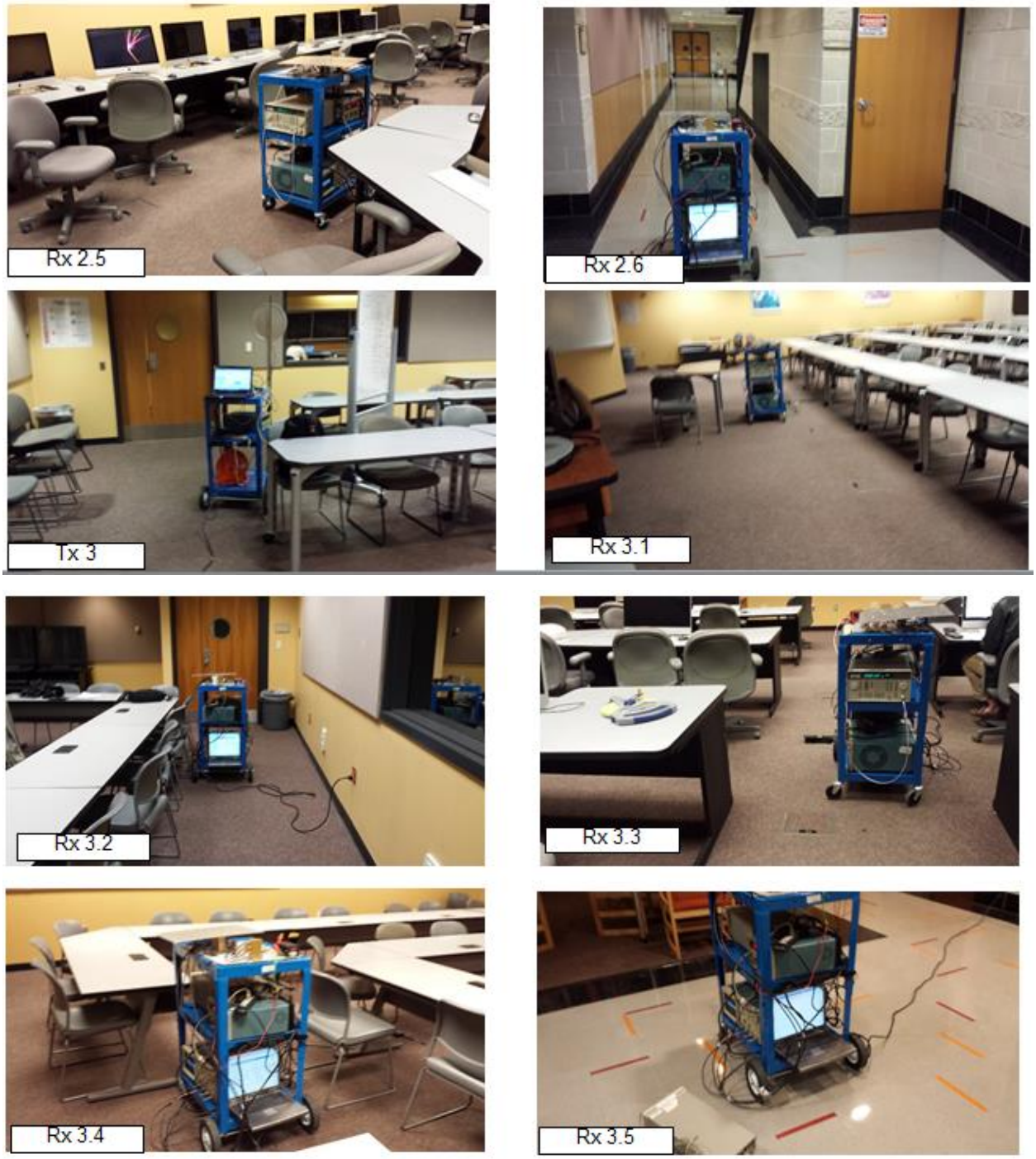

Figure A.7: Site photos for Scenario 3: Tx 3, Rx 2.5 – 2.6, Rx 3.1 – 3.5

Figure A.8: Site photos for Scenario 3: Rx 3.6

A.4 Scenario 4 (Hospital)

Figure A.9: Site photos for Scenario 4: Tx 1, Tx 2, Tx 3, Rx 1.1 – 1.2, Rx 2.1 – 2.2, Rx 3.1

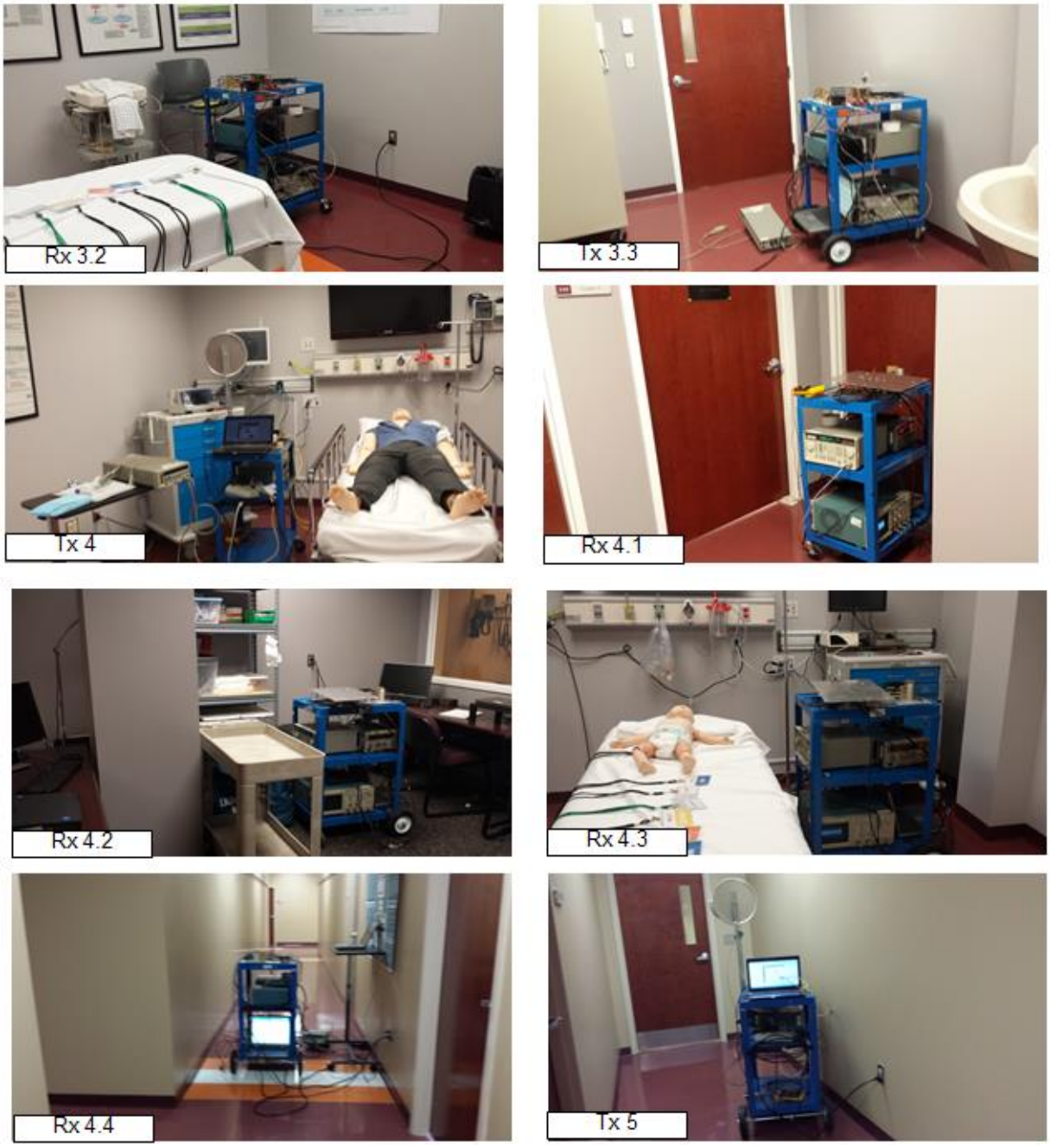

Figure A.10: Site photos for Scenario 4: Tx 4, Tx 5, Rx 3.2 – 3.3, Rx 4.1 – 4.4

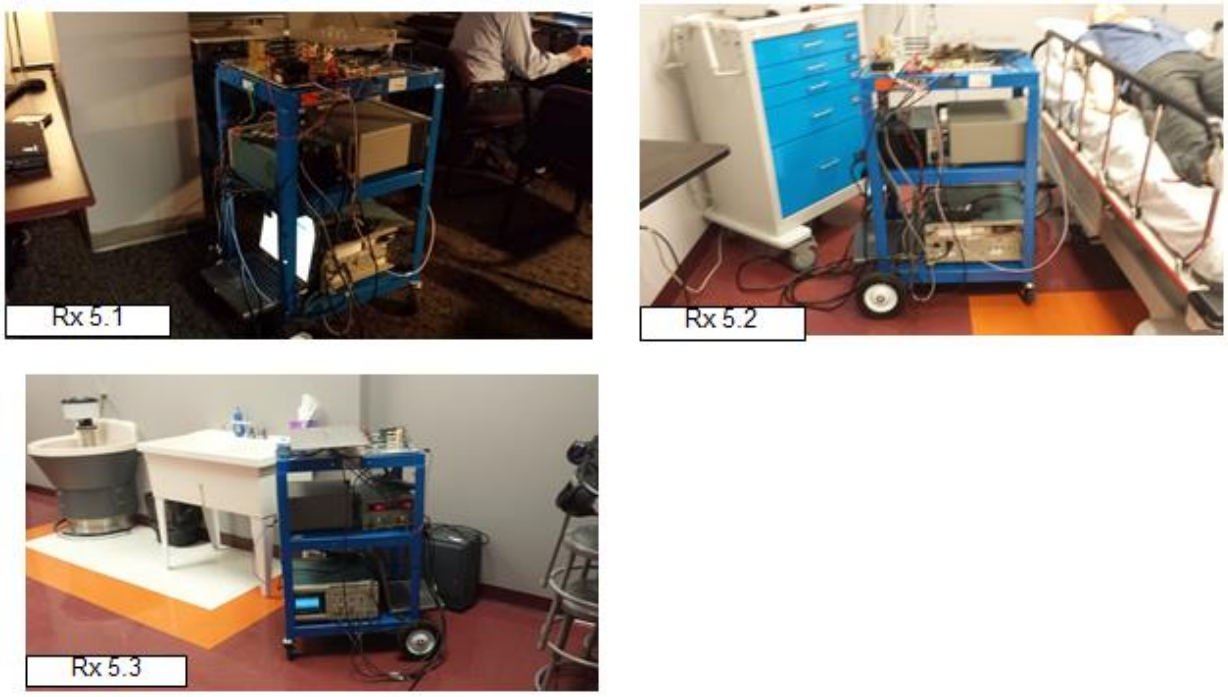

Figure A.11: Site photos for Scenario 4: Rx 5.1 – 5.3

A.5 Scenario 5 (Indoor-to-Outdoor)

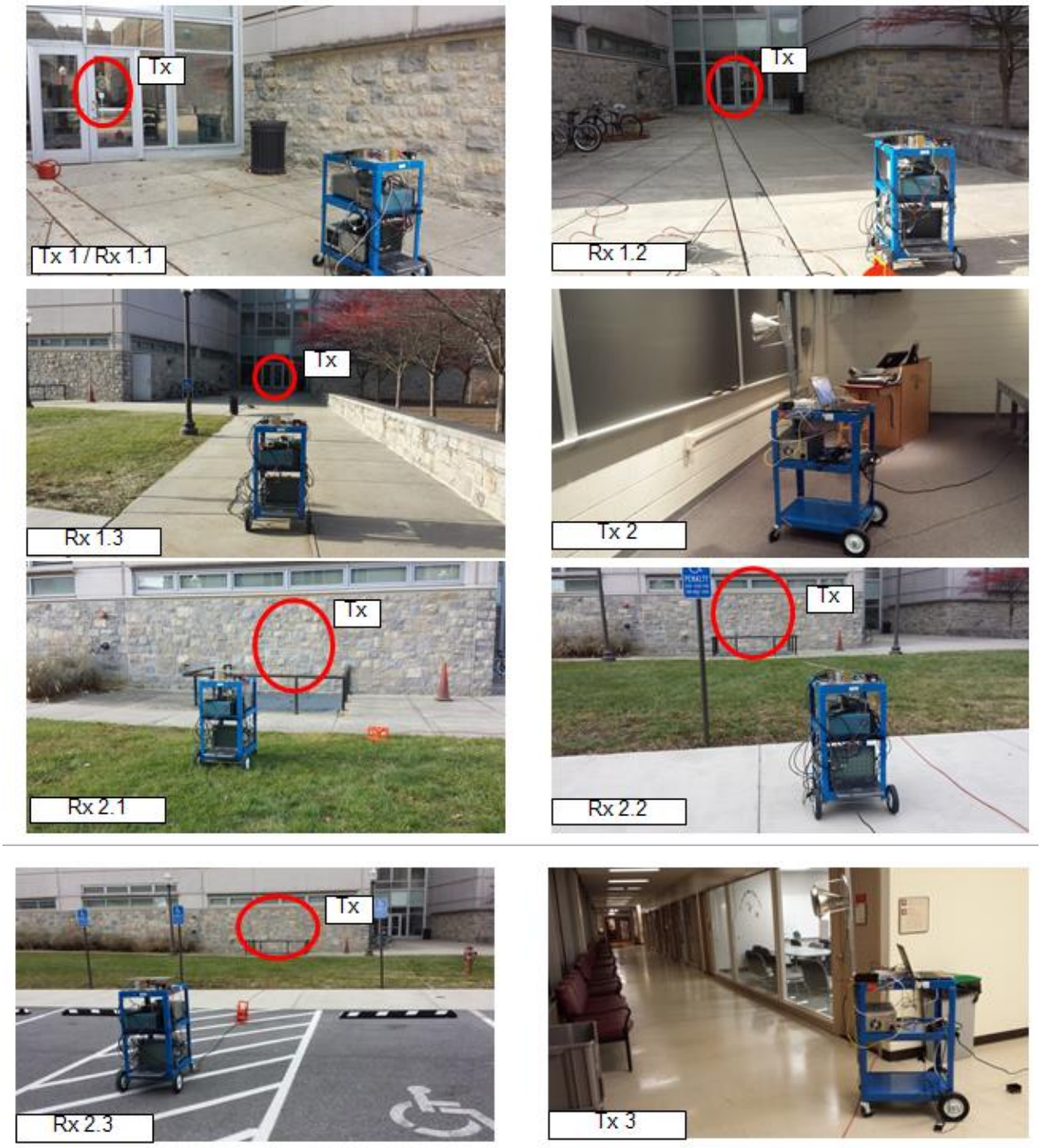

Figure A.12: Site photos for Scenario 5: Tx 1, Tx 2, Tx 3, Rx 1.1 – 1.3, Rx 2.1 – 2.3

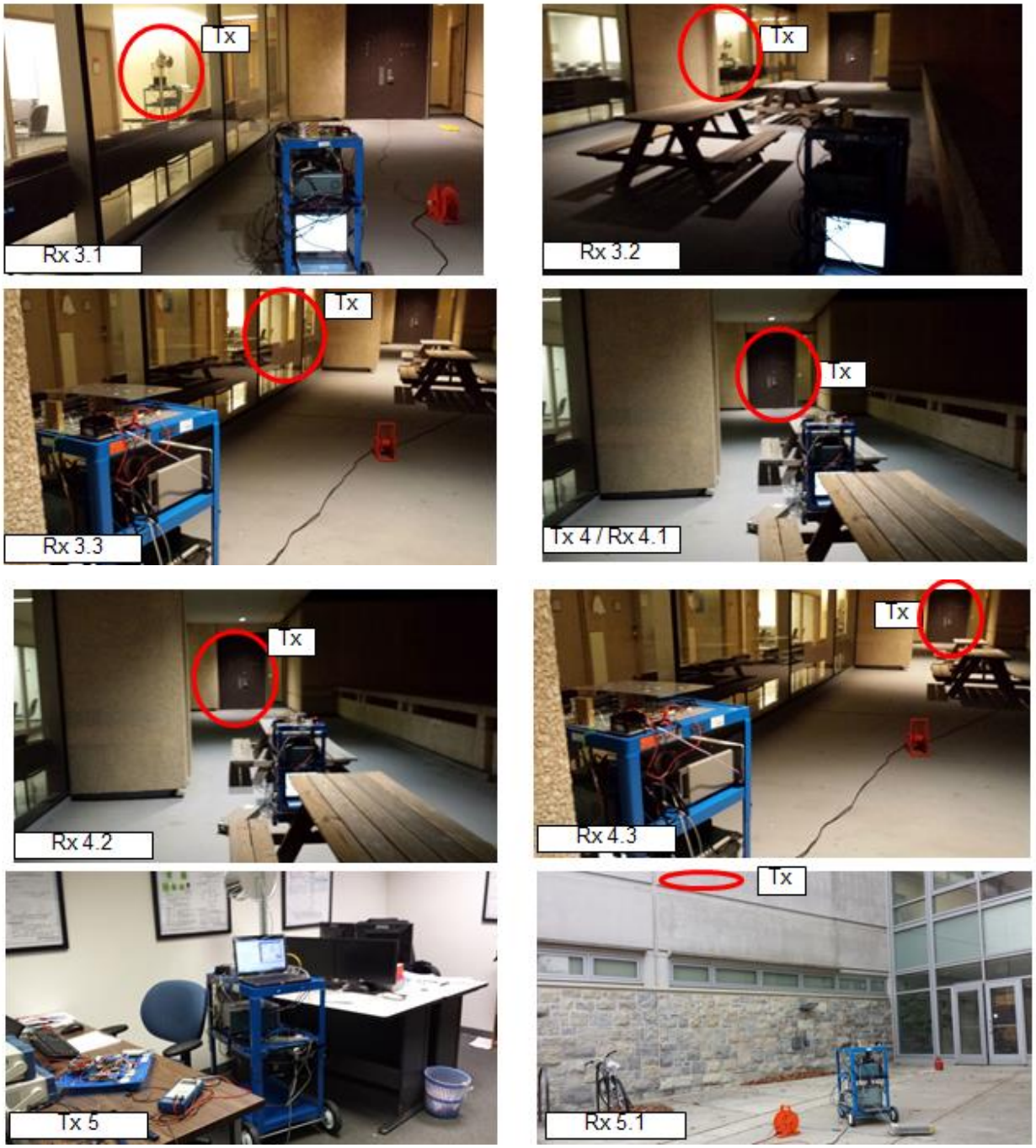

Figure A.13: Site photos for Scenario 5: Tx 4, Tx 5, Rx 3.1 – 3.3, Rx 4.1 – 4.3, Rx 5.1 – 5.3

Figure A.14: Site photos for Scenario 5: Tx 6, Rx 5.2 – 5.3, Rx 6.1 – 6.3

Appendix B

Average Power Delay Profiles

B.1 Scenario 1 (Office)

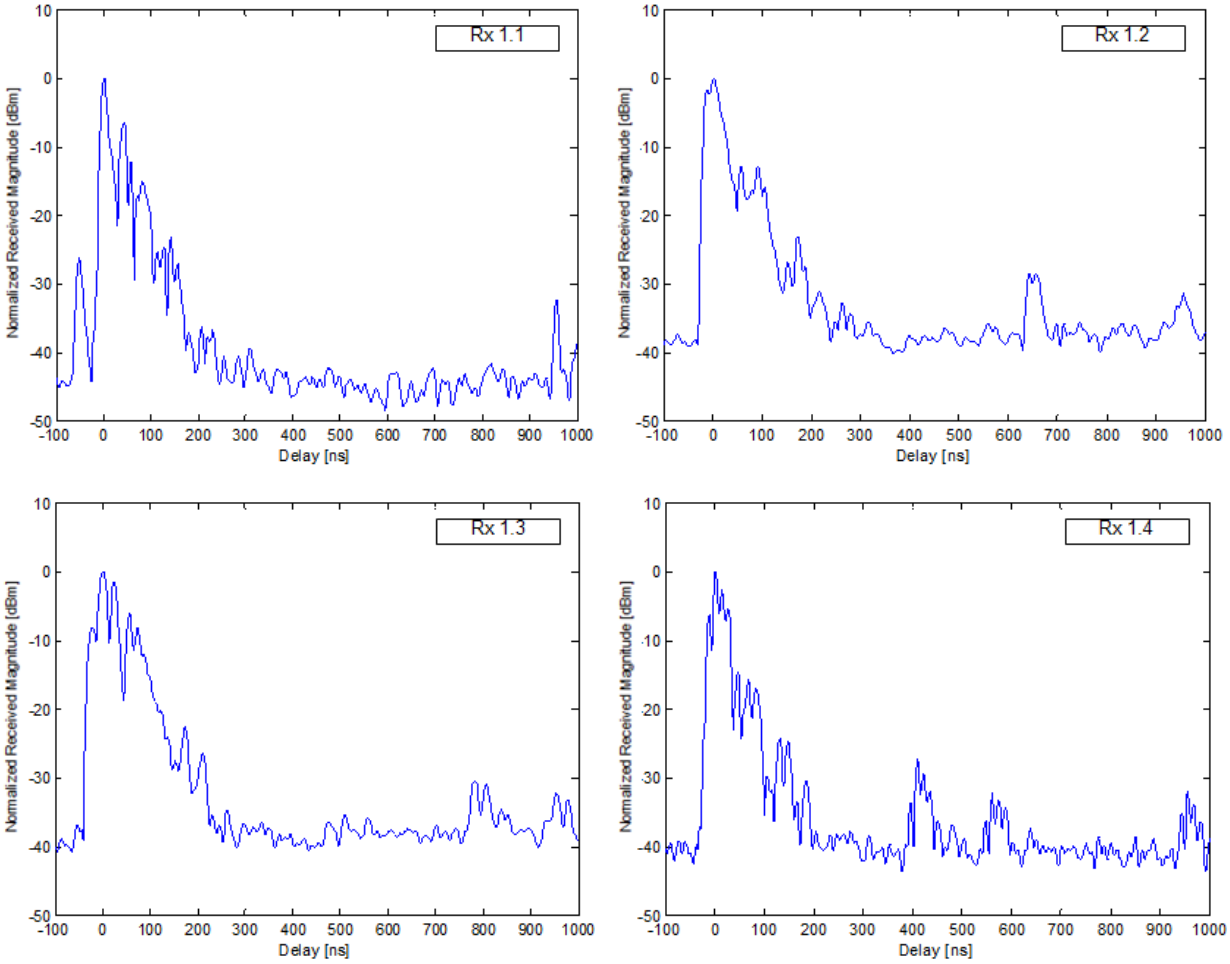

Figure B.1: Average power delay profiles for Scenario 1: Rx 1.1 – 1.4

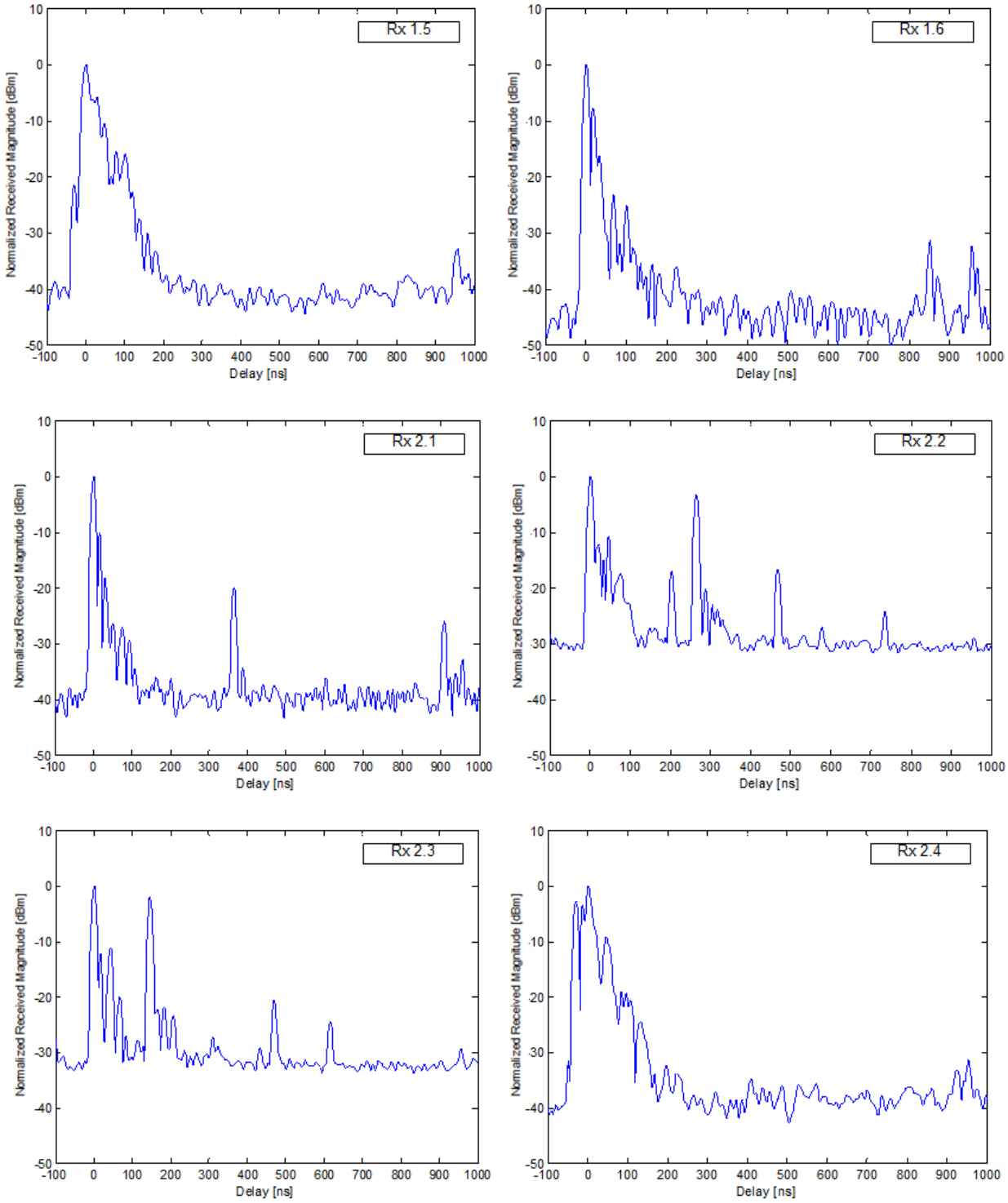

Figure B.2: Average power delay profiles for Scenario 1: Rx 1.5 – 1.6, Rx 2.1 – 2.4

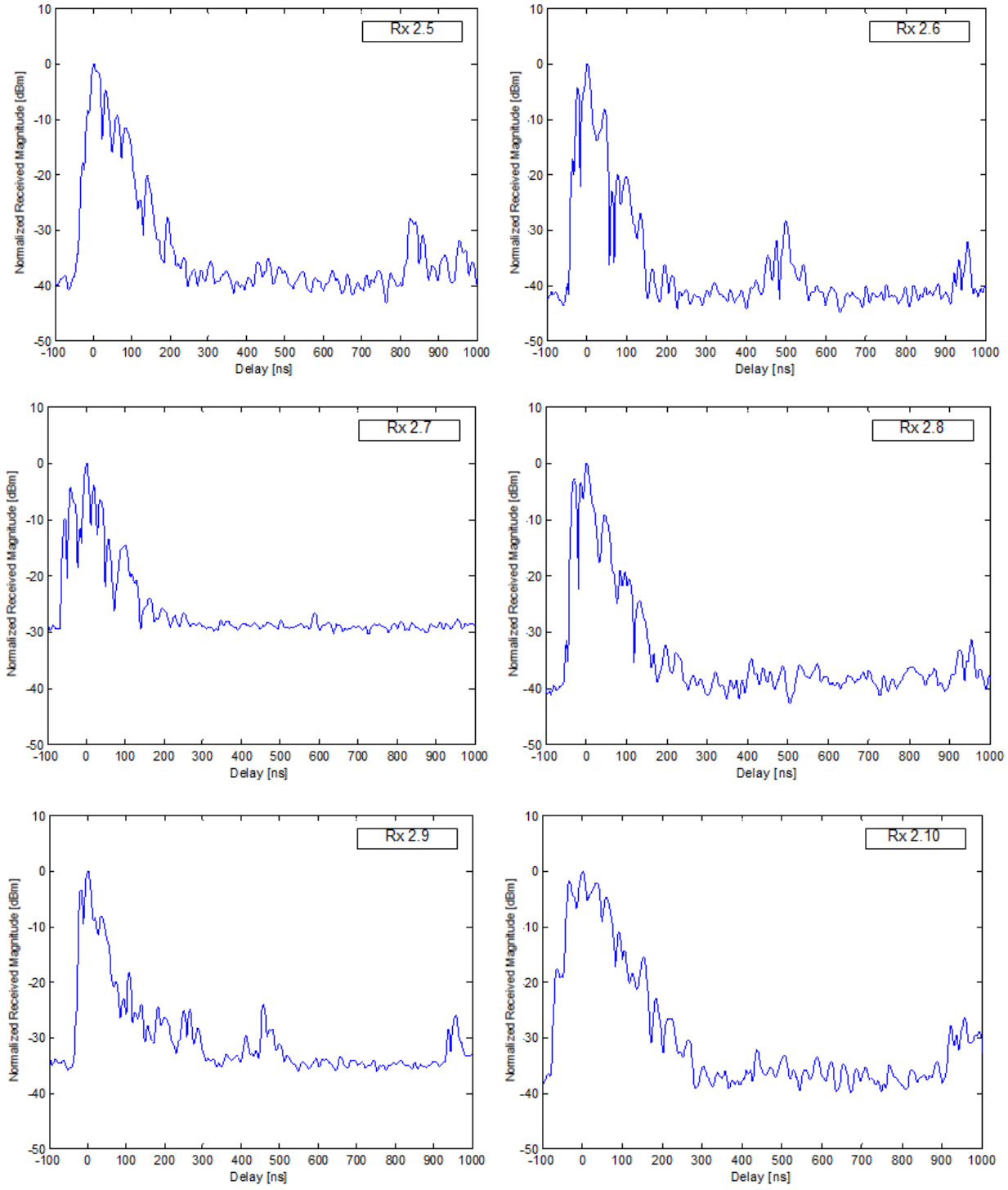

Figure B.3: Average power delay profiles for Scenario 1: Rx 2.5 – 2.10

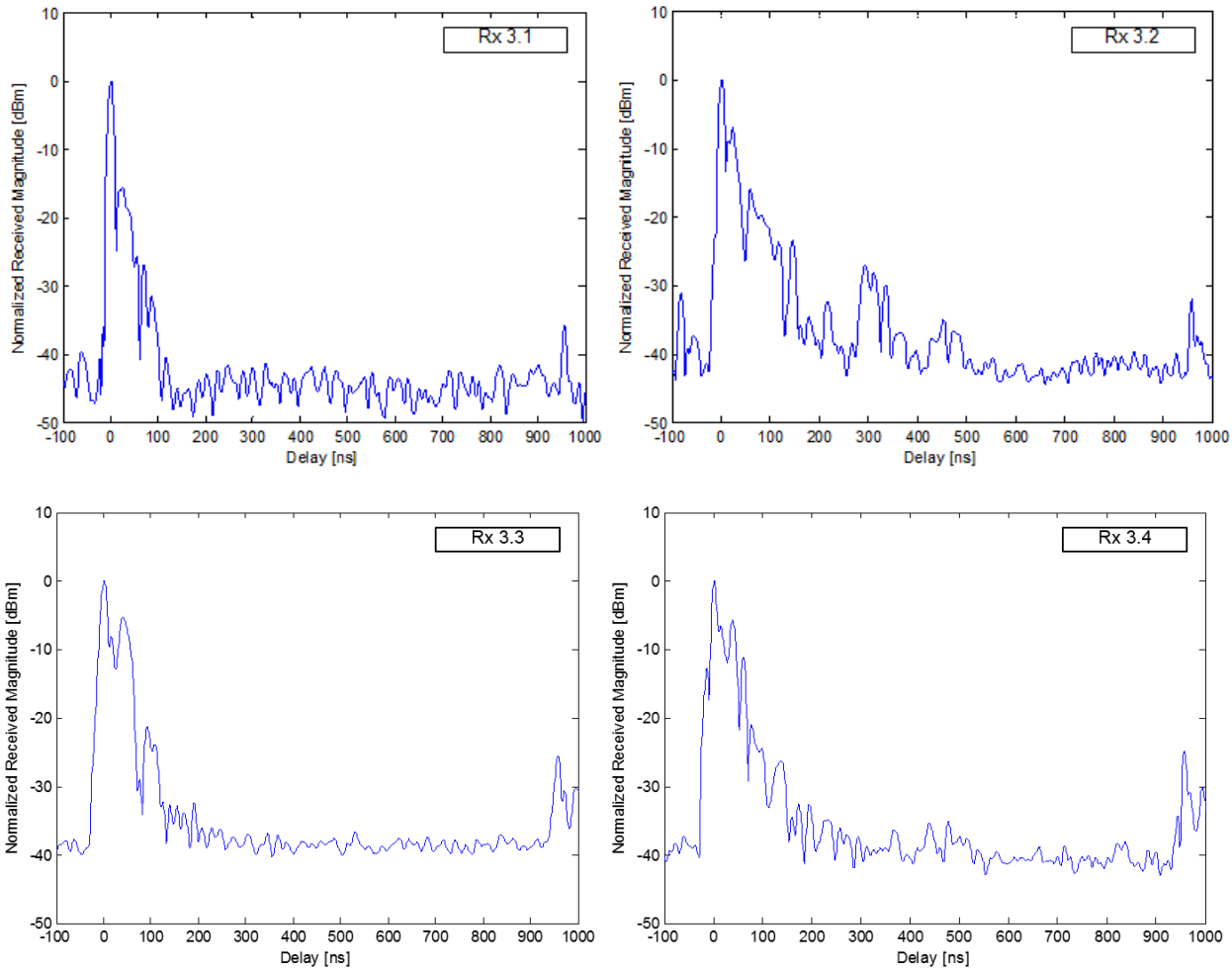

Figure B.4: Average power delay profiles for Scenario 1: Rx 3.1 – 3.4

B.2 Scenario 2 (Classroom/Computer Laboratory)

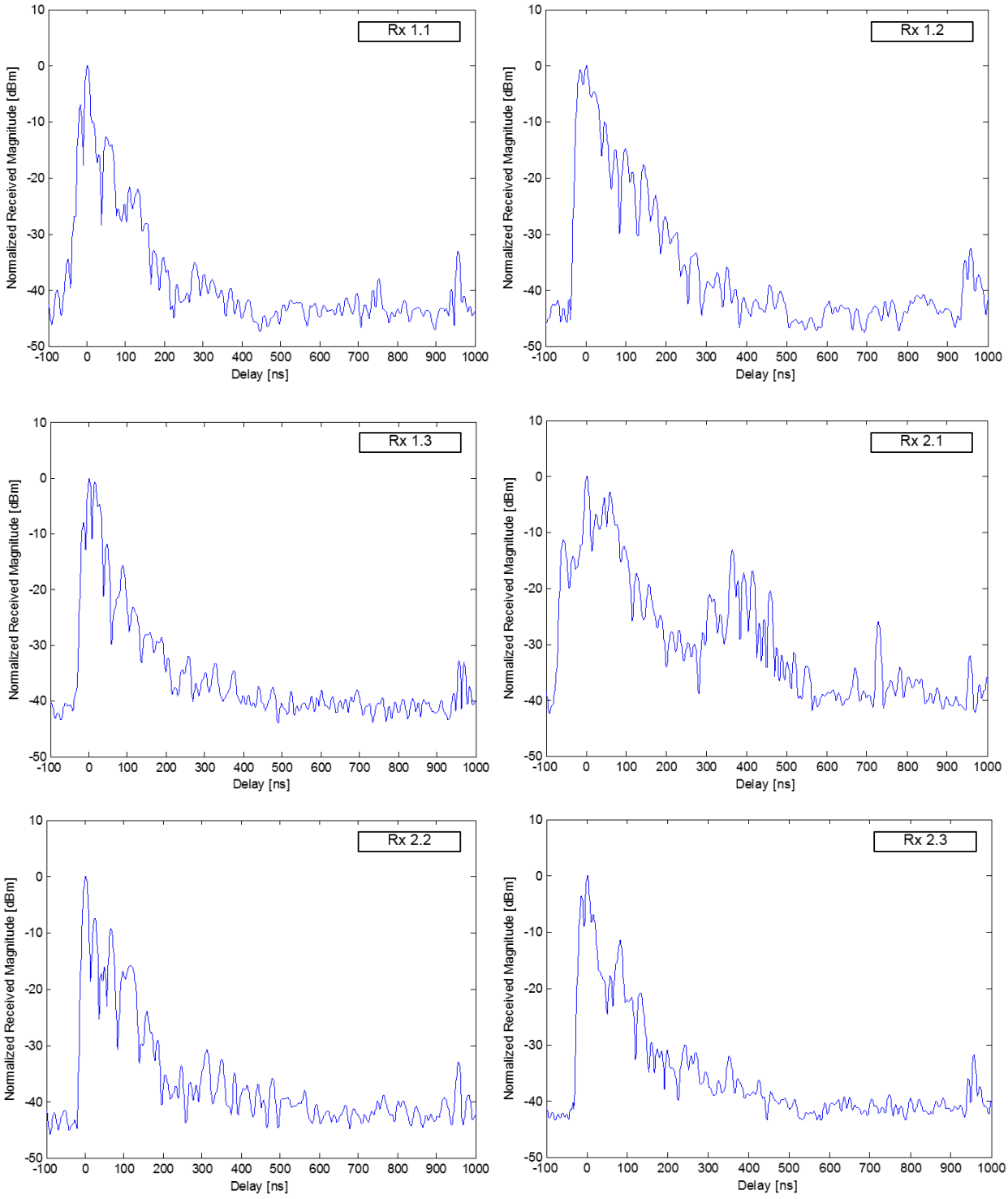

Figure B.5: Average power delay profiles for Scenario 2: Rx 1.1 – 1.2, Rx 2.1 – 2.3

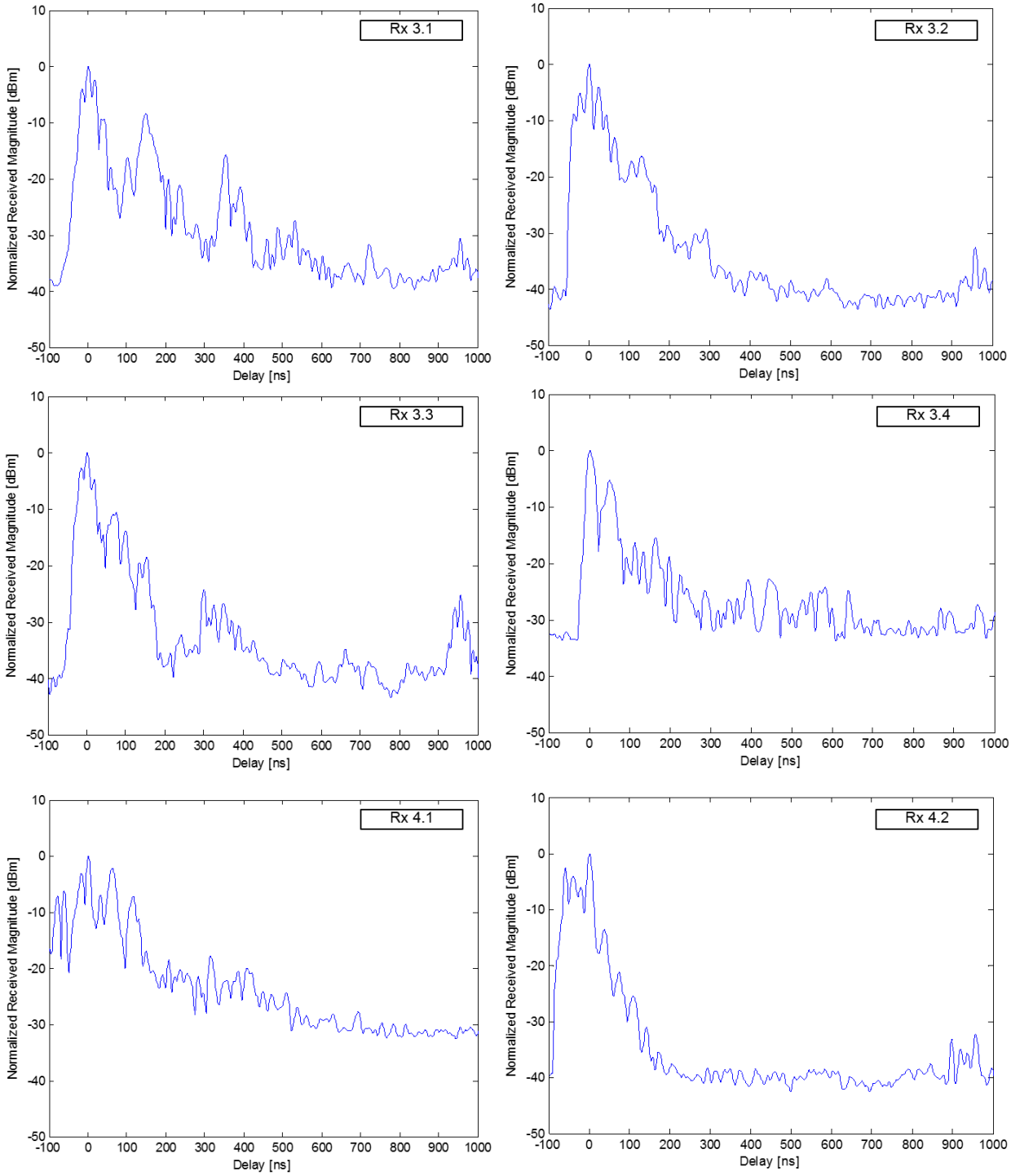

Figure B.6: Average power delay profiles for Scenario 2: Rx 3.1 – 3.4, Rx 4.1 – 4.2

B.3 Scenario 3 (Atrium)

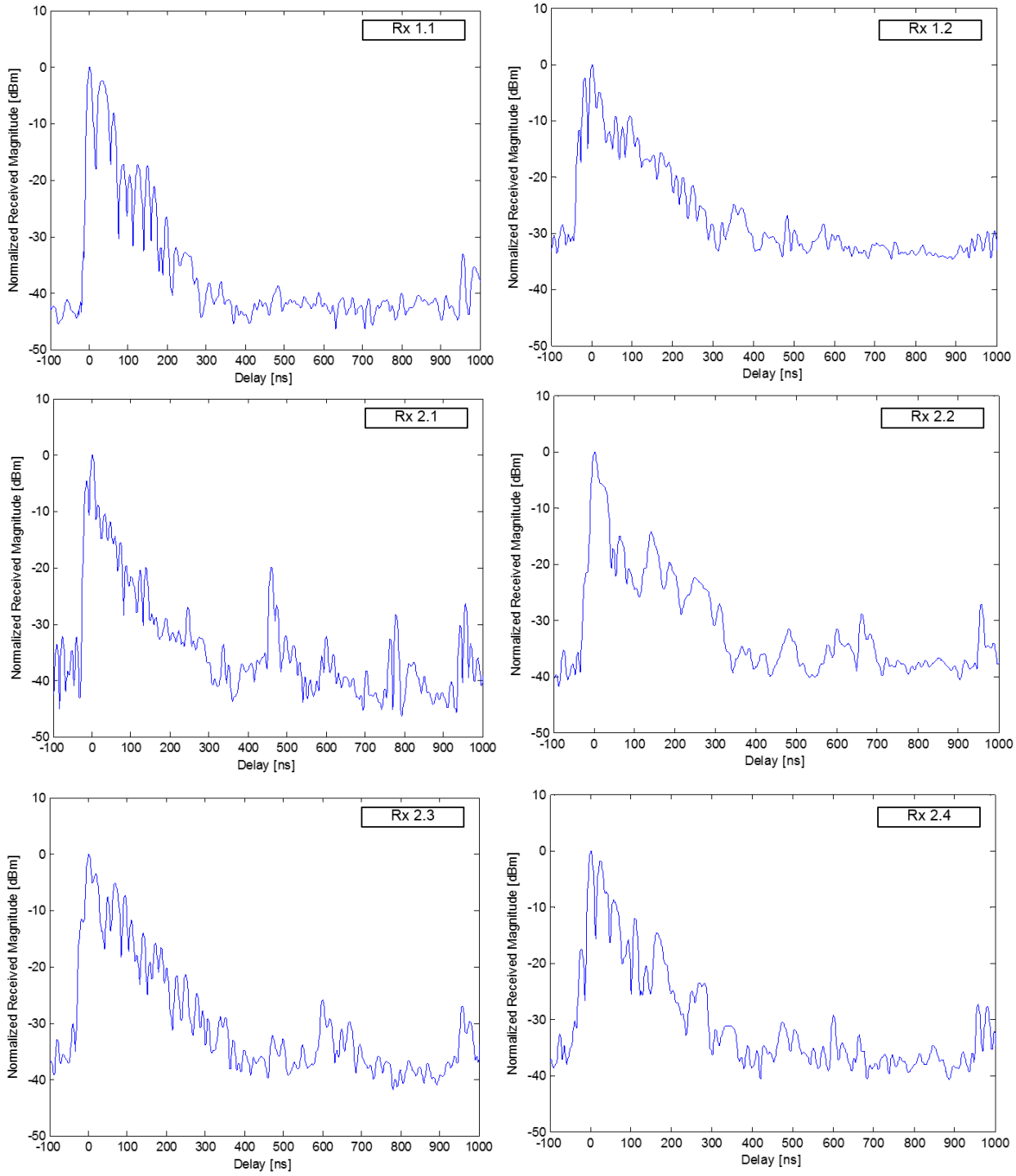

Figure B.7: Average power delay profiles for Scenario 3: Rx 1.1 – 1.2, Rx 2.1 – 2.4

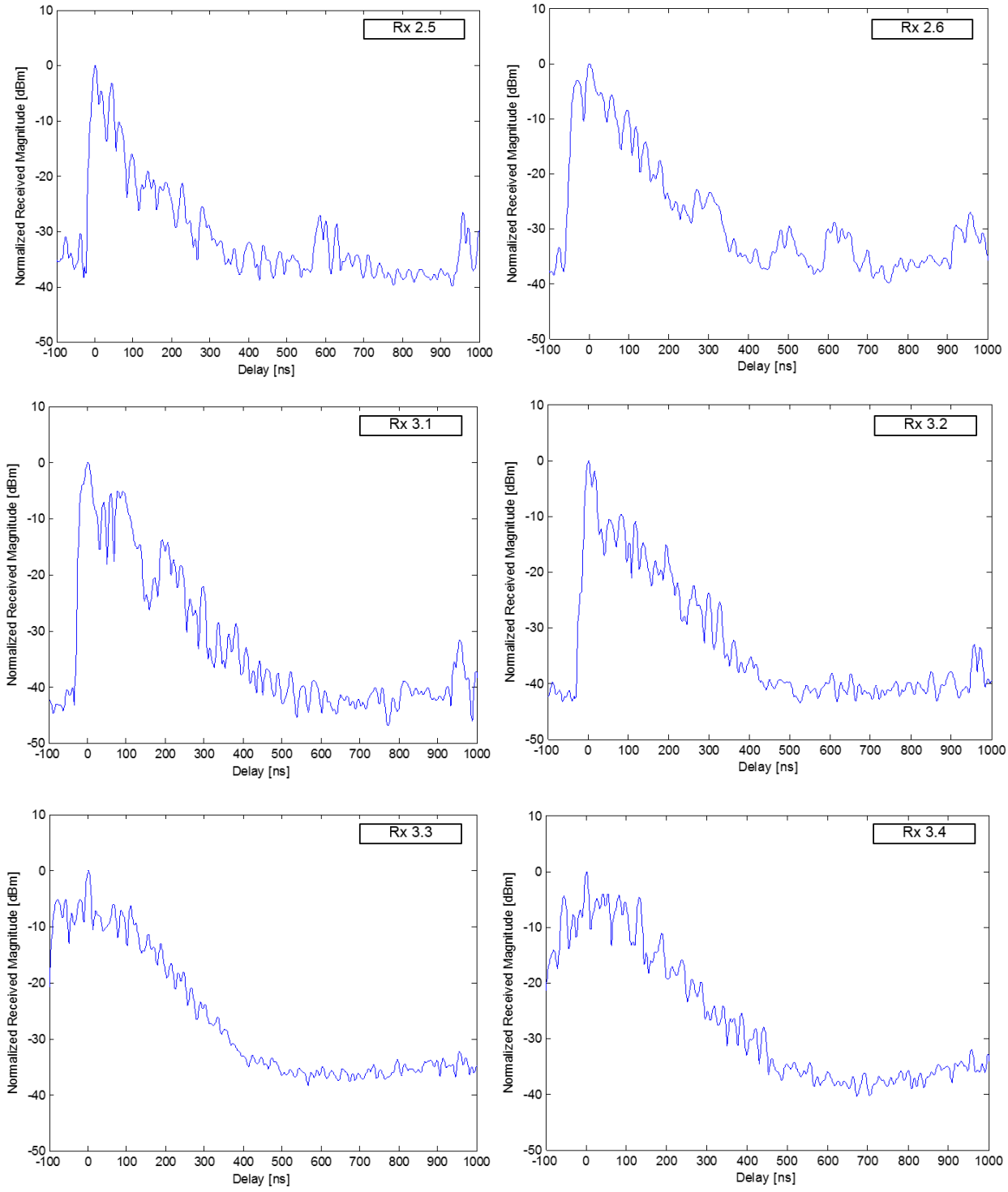

Figure B.8: Average power delay profiles for Scenario 3: Rx 2.5 – 2.6, Rx 3.1 – 3.4

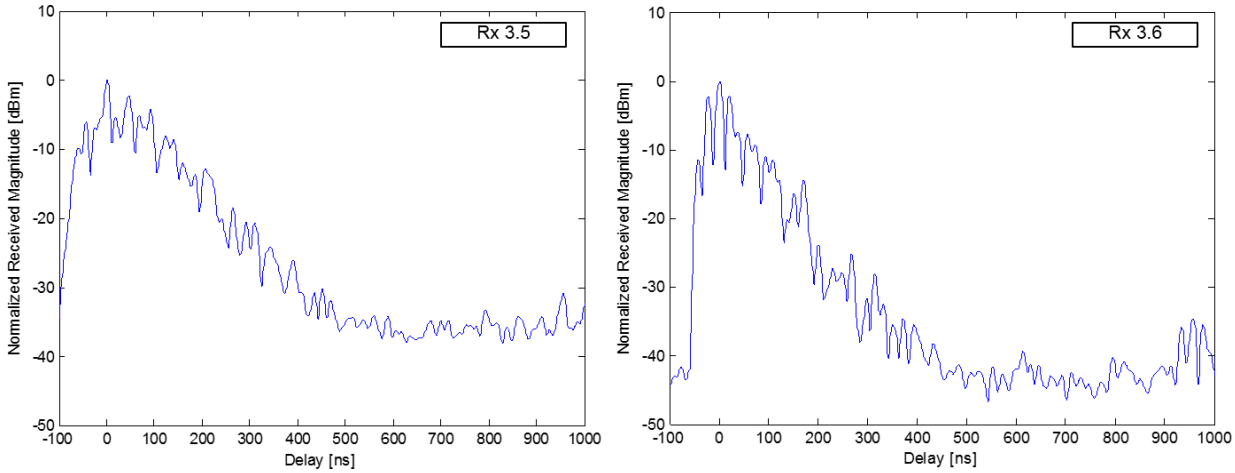

Figure B.9: Average power delay profiles for Scenario 3: Rx 3.5 – 3.6

B.4 Scenario 4 (Hospital)

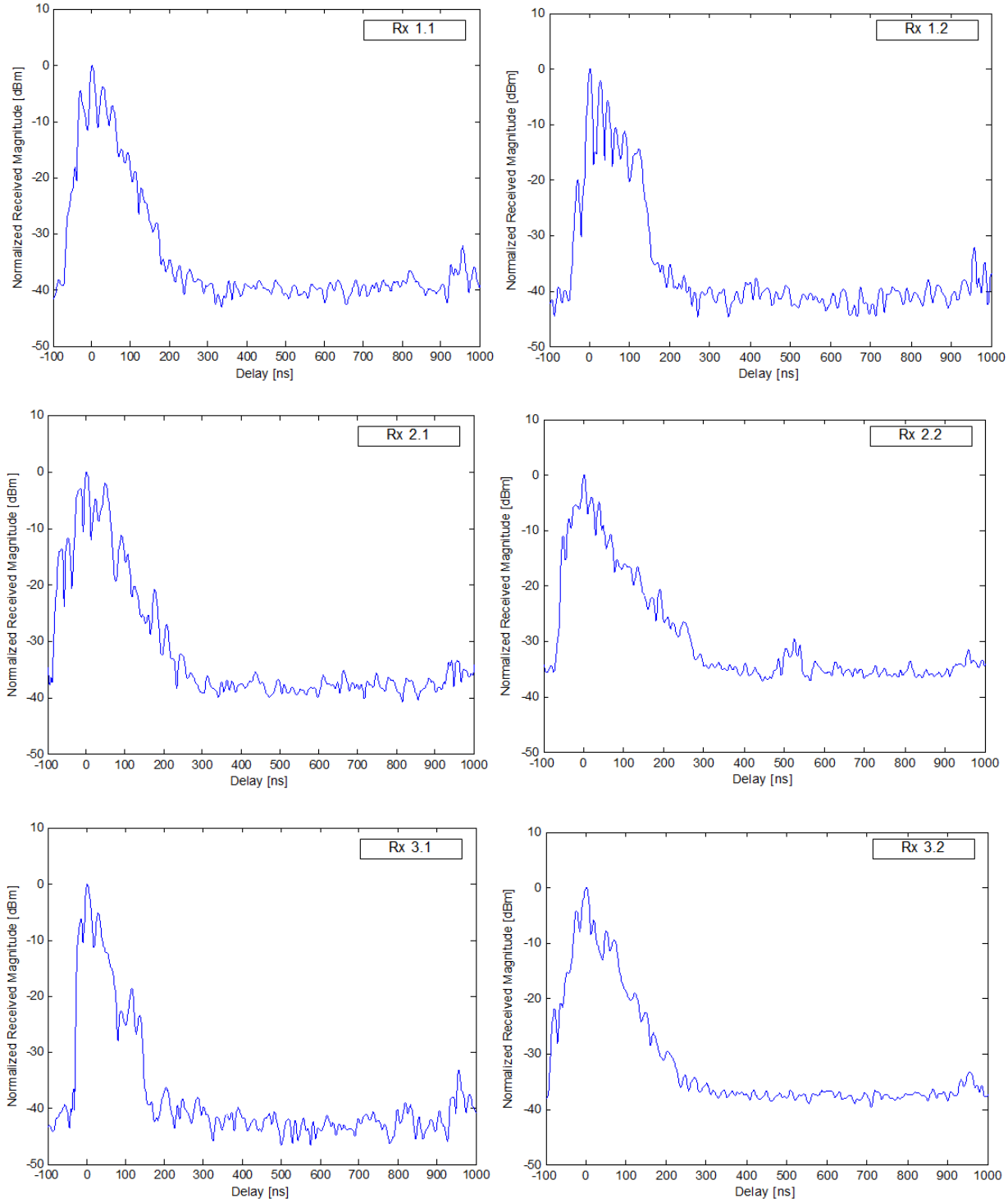

Figure B.10: Average power delay profiles for Scenario 4: Rx 1.1 – 1.2, Rx 2.1 – 2.2, Rx 3.1 – 3.2

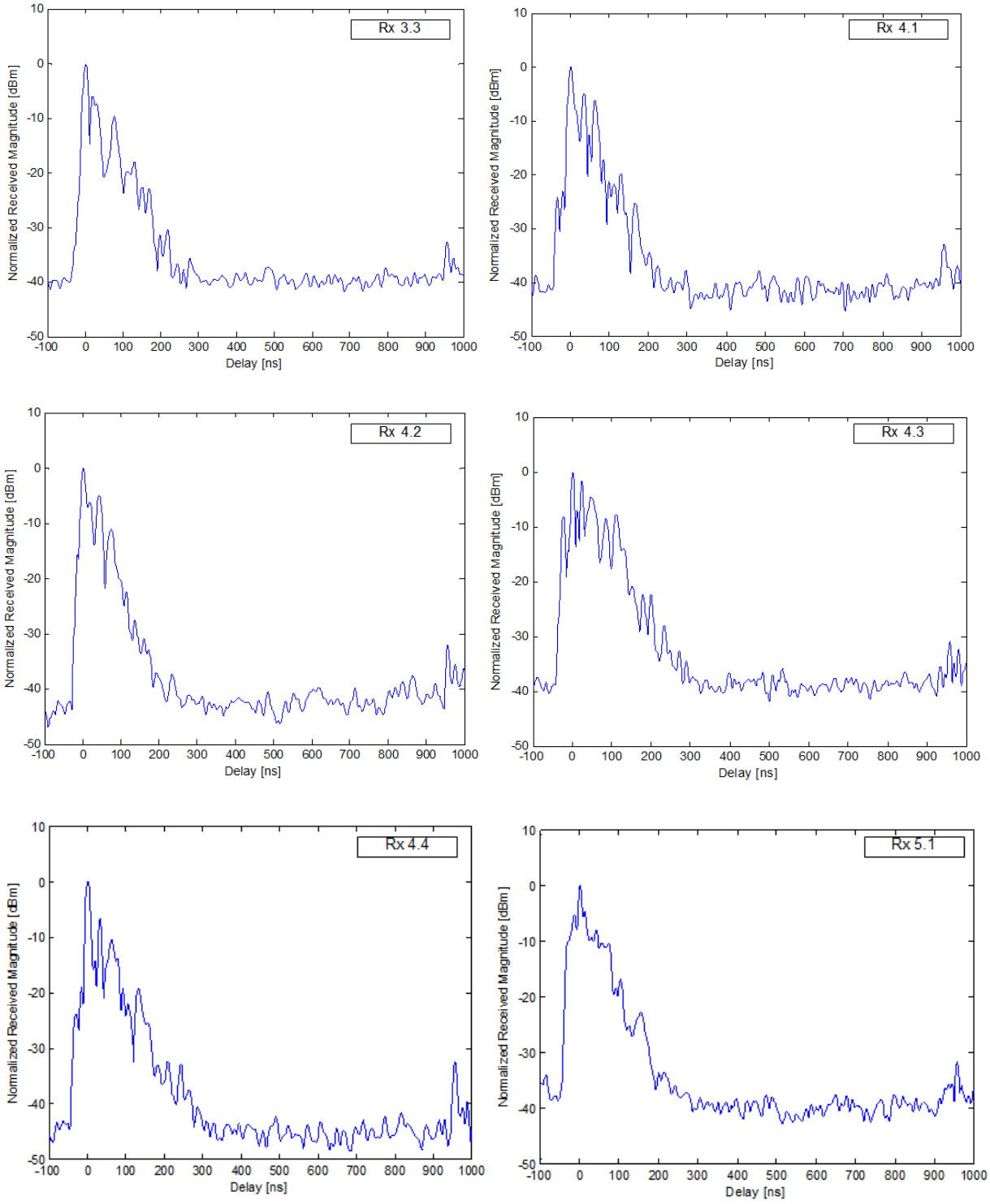

Figure B.11: Average power delay profiles for Scenario 4: Rx 3.3, Rx 4.1 – 4.4

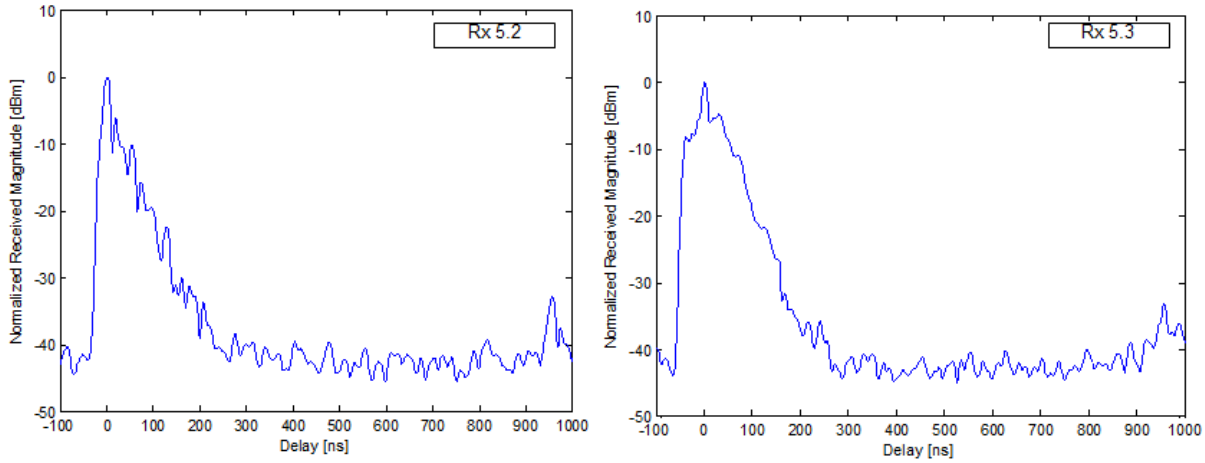

Figure B.12: Average power delay profiles for Scenario 4: Rx 5.2 – 5.3

B.5 Scenario 5 (Indoor-to-Outdoor)

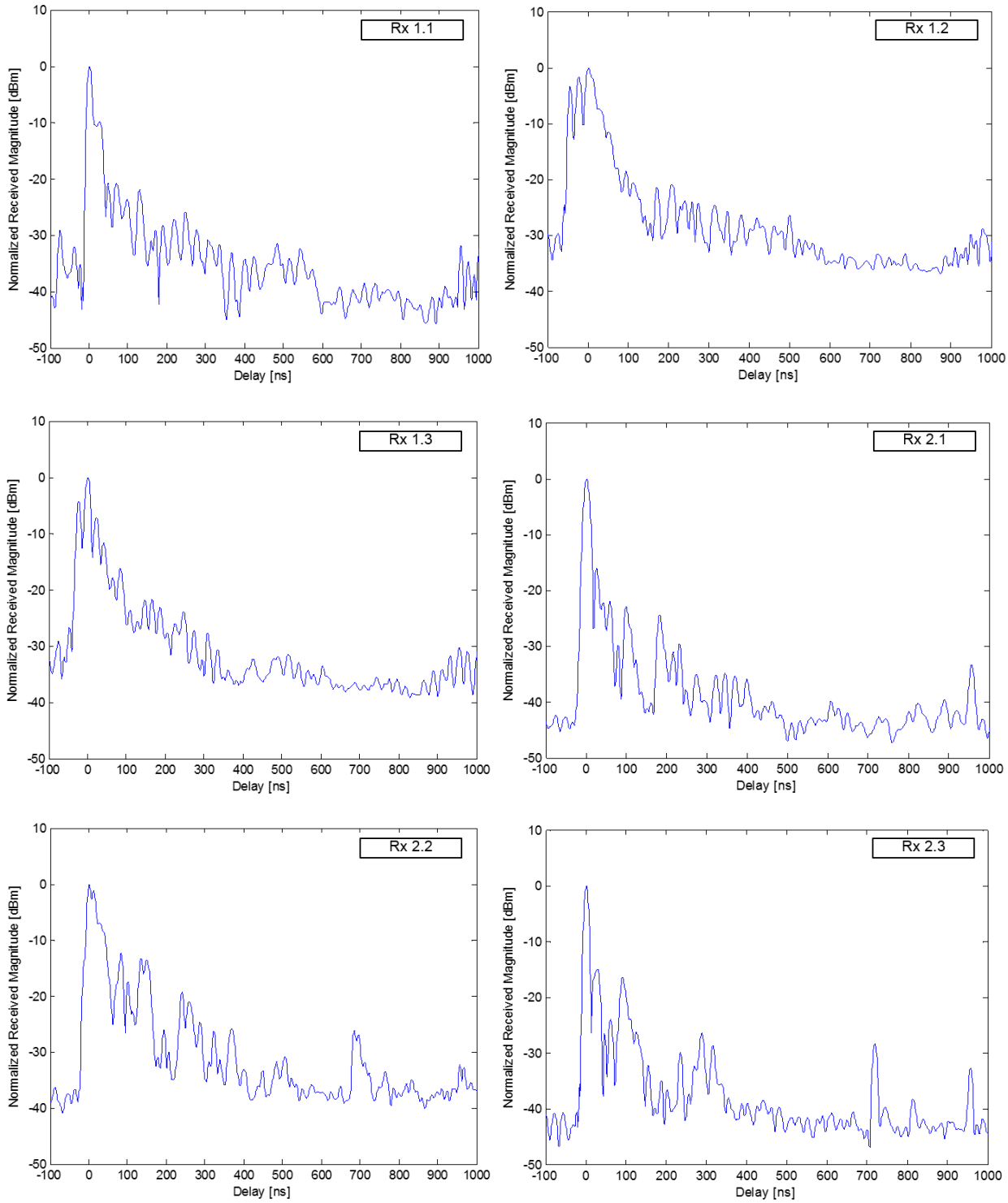

Figure B.13: Average power delay profiles for Scenario 5: Rx 1.1 – 1.3, Rx 2.1 – 2.3

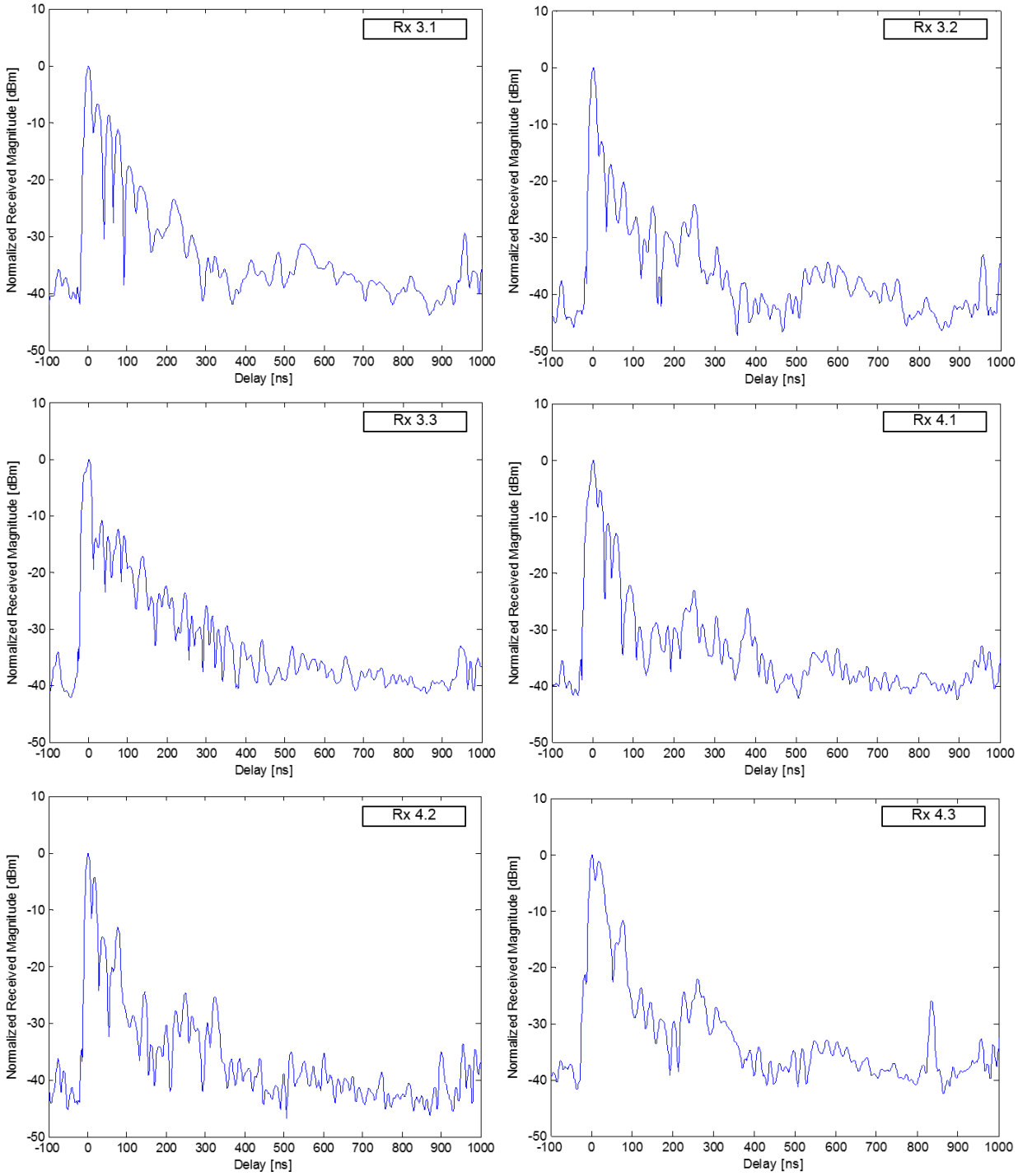

Figure B.14: Average power delay profiles for Scenario 5: Rx 3.1 – 3.3, Rx 4.1 – 4.3

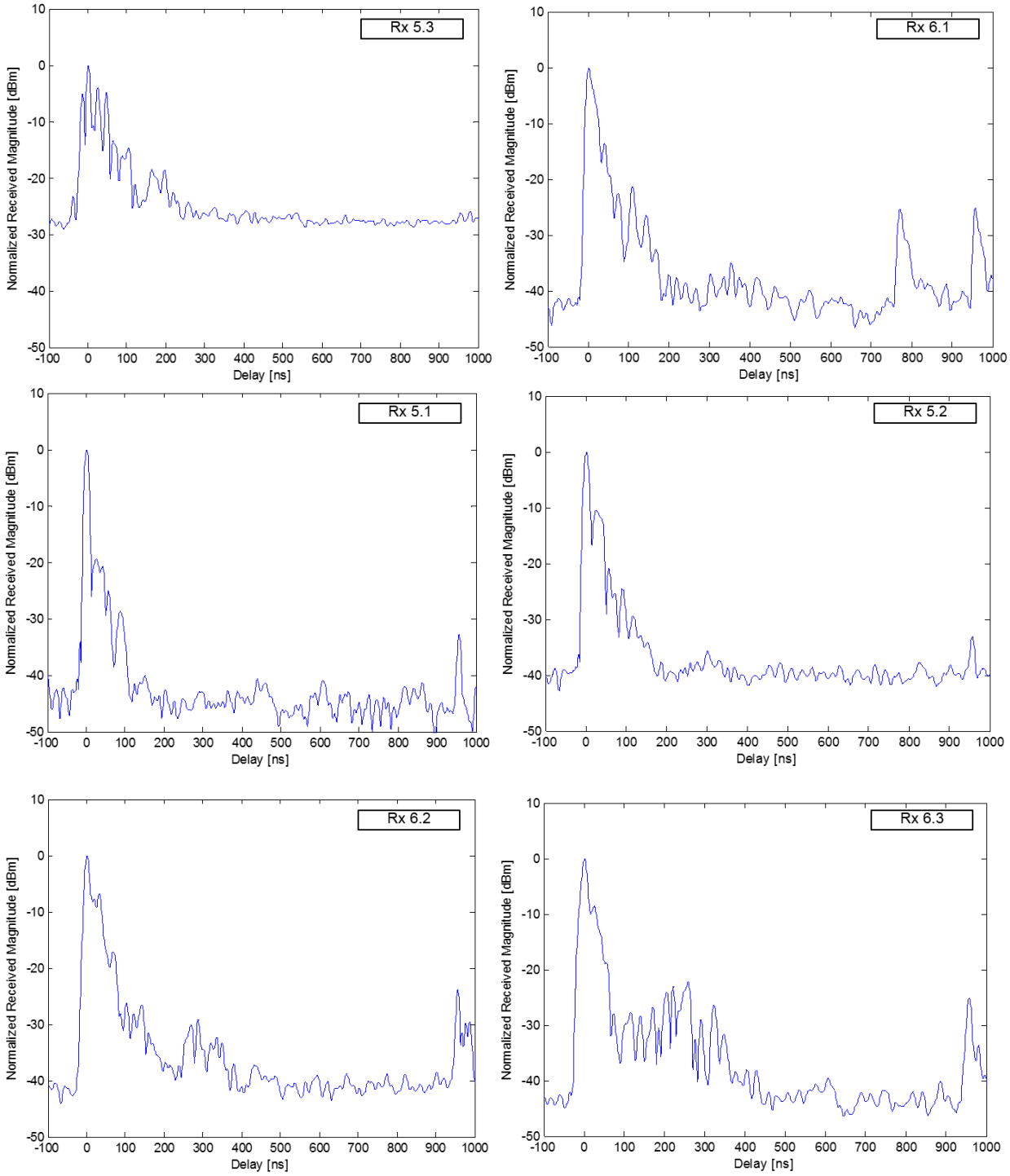

Figure B.15: Average power delay profiles for Scenario 5: Rx 5.1 – 5.3, Rx 6.1 – 6.3